This is to certify that the
thesis entitled

POLYMER NANOPARTICLES AND NANOPARTICLE ARRAYS

presented by

JIWU LIU

has been accepted towards fulfillment
of the requirements for the

Ph.D. degree in Physics and Astronomy

Major Professor's Signature

8/19/2009

Date

POLYMER NANOPARTICLES AND NANOPARTICLE ARRAYS

By

JIWU LIU

A DISSERTATION

Submitted to
Michigan State University
in partial fulfillment of the requirements
for the degree of

DOCTOR OF PHILOSOPHY

Physics and Astronomy

2009

ABSTRACT

POLYMER NANOPARTICLES AND NANOPARTICLE ARRAYS

By

Jiwu Liu

The manufacturing of polymeric nanoparticles by intramolecular crosslinking is studied by molecular dynamics simulation. Firstly an overview of the intramolecular crosslinking process is obtained by the simulations of benzocyclobutene(BCB)/styrene copolymers using an atomistic model. Then various coarse grained models, including Freely Jointed Chain (FJC), Freely Rotating Chain (FRC) and stiff chain models, are adopted for studying general properties of intramolecular crosslinking of polymers. A temperature series simulation on the FJC model reveals that the change of ambient temperature results in the formation of nanoparticles with distinct morphologies. To describe their structures, a quantity referred to as chemical distance density is introduced, with a quantitative relation between it and the radius of gyration being found. The subsequent study of rigidity effects adopts FRC and stiff chain models. It is found that in the rigid regime, the crosslinking process leaves a substantial number of crosslinkers unlinked, and forms nanoparticles that are significantly larger than their non-rigid counterparts. The Maxwell constraint counting method is used to determine the rigidity thresholds, which yields good agreements with the simulation data. In the last chapter, the atomistic model for polystyrene in the previous crosslinking simulations is employed for a study of polystyrene chains on attractive substrates. The phase diagram and a rough overview of chain dynamics on substrates are obtained.

To my family

ACKNOWLEDGMENTS

At the time when I finish my PhD thesis, I would like to thank those who have helped me to accomplish this important goal in my life.

First of all, I want to give my deepest thanks to my advisor, Professor Phillip Duxbury, for guiding me through my PhD study with his expertise, insights and great patience. My future work will continuously benefit from what I have learned from him.

I am grateful to all professors in my PhD guidance committee, Subhendra D. Mahanti, Simon Billinge, Chong-Yu Ruan, Gregory Baker and Michael Mackay, for all the help and advice they have offered me.

I would also like to acknowledge all my officemates. Radu Cojocaru gave me suggestions on my thesis writing. I learned many things about scientific research and computer techniques from working with Chris Farrow and Erin McGarrity. And Dan Olds, Saurabh Gujarathi, Luke Granlund and Kanokkorn Pimcharoen make the office an enjoyable place to work in. Saurabh Gujarathi has proof read my thesis and given me valuable advice on my writing.

Thanks to all my friends in graduate school, Teng Yang, He Huang, Wenduo Zhou, Yuping Huang, Zhensheng Ding, Gaoming Zhang, Zhiyi Bao and many others, for standing by me and giving me help whenever I need.

Most importantly, my great gratitude to my parents, my brothers and my sister. You have given me enormous support and love. This work is dedicated to you.

Table of Contents

List of Tables

List of Figures

Chapter 1

Introduction to polymer physics

Polymers, also referred to as macromolecules, are large molecules made of repeating chemical units connected by covalent bonds. They are primary materials of modern civilization. The use of polymers by mankind started since ancient times, but it was then limited to the naturally available polymers such as wood, fiber, natural rubber and so on. It was since 19th century when the synthetic polymers were invented that the polymer industry started growing rapidly. Thousands of new types of polymers have been synthesized, and have found tremendous use in almost every aspect of our daily lives.

The applications of polymers keep expanding owing to the fast evolving polymer technology. Among other things, a recent experiment showed that nanoparticles can be made by the intramolecular crosslinkings of polymers[4], opening the door for polymers to enter nanoparticle world. Polymeric nanoparticles have many promising applications ranging from constituents of new nanomaterials to functional parts of novel nano-devices. This thesis shall focus on the study of their properties and syntheses from the point of view of physics.

A brief introduction to polymer physics is given in the following three sections, with emphases on issues that are relevant to this thesis. Section 1.1 covers some basic

knowledge about polymers, such as their classifications and descriptions. In section 1.2, two basic theoretical models of polymers are introduced. The last section describes different phases of polymer chains and of bulk polymers. More about polymer physics can be found in many good textbooks[5, 6, 7, 2].

1.1 Basics of polymers

The elementary units of a polymer are termed *monomers*. A polymer is called a *homopolymer* when all monomers in it are of the same type. On the contrary, a polymer is called a *heteropolymer* or *copolymer* if its constituent monomers are of different types. Copolymers can be classified by the orderings of their monomers. Some typical types of copolymers are:

- Block copolymer: —A—A—A—A—A—A—A—B—B—B—B—B—B—B—
- Alternate copolymer: —A—B—A—B—A—B—A—B—A—B—A—B—
- Random copolymer: —A—B—B—B—A—B—A—A—B—B—A—B—

Biopolymers such as DNA and proteins are well known examples of copolymers. DNA consist of 4 types of nucleotides (denoted as A,T,C,G) whereas proteins are made from 20 different amino acids. The ordering of monomers in a biopolymer carries rich information. It makes biopolymers complex enough to serve as fundamental units of life.

Polymers show vast diversity in their chemical and physical properties due to differences in their constitutions, syntheses as well as processings. In order to fully describe a polymer, three levels of charatersiscs are required, namely *constitution* , *configuration* and *conformation.*

Constitution of a polymer specifies all the chemical units of the polymer as well as their connections. It thus defines the size, the type and the basic structure of a

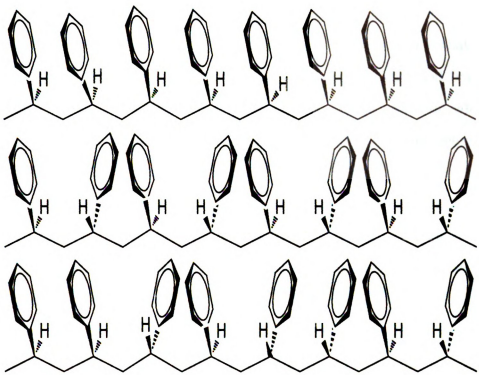

Figure 1.1: Isotactic(top), syndiotactic(middle), and atactic(bottom) polystyrenes. The polymer backbone is in the plane of the paper, and the solid and dashed wedges indicate groups above and below the plane, respectively.

polymer.

Configuration refers to the spatial arrangement of atoms in a polymer, in particular the orientations of its substituents, so that polymers of the same constitution, namely isomers, can be distinguished. A polymer can not change from one configuration to another without breaking its chemical bonds. Figure 1.1 shows three configurations of a polystyrene chain, *i.e.*, isotactic, syndiotactic and atactic configurations. The difference among them resides in the locations of the phenyl groups. In the isotactic configuration, phenyl groups are located on the same side of the backbone. In the syndiotactic configuration, phenyl groups distribute alternatively on both sides of the backbone. In the atactic configuration, the locations of phenyl groups are random. Different tacticities of polymers can lead to their different physical and chemical behaviors. For example, an isotactic polymer is easier to crystallize

due to its ordered structure.

Conformation specifies the dihedral angles about covalent bonds that connect monomers. To change from one conformation to another no chemical bonds need to be broken. Instead it is achieved through the rotation of atoms or side groups about covalent bonds. Therefore the conformation of a polymer is also referred to as *Rotational Isomeric State* (RIS).

N-butane provides a starting point for the analysis of conformations of polymers. In fig. 1.2, three representative rotational isomeric states of *n*-butane are shown, namely *trans*, *gauche* and *eclipsed*. The potential energies of polymers at different conformations are different, too. Fig. 1.3 shows the potential energy of a *n*-Butane as a function of its dihedral angle. It has three minima, corresponding to *trans*(t), *gauche*$^+$(g^+) and *gauche*$^-$(g^-) conformations, respectively. Among them, the global minimum is achieved at the dihedral angle of 180°, which is the trans conformation. On the other hand, the global maximun occurs when the dihedral angle is 0°, *i.e.*, eclipsed conformation.

The probability for a n-butane to take on the trans or gauche states are significant because of their low potential energies. Likewise, a rotational isomeric state of a long polymer chain consists of predominantly trans and gauche. So it can often be written as a sequence of them, *e.g.*, $tg^+ttg^- \cdots\cdots$. The number of total rotational isomeric states grows exponentially with the number of monomers, and can become enormous for a long polymer.

Radius of gyration (R_g) is the primary parameter to describe the dimension of a polymer. A simple definition of R_g is:

$$R_g^2 = \frac{\sum_i m_i(\vec{R}_i - \vec{R}_0)^2}{\sum_i m_i} \tag{1.1}$$

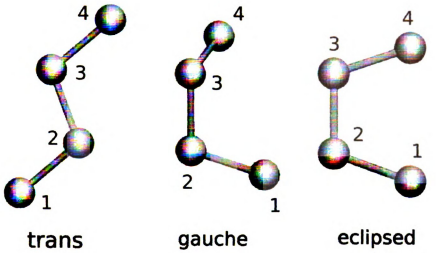

Figure 1.2: Conformations of *n-butane*

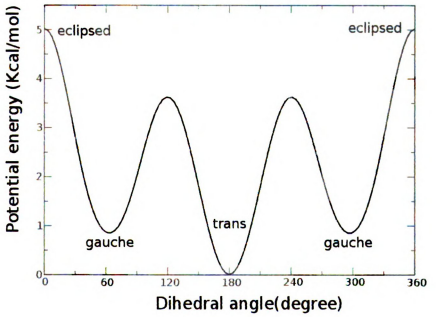

Figure 1.3: Rotational potential of *n-butane*

where $\vec{R_0}$ is the center of mass of the polymer, and m_i and $\vec{R_i}$ are the mass and position vector of the ith atom in the polymer. Another equivalent definition is

$$R_g^2 = \frac{\sum_{i=1}^{N} \sum_{j=i+1}^{N} (m_i \vec{R_i} - m_j \vec{R_j})^2}{(\sum_i m_i)^2} \tag{1.2}$$

The mass factors in the definitions of R_g are not always essential. When all types of atoms are evenly distributed in the polymer (which is true for homopolymers and random copolymers), all mass factors can be set to unity with little change to the value of R_g.

Persistence length of a polymer is the parameter to describe its stiffness. A polymer with persistence length l_P satisfies the equation below:

$$< cos\theta_l >= e^{-l/l_p} \tag{1.3}$$

where θ_l is the angle between the tangents at two points on the chain separated by a contour distance of l.

1.2 Chain models

A polymer can be modeled as a chain of many segments connected together, where a single segment may represent one or more monomers. The chain model can be applied not only to linear polymers, but also to complex polymers consisting of branches, loops or crosslinks, for they can be regarded as multiple linear chains connected together. This brief introduction is limited to linear polymers only.

The simplest chain model of polymers is the *ideal chain* (also known as *Gaussian chain*, *unperturbed chain* or *Brownian chain*) model. In this model the segments of a

chain are chosen to be appreciably longer than the persistence length of the polymer such that they are independent of each other. One segment can acquire arbitrary orientation with respect to other segments. Furthermore, there is no interactions among the segments.

Consider an ideal chain with N segments, $\vec{l}_1, \vec{l}_2, ..., \vec{l}_N$. The mean square of its end to end distance is defined as:

$$< R^2 >=< (\sum_{i=1}^{N} \vec{l}_i)^2 > \tag{1.4}$$

As there is no correlation between two segments, the sum of ensemble average $< \vec{l}_i \cdot \vec{l}_j >$ vanishes when $i \neq j$. If each segment has an average length $b = \sqrt{< l^2 >}$, it can be easily derived:

$$< R^2 >= N < l^2 >= Nb^2 \tag{1.5}$$

Analogy can be drawn between an ideal chain and a random walk. The contour of an ideal chain can be directly compared to the trajectory of a random walk. It can be seen that the above result agrees with the random walk model as expected.

The mean square of R_g of an ideal chain is [5]:

$$< R_g^2 >= \frac{< R^2 >}{6} = \frac{Nb^2}{6} \tag{1.6}$$

So the size of ideal chain shows a power law dependence on the number of monomers N in a polymer:

$$R \sim N^{1/2} \tag{1.7}$$

The *real chain* (or *perturbed chain*) model is derived on the basis of the ideal chain model. It takes into account the hard core repulsion between the segments, so that it is a more realistic description of polymers compared to the ideal chain. Mathematical treatment of the perturbed chain is more difficult. It turns out a similar power law

dependence of R_g on the number of monomers can be found:

$$R \sim N^{3/5} \tag{1.8}$$

The exponent is bigger than that of the ideal chain model due to the excluded volume effect.

The chain models for polymers are the so-called coarse-grained models. In addition to them, polymers can also be modeled in other ways, as illustrated in fig. 1.4. The *ab initio* method employs quantum mechanics to study the processes in polymers that take place at very small time and length scales. Atomistic and coarse-grained models are often adopted in the molecular dynamics or Monte Carlo simulation of polymers. They rely on classical force fields to describe polymers. And the properties of large polymer systems, such as bulk polymers, can be studied with fluid models or finite element methods.

1.3 Phases for single and bulk polymers

A long polymer can exhibit two distinct phases, namely *coil* and *globule*, which have been extensively studied in the past [8]. Basically, for a polymer at low temperatures, the attraction between monomers is dominant, so that it forms a globule, with R_g approximately scaling as $N^{1/3}$. While at high temperatures, a polymer tends to expand to acquire a larger conformational entropy, therefore it takes on the coil state, where the thermal effect completely overcomes the attraction between monomers, and leads to a net excluded volume effect in the polymer. In this case polymers behave like perturbed chains, with R_g being proportional to $N^{3/5}$. In fig. 1.5, R_g of polystyrene chains in cyclohexane is plotted against temperature, where a transition from the globule to the coil state can be observed.

In the transition from the globule to the coil state, there is a special temperature

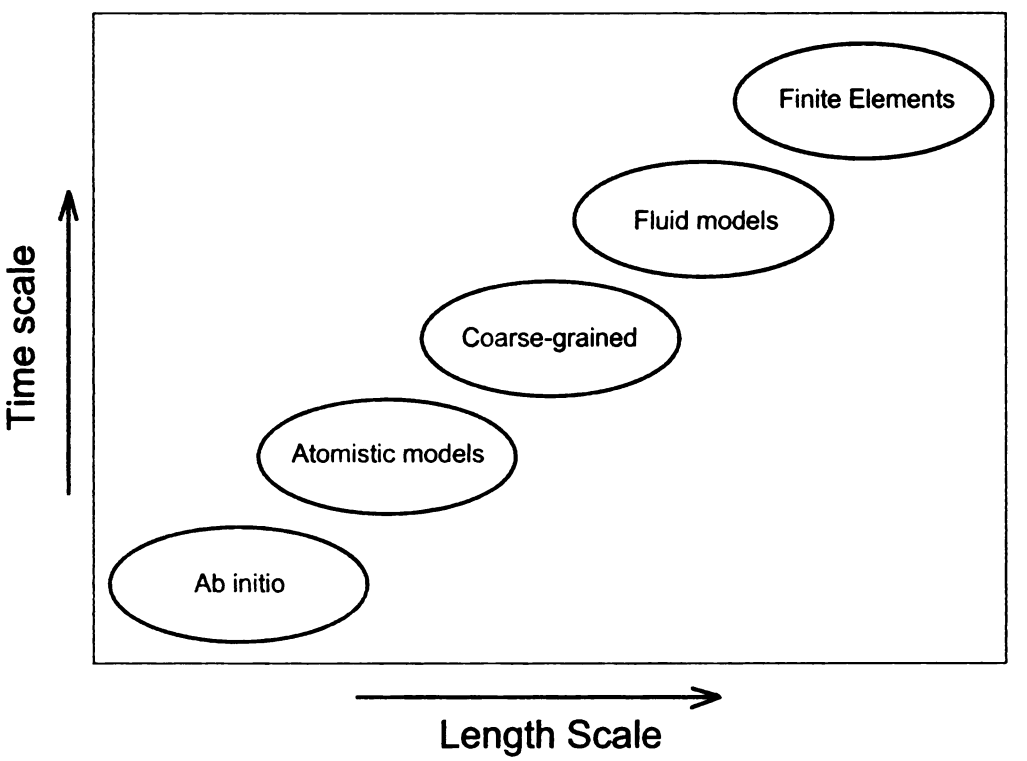

Figure 1.4: Polymer models at different time and length scales.

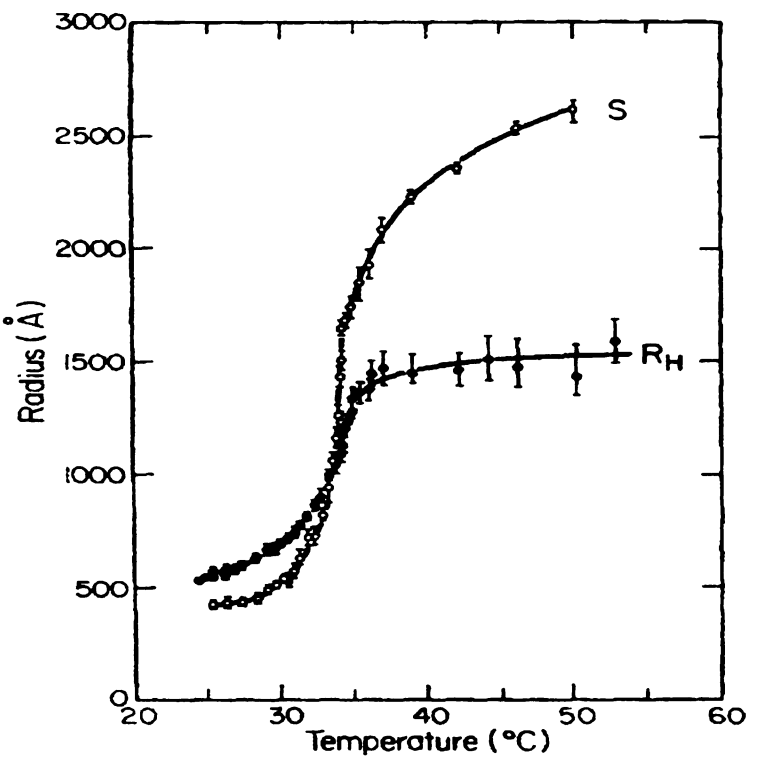

Figure 1.5: Coil-globule transition of polystyrene ($M_w = 2.6 \times 10^7$) in cyclohexane. S is the radius of gyration. R_H is the hydrodynamic radius[1].

point where the attraction between the monomers exactly cancels the effective hard core repulsion, so that the excluded volume effect vanishes. It appears that the monomers do not interact with each other, and polymers behave as if they were ideal chains. This special temperature is called the Θ(theta) temperature.

In addition to the temperature, the solvent quality can induce the coil globule transition, too. Since the attraction between the monomers and the solvent molecules offsets the attraction between the monomers themselves and results in an expansion effect, the solvent plays a similar role as the temperature. The solvent that causes a polymer to expand is called a *good solvent* of this polymer, otherwise a *poor solvent.* The solvent satisfying theta condition is called Θ *solvent*, accordingly.

The quality of a solvent is changeable. A solvent can be poor at low temperatures and become good at high temperatures. If a solvent is made of the same molecules as the monomers, it will always offset the attraction between the monomers. Consequently, polymers stay in the perturbed chain state at all temperatures. Such a solvent is called an *athermal solvent.*

Bulk polymers have different phase behaviors, which can be indicated by the Young's modulus as in fig. 1.6. Firstly, at very low temperatures, most bulk polymers do not crystallize. Instead, they are trapped in the glassy state (region 1). When the temperature rises, they undergo a transition from the glassy state to the rubbery state (region 3). The transition is marked by region 2. And at very high temperatures, bulk polymers start melting and change into polymer melts eventually, which are indicated by region 4 and 5 in the figure.

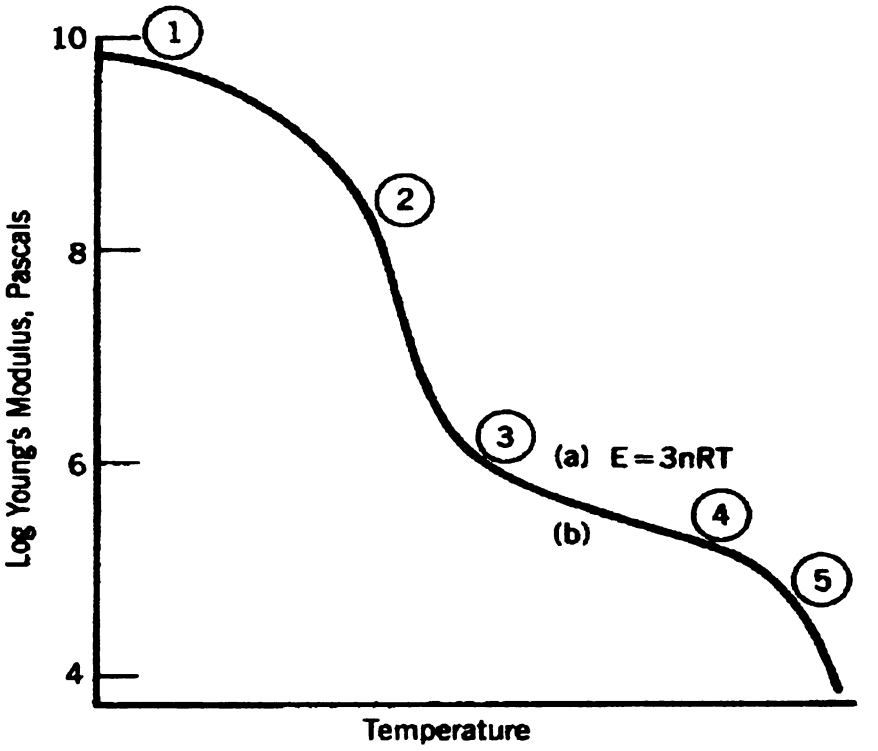

Figure 1.6: Temperature dependence of Young's modulus of bulk polymers [2].

Chapter 2

Molecular dynamics simulation of polymers

Computer simulations have been extensively used to study polymers for the past few decades. They are applied to a wide variety of polymer systems, such as polymer chains, polymer melts, polymer membranes and polymer solutions *etc.* They are also adopted in the emerging areas of polymer science, *e.g.*, polymer nanocomposites and polymeric nanoparticles. It can be foreseen that computer simulations will play a more important role in polymer science in the future.

Molecular dynamics (MD) and Monte Carlo (MC) are two major simulation techniques in the study of polymers. Both of them are capable of simulating a polymer system at equilibrium, which is done by firstly generating an ensemble of microscopic states for the system being studied and then evaluating its properties by averaging over the whole ensemble. These two methods yield results with same accuracy and are equally efficient. However, they differ from each other in their ways of generating their ensembles of microscopic states. A Monte Carlo simulation does it in a stochastic way, where the microscopic states are generated randomly; while a molecular dynamics simulation does it by integrating the equations of motion of the system, so that the

microscopic states it generates also follows the trajectory of the system in its phase space. Therefore, the study of the system dynamics can only be done by molecular dynamics simulations.

This chapter focuses on the molecular dynamics simulations of polymers only. Firstly, section 2.1 provides an overview of molecular dynamics. Then in section 2.2 its application to polymer systems is discussed. Finally, in section 2.3 and section 2.4 some basics of molecular dynamics and force fields are introduced.

2.1 Introduction

As an input to a molecular dynamics simulation, the initial configuration of the system under study has to be created prior to the simulation. An initial configuration specifies the coordinates and velocities of all particles in the system. It can be prepared in many different ways, which can be realistic or not. Sometimes the initial configurations may be created far from equilibrium, so that the subsequent molecular dynamics simulation fails. To cope with this problem, an energy minimization usually is applied before the real molecular dynamics simulation. It drives the system to a stable state, corresponding to a local minimum in the potential energy landscape. Another approach is to introduce a so called "soft potential" for a short period of time. Unlike physical potentials such as the Lennard-Jones potential, soft potentials remain finite even when particles overlap with each other. Thus they are able to push particles apart gradually and leave the system in a safe state.

A typical molecular dynamics simulation comprises of two parts. The first part is the equilibration run where the system is brought to its equilibrium. The second part is the production run where a number of snapshots of the system are taken to calculate its properties. In some cases, an energy minimization may be performed on those snapshots prior to the calculation to eliminate thermal noises.

Molecular dynamics employs classical mechanics to describe the motion of a molecular system being studied. Though quantum mechanics is a more accurate description of such a microscopic system, it is not feasible because of the tremendous difficulty in solving the Schrödinger equation that involves a large number of atoms. Since classical mechanics can only provide approximate descriptions of microscopic systems, it inevitably causes errors in molecular dynamics simulations. Consider a simple oscillator with a resonant frequency ν. When its energy quantum $h\nu$ is greater than $k_B T$, it should have a large probability of staying at the ground state according to quantum mechanics. However, classical mechanics allows the oscillator to absorb heat continuously so that it can rise to higher energy levels. Hence corrections have to be made to the kinetic energy and specific heat of the system[9]. Basically, when there are strong quantum effects such as electron excitation/transfer/tunneling, molecular dynamics has to be corrected or replaced with its quantum mechanics counterpart.

A molecular dynamics simulation is divided into discrete time steps. At each time step, coordinates and velocities for all atoms are computed by integrating the equations of motion. However, since the integration algorithms neglect higher order terms in Taylor's expansions of coordinates and velocities, large errors can arise if the time step is too big. To reduce this error, it is usually required that the integration time step is appreciably shorter than the period of the fastest oscillation in the system.

On the other hand, the computing time of a simulation is not proportional to the real time period being simulated, but the number of integration steps to run, which simply is the real time period divided by the integration time step. Thus, the longer each integration time step is, the shorter computing time the simulation takes. Basically there are two ways to enable a longer time step. One is to replace fast harmonic oscillators, *e.g.*, that of the bond stretching and bond bending, with hard constraints. Another way is to use relatively less rigid harmonic potentials to describe those oscillators.

In a molecular dynamics simulation, the force field that describes the system is of the central importance. Force fields are designed "artificially" in order to reproduce by computer simulations the real dynamics of molecular systems, using parametrized classical potential functions . So a force field by its nature is not a precise account of real systems, even though its parameters have often been carefully fit to the experimental data. Furthermore, an additional "transferability" error can occur[10] when a force field is applied to systems that it is not trained for. And it can also occur when calculating some physical properties whose experimental data are not incorporated in the fitting of the force field. More about force fields are discussed in section 2.4.

Overall, molecular dynamics is an effective technique to study complex systems, though with certain approximations. Usually, the larger the system is, the more approximations one has to introduce. So the result of a molecular dynamics simulation should always be checked with experiments.

2.2 Difficulties in the simulation of polymers

The simulation of polymers has intrinsic difficulties due to their complex nature[11]. Firstly, polymers are inhomogeneous systems which exhibit distinct structures at different length scales. To study their properties the samples have to be large enough to take into account all the inhomogeneities. For example, to study the properties of a polymer chain, the sample has to be of a size equal to the full chain, which is typically of tens of thousands of atoms. The samples have to be even larger when it comes to bulk polymers such as polymer melts. Compared to simple liquids which are homogeneous above a length scale about 10 Å (so that a small number of atoms are sufficient to show its properties), polymer systems are significantly more complicated.

Secondly, the simulation of a polymer system usually takes a long computing time because the time scales of its processes are vastly different. Vibrations of chem-

ical bonds in a polymer take place at a time scale of 10^{-13} second, while it takes about 10^{-11} second for a polymer to overcome the torsional potential barriers. The equilibration time for a large polymer system is significantly longer, ranging from 10^{-8} to 10^{-5} second. As mentioned in section 2.1, the time period of a single integration step has to be appreciably shorter than the period of the fastest oscillation in the system. Therefore, a time step of 10^{-15} second is usually adopted for a realistic polymer simulation. Consequently, the whole simulation of a polymer system may take tens of millions of steps to reach equilibrium, making it a CPU intensive task.

Thirdly, polymers have large configurational varieties such that their physical properties vary greatly. To better account for this diversity, it is often needed to study a number of polymers with various configurations, or a very long chain. The use of a long sample or multiple short samples can also improve the ergodicity of a simulation. Ergodicity ensures that the phase space of a system is faithfully sampled according to its equilibrium distribution, but is often hard to achieve for a molecular dynamics simulation which typically corresponds to a very short period of real time.

In answering those difficulties, the rapidly evolving computer technology as well as the advances in simulation techniques greatly improve our ability of handling the simulation of polymers. A comprehensive introduction to the simulation of polymers can be found in many good books[11, 12].

2.3 Basics of molecular dynamics simulation

2.3.1 Units

Real units and Lennard-Jones reduced units are two widely adopted units for molecular dynamics simulations. The real units are often used in atomistic models of polymers. In real units, energy is measured in Kcal/mol, mass in g/mol, temperature in K and distance in $\mathring{A}$. The units for other quantities can be determined accordingly.

The Lennard-Jones reduced units are more suitable for theoretical models of polymers. They are based on the parameters in the Lennard-Jones potential:

$$U_{LJ} = 4\epsilon \left[\left(\frac{\sigma}{r}\right)^{12} - \left(\frac{\sigma}{r}\right)^{6} \right] \tag{2.1}$$

ϵ and σ are chosen to be the unit for energy and distance respectively, and the mass of a proton is adopted as the third basic unit. Other units are derived from these three. In particular, the unit of temperature is $T = \epsilon/k_B$, and the unit of time is $t = \sqrt{m\sigma^2/\epsilon}$.

2.3.2 Boundary condition

In a molecular dynamics simulation, the system to be studied is enclosed in a simulation box for which the boundary condition has to be set.

The simplest way is to use the free boundary condition. It is good for an isolated system, such as a single polymer chain in vacuum. A direct consequence of the free boundary condition is the lack of pressure because pressure is exerted by the walls of the simulation box, which, however, are not fixed under the free boundary condition.

Most real systems exist in nontrivial environments to which the free boundary condition does not apply. In this case, the periodic boundary condition is often used. It assumes that a simulation box is surrounded by translated images of itself in three directions. And particles can interact with their image particles across the boundary. Those particles that exit from one side of the simulation box should re-enter from the opposite side.

The periodic boundary condition is more realistic compared to the free boundary condition. But it has one side effect, *i.e.*, the fake periodic correlation. So it is important to use a large enough system such that the fake correlation is negligible. And many trial simulations may be performed in order to find the appropriate size

of the simulation box.

2.3.3 Verlet algorithm

Verlet algorithm is the most popular algorithm of integrating the equations of motion in molecular dynamics. It updates the positions and velocities of particles by the following formula[13]:

$$\mathbf{r}(t+\Delta t) = 2\mathbf{r}(t) - \mathbf{r}(t-\Delta t) + \ddot{\mathbf{r}}\Delta t^2 + O(\Delta t^4) \tag{2.2}$$

$$\mathbf{v}(t) = [\mathbf{r}(t+\Delta t) - \mathbf{r}(t-\Delta t)]/(2\Delta t) \tag{2.3}$$

This Verlet algorithm has been modified to form two slightly different integration algorithms. They are referred to as *leap-frog Verlet* and *velocity Verlet* respectively. In the leap-frog Verlet algorithm, velocities are computed at the midpoint of a time step and are used to update positions:

$$\mathbf{v}(t+\frac{\Delta t}{2}) = \mathbf{v}(t-\frac{\Delta t}{2}) + \ddot{\mathbf{r}}\Delta t \tag{2.4}$$

$$\mathbf{r}(t+\Delta t) = \mathbf{r}(t) + \mathbf{v}(t+\frac{\Delta t}{2})\Delta t \tag{2.5}$$

In the velocity Verlet algorithm, the equations for updating positions and velocities are:

$$\mathbf{r}(t+\Delta t) = \mathbf{r}(t) + \mathbf{v}(t)\Delta t + \ddot{\mathbf{r}}(t)\frac{\Delta t^2}{2} \tag{2.6}$$

$$\mathbf{v}(t+\Delta t) = \mathbf{v}(t) + [\ddot{\mathbf{r}}(t) + \ddot{\mathbf{r}}(t+\Delta t)]\frac{\Delta t}{2} \tag{2.7}$$

It can be verified that all those Verlet algorithms are consistent.

The Verlet algorithms are not the most accurate ones to integrate the equations of motion. For example, *Gear* algorithm yields better accuracy. However, Verlet

algorithms obey the time reversibility and maintain the conservation of energy. They are easy to implement, too. So Verlet algorithms are by far the most widely used ones in molecular dynamics.

2.3.4 Thermostat and barostat

The integration of the equations of motion in molecular dynamics updates a system according to Newtonian equations. It generates microscopic states that follow the microcanonical distribution. To study more general cases, namely the canonical and grand canonical distribution, thermostat and barostat have be incorporated. They ensure a system to stay at a constant temperature or pressure. In below two major thermostat/barostat techniques are briefly introduced, *i.e.*, *Nosé-Hoover* and *Berendsen.*

In 1984, Nosé proposed a method to couple a dynamical system to a heat bath[14], which later was improved by Hoover[15, 16] and thus was referred to as *Nosé-Hoover* method. Basically the method adds an extra degree of freedom s to the Hamiltonian of the system to describe the effect of the heat bath, which leads to one additional kinetic energy term T_s and one additional potential energy term V_s:

$$T_s = \frac{p_s^2}{2Q} \tag{2.8}$$

$$V_s = gk_BTln(s) \tag{2.9}$$

where g is the number of the degrees of freedom of the system, and Q is the effective mass for the new degree of freedom s. Based on the new Hamiltonian it can be derived that[17]:

$$\ddot{r} = \frac{F}{m} - \zeta v \tag{2.10}$$

$$\dot{\zeta} = \frac{1}{Q}(T - T_0) \tag{2.11}$$

where T and T_0 are the temperature of the system and the heat bath respectively, and ζ is essentially a friction parameter. It can be seen that Nosé-Hoover method basically adds a frictional force ζv to the system to achieve the coupling to the heat bath. Its time derivative is proportional to the difference between current system temperature and the temperature of the heat bath.

Nosé-Hoover method generates the canonical ensemble of the microscopic states of the system in a continuous, deterministic way. And in the mean time, the time reversibility is followed. Due to its nice features, Nosé-Hoover method is widely employed in molecular dynamics simulations.

The algorithm introduced by Berendsen *et al.*[18] implements the thermostat/barostat in a simpler way. The coupling of a system to its environment is made explicit without any change of the Hamiltonian. Berendsen method requires that the temperature and pressure of the system obey two equations in below:

$$\frac{dT}{dt} = \frac{T - T_0}{\tau_T} \tag{2.12}$$

$$\frac{dP}{dt} = \frac{P - P_0}{\tau_P} \tag{2.13}$$

where T and P are the current temperature and pressure of the system, while T_0 and P_0 are those of the environment. The system temperature and pressure are changed by rescaling velocities and positions of all atoms directly.

Berendsen algorithm allows a desired coupling strength to be chosen by selecting appropriate values for τ_T and τ_P, which determine how frequently the positions and velocities of atoms are rescaled. Usually in the equilibration part of a simulation a short $\tau_T(\tau_P)$ is chosen for the system to reach equilibrium quickly, while in the production part a longer $\tau_T(\tau_P)$ is used to ensure that the perturbation to the dynamics of the system is negligible when its properties are evaluated.

2.4 Force field

2.4.1 Overview

A force field defines the interactions between particles. Depending on the level of abstraction, a particle can represent a real atom, a united atom or a group of atoms. Accordingly, the force field is referred to as an *all atom* force field, a *united atom* force field or a *coarse grained* force field respectively. An all atom force field defines the interactions between real atoms in the system. A united atom force field treats a carbon atom with all hydrogen atoms bonded to it as a single particle, *i.e.*, a united atom. It only defines the interactions between those united atoms. In a coarse grained force field, a large number of atoms are grouped together to be considered as a whole body, *e.g.*, the bead spring model. It leads to a highly simplified force field without chemical details. Only the interactions between those abstract "particles" are considered to determine the primary conformations of polymers.

Force fields can be derived by either the empirical method or the *ab initio* computation method. The empirical method fits the force fields to experiment data to determine their parameters. Sometimes data obtained from quantum chemistry computation of small molecules are also used in the fitting. Most popular force fields are obtained through this approach, such as CHARMM[19, 20, 21], AMBER[22, 23, 24, 25, 26], and MM2/MM3/MM4[27, 28, 29]. On the other hand, the *ab initio* computation method derives force fields by direct quantum chemistry computations. It is utilized in the derivations of MMFF94[30] and CFF[31] force fields. The *ab initio* computation method builds a force field on a consistent ground. It is not affected by errors or incompleteness of experimental data. Due to this advantage, the *ab initio* computation method is very promising in the future derivations of force fields.

A short introduction to force fields is given in the following two subsections. Further readings can be found in some review papers [32, 33, 34] and references cited

therein.

2.4.2 Implementation

A force field consists of different types of potentials. In general, they can be separated into two classes, bonded interactions and pair (non-bonded) interactions. Bonded interactions consists of *bond*, *angle*, *dihedral* and *improper* interactions, while pair interactions include *van de Waals* and *Coulomb* interactions. The total potential energy of a system can be written as:

$$U = U_{bonded} + U_{pair} \tag{2.14}$$

$$U_{bonded} = U_{bond} + U_{angle} + U_{dihedral} + U_{improper} \tag{2.15}$$

$$U_{pair} = U_{vandeWaals} + U_{Coulomb} \tag{2.16}$$

The potential functions in a force field can take on various forms. The simplest one is denoted as the class-I additive potential energy functions, which are supported by most force fields. They are defined as the following:

$$\begin{aligned}
U_{bond} &= \Sigma K_r (r - r_0)^2 \\
U_{angle} &= \Sigma K_\theta (\theta - \theta_0)^2 \\
U_{dihedral} &= \Sigma K_\phi (1 + cos(n\phi - \delta)) \\
U_{improper} &= \Sigma K_\chi (\chi - \chi_0)^2 \\
U_{vandeWaals} &= \Sigma 4\epsilon \left[\left(\frac{\sigma}{r}\right)^{12} - \left(\frac{\sigma}{r}\right)^{6} \right] \\
U_{Coulomb} &= \Sigma \frac{C q_i q_j}{\epsilon r}
\end{aligned}$$

The class-I functions contain only harmonic terms, which are adequate in the vicinities of the potential minima. But in order to study states far from equilibrium, a class-II

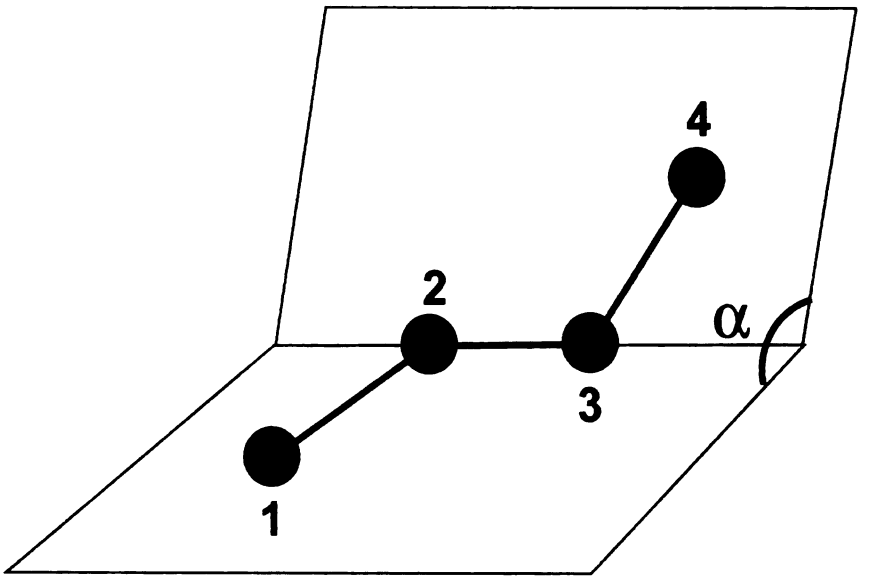

Figure 2.1: Dihedral angle α defined for the particle sequence 1-2-3-4.

force field is often needed since it contains higher order terms so that it can treat large deviations from equilibrium more accurately. A class-II force field is more elaborate and provides a better description of the potential energy[34].

Four types of bonded interaction are bond, angle, dihedral and improper interactions. Bond interaction defines the bond stretching motion between two chemically bonded atoms, and angle interaction defines the bond bending motion for three consecutively bonded atoms.

Dihedral interaction is described by dihedral potentials. A dihedral potential applies to two atoms that are separated by three consecutive bonds. In fig. 2.1, the dihedral angle for four consecutively bonded atoms 1,2,3 and 4 is defined, which is the angle α between plane 123 and 234. The corresponding class-I dihedral potential energy function is simply:

$$U_{Dihedral} = K(1 + cos3\phi) \tag{2.17}$$

It has three minima at 60°, 180° and 300° corresponding to one *trans* and two *gauche*

conformations, with the *trans* conformation at $\alpha = 180°$. This definition of a dihedral angle is used in the LAMMPS[35] software. Other molecular dynamics software may use a different definition, where the *trans* angle becomes 0° and the dihedral potential energy function form changes accordingly.

Improper interaction can maintain chemical stericity. Typically, an improper potential should be enforced about a sp^2 hybridized carbon atom to ensure its planarity. Furthermore, in united atom force fields, an improper potential can also be enforced about a sp^3 hybridized carbon atom that is bonded with one hydrogen atom and two other atoms. Because the hydrogen atom is not explicitly represented in united atom force fields, an improper potential is required to prevent those four atoms from collapsing into a plane.

The definition of an improper angle involves 4 atoms i, j, k and l. It is the angle between plane ijk and plane jkl. Usually atom i is the center atom, to which atoms j, k and l are bonded, while there are usually no bonds between atoms j, k and l. In fig. 2.2, the improper angle χ for four atoms labeled as 1,2,3 and 4 is illustrated. It is the angle between plane 123 and 234.

According to this definition, improper angles in some common cases can be found. For a sp^2 hybridized carbon atom, the improper angle is 0°. For a sp^3 hybridized carbon atom, the improper angle is approximately 35.26°.

Those bonded potentials have different strengths. Dihedral potentials are important in determining the conformation of a polymer. They are usually weak such that polymers can overcome dihedral potential barriers to arrive at other conformations easily. On the contrary, other bonded potentials, *i.e.*, bond, angle and improper potentials are typically strong. They are key to maintain the configurations of polymers but have little to do with their conformational changes.

There are two types of pair interaction, van de Waals and Coulomb interaction. Van de Waals interaction is commonly described by the Lennard-Jones 12-6 potential,

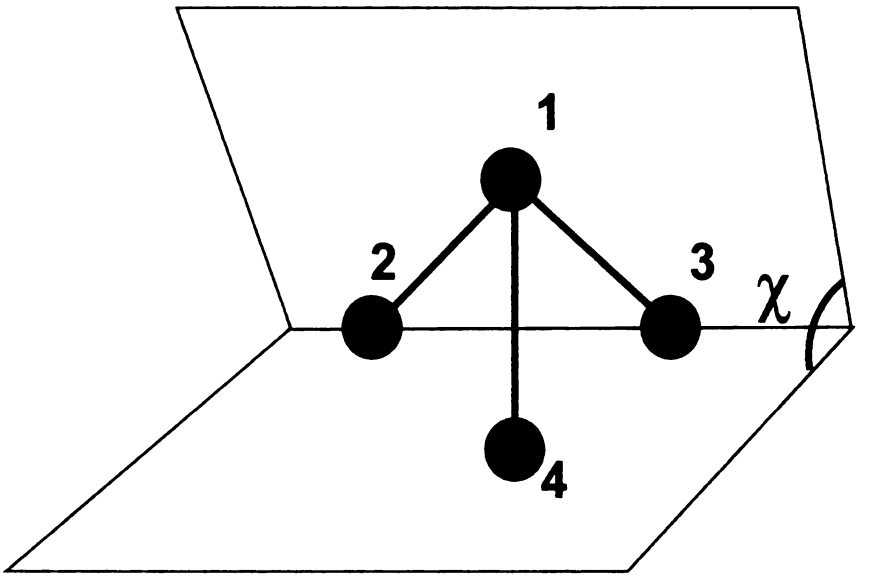

Figure 2.2: Improper angle χ defined for the particle sequence 1-2-3-4.

but subtle differences exist between different force fields. Firstly, the so called 1-2,1-3 and 1-4 pair interactions may be treated differently. Those pairs refer to two atoms that are separated by one, two and three bonds, respectively. The atoms separated by one bond have a direct bond potential between them, while atoms separated by two bonds usually have an angle potential defined. Bond potentials and angle potentials are much stronger than Lennard-Jones potentials, thus the 1-2 and 1-3 pair interactions are often excluded from the total potential energy. As for the 1-4 pair interaction, usually it is included but scaled by a factor γ ($\gamma < 1$), with γ assuming different values in different force fields.

The second difference resides in the mixing rules for the parameters of various Lennard-Jones potentials. The parameters in Lennard-Jones potentials are typically defined on a per-type basis, namely, each type of atom has the same parameter set. The mixing rules are employed to determine the parameters for the van de Waals interaction between two different types of atoms. A commonly used set of mixing

rules is:

$$\epsilon = \sqrt{\epsilon_1 \epsilon_2} \tag{2.18}$$

$$\sigma = (\sigma_1 + \sigma_2)/2 \tag{2.19}$$

Thirdly, the cut-off distances of Lennard-Jones potentials vary from one force field to another. To save computing time, all force fields exclude from the potential energy calculation those pairs of atoms that are too far apart, *i.e.*, beyond the cut-off distances. The cut-off distances are basically artificial choices, but they may be slightly correlated with the parameters of Lennard-Jones potentials because force fields are fit to experiment data as a whole.

The last term in the potential energy is the Coulomb interaction, which is important for charged polymers. Since this thesis does not involve charged polymers, Coulomb interaction is not to be discussed here. Details about it can be found in the aforementioned references.

2.4.3 Comparison

The designs of force fields are far from converging. They differ not only in the potential function forms and parameters, but also in the subtle issues such as the treatment of the 1-4 pair interaction[34]. However, the apparent discrepancy between them is largely due to the fact that each force field is designed for a particular type of systems, and is thereby only fit to the relevant experiment data. Basically, all force fields perform well in their own fields, as was verified by numerous simulation work in the past.

A force field should only be applied to what it is designed for. In general, the use of a force field for a system that it is not trained for can cause excessive errors, which is referred to as the "transferability" issue[10, 36]. It is thus important

to know the applicable area of each force field[34]. In short, CHARMM, AMBER, GROMACS[37, 38] are primarily designed for macromolecules in condensed phases or in solutions. However, since AMBER took into account the transferability issue when it was developed, it has a wide range of applications that include the gas phase. MM2/MM3/MM4, MMFF94, COMPASS[39, 40], CFF[31], Dreiding[41] and UFF[42] deal primarily with small molecules in the gas phase. Except for MMFF94 and COMPASS, all of them focus on the local structures of molecules. Since little experiment data of condensed phases were used to derive them, the nonbonded interactions are described with less accuracy.

In addition to the applicability, the performance of each force field is another factor to consider when choosing a force field. Various popular force fields have been assessed in some previous works [36, 43, 44, 45]. It turns out that all force fields have their own strengths and weaknesses. Among all the force fields, MMFF94 force field stands out, partly being attributed to its full quantum chemistry foundation. Furthermore, AMBER force field is good in finding the correct ground state structure but produces relatively large errors in the energy calculation. MM2/MM3/MM4 force fields are fit to most comprehensive experiment data, so that they can serve as a touchstone for evaluating other force fields. UFF and DREIDING force fields are two universal force fields. They are designed to work with all systems. However, since they are not optimized by experiment data, when studying a specific system, they yield less accurate results than a parametrized force field that is fit to the particular data.

Chapter 3

Intramolecular crosslinking of BCB-styrene copolymers

3.1 Introduction

The intramolecular crosslinking of a polymer is a process in which chemically active monomers react with one another to form additional covalent bonds. Active monomers are referred to as "crosslinkers" to distinguish them from monomers that can not crosslink. The intramolecular crosslinking process permanently alters the structure of a polymer. As the density of intramolecular crosslinks increases a polymer becomes more compact, and eventually transforms into a particle-like object. The feasibility of synthesizing nanoparticles by intramolecular crosslinking of polymers has been demonstrated in several recent experiments[4, 46, 47, 48], opening the door to fabrication of designed nanoparticles by crosslinking of carefully controlled unimolecular precursors.

Nanoparticles have abundant applications, such as bio-integration [49], polymer nano-composite materials[50], drug delivery[51], stabilization of polymer films[52, 53], facilitation of polymer processing[54, 55] and so on. Those applications typically rely

on nanoparticles with specific chemical and physical properties, which entails the ability to customize nanoparticles. Moreover, industrial production of nanoparticles requires an effective control over the manufacturing process. Therefore, a good understanding of the intramolecular crosslinking process is indispensable for its application to nanoparticle manufacturing.

The percentage of crosslinkers in a precursor polymer is a first factor that can be utilized to direct intramolecular crosslinking processes, as it is easily tuned yet has a direct impact on the structure of the polymer nanoparticle end product. A polymer with more crosslinkers is more rigid and usually, though not always, it is also more compact. The percentage of crosslinkers also affects other aspects of the crosslinking process including the reaction rate and and the fraction of crosslinkers that are never able to find a partner, i.e. the reaction completeness.

Intramolecular crosslinking of a polymer bears some resemblance to the folding of a protein as both of them involve the collapse of chains due to the interaction between their segments. In particular, the rigidity effect has been studied in protein folding processes[56]. One thus can expect that the rigidity of a polymer has a similar dependence on its intramolecular crosslinking density, as demonstrated here by the studies of the conditions under which the rigidity transition may occur due to irreversible crosslinking.

In this chapter, the intramolecular crosslinkings of BCB/styrene copolymers with a full range of crosslinker concentrations were studied by molecular dynamics simulations using the LAMMPS software[35]. It is organized as follows. In section 3.2, the experiment on the intramolecular crosslinking of BCB/styrene copolymers is introduced. In section 3.3 a united atom model of BCB/styrene copolymers is presented. And in section 3.4 the procedure of the crosslinking simulation is described in detail. In section 3.5 the crosslinking reaction rate of BCB/styrene copolymers is studied and the fraction of BCB monomers that are unable to crosslink is also found. In section

3.6 the rigidity effect on the intramolecular crosslinking of BCB/styrene copolymers is discussed. Simple theoretical models are provided to help understand the systematics of the data. In the last section, the simulation studies are summarized and the overall understanding derived from them is given.

3.2 Experiment

The simulation work on the intramolecular crosslinking of BCB/styrene copolymers was motivated by a recent experiment[4], where it was demonstrated that nanoparticles with radii of gyration ranging from 5nm to 20 nm can be manufactured by the intramolecular crosslinking of BCB/styrene copolymers. The experiment was performed in a good solvent so that the precursor polymers achieved expanded morphologies. A typical precursor polymer in the experiment had 1000 monomers, among which about 20% were BCB monomers. When heated to $250^{\circ}C$, the BCB monomers started reacting with one another to form crosslinks. The crosslinked polymers exhibited considerable contraction and formed nanoparticles eventually.

In practice, two different types of crosslinking can occur in a crosslinking experiment, namely intramolecular and intermolecular crosslinking. Intramolecular crosslinking connects monomers within a single polymer, while intermolecular crosslinking connects monomers from different polymers.

The key point of an intramolecular crosslinking experiment is to suppress unwanted intermolecular crosslinkings. Typically, this can be accomplished by reducing the concentration of polymers in the solution so that an ultra dilute solution is often required for the ideal effect. In the ultra dilute solution, it is very unlikely for two polymers to come close enough to form an intermolecular crosslink. However in the ultra dilute solution there is only a nominal amount of the reactants, *i.e.*, the precursor polymers, so this approach is not suitable for mass production.

The authors introduced another technique to address this difficulty, which was referred to as "slow addition" method[4]. In this procedure, the precursor polymers were added into the reaction container slowly to allow enough time for each individual polymer to crosslink by itself. At any time of the process, the concentration of the precursor polymers was low enough such that the intermolecular crosslinking was unlikely to occur. But the concentration of final polymeric nanoparticle product increased steadily as the experiment went on. Those nanoparticles could not react further with each other because nearly all their BCB monomers were already crosslinked during the addition.

Compared to the approach of crosslinking the polymer in an ultra dilute solution, the slow addition method has obvious advantages. It requires much less solvent yet yields highly concentrated products. However, its applicability depends on the number of crosslinkers that are left unreacted as unreacted monomers in a nanoparticle may lead to crosslinking with nanoparticles that are formed later. The concept can not work in the case where a considerable number of crosslinkers are unable to find a partner.

3.3 Model

The structure of a BCB/styrene copolymer is very similar to that of a polystyrene. The only difference between them is that the former contains BCB monomers. A BCB monomer, however, is basically a styrene bonded with two extra CH units. Hence, it is not difficult to derive an atomistic model for BCB/styrene copolymer based on one for polystyrene.

In the past, a plethora of simulation works have been done on polystyrene, where a variety of atomistic models were employed. In 1990's, Mondello *et al.*[57, 58, 59] applied a united atom model to simulate polystyrene. It is shown that the model

led to good agreements with X ray and Neutron diffraction data. Recent simulations of polystyrenes using this model also proved to be successful[60, 61, 62, 63]. As a comparison, their all-atom model surprisingly failed to yield a result of same accuracy. *TraPPE-UA* is another united atom force field that has been applied to the simulations of polystyrenes[64, 65]. It is relatively simple yet has been demonstrated to produce high quality results for some properties such as density, self diffusion *etc.* Boyd *et al.*developed an anisotropic united atom model [66, 67, 68], where they proposed that centers of united atoms should be shifted from carbon atoms towards hydrogen atoms. This modification was found to lead to better results for PVT simulations. Jorgensen *et al.*designed an all-atom model [69] which has been utilized in a number simulations of polystyrenes [70, 71]. It assigns partial charges to phenyl groups in order to reproduce their electric quadruple moments. The universal force field DREIDING [41] has also been used in the simulations of polystyrenes[72, 73]. Though it is not particularly optimized for macromolecules, it was found to produce results with a reasonable accuracy. In addition, some coarse grained models for polystyrene are also developed[65, 74]. They aim to generate facile representations of polystyrene as well as their mappings to atomistic models, in order to provide efficient approaches for the large scale simulations of polystyrenes.

Among all those models, the united atom model by Mondello *et al.*[57] was chosen for the crosslinking simulations of BCB/styrene copolymers in this chapter. This model treats a carbon atom with its bonded hydrogen atoms as a single particle, *i.e.*, a united atom. A widely used united atom force field[22] is incorporated in this model. Though the force field has been considerably updated in the past few decades[23, 24, 25, 26], the original version is still in use and is valid for molecular dynamics simulations in vacuum.

The crosslinking simulations in this chapter were also performed in vacuum. However, the experiment [4] was done in a good solvent with temperature $T = 523K$.

Consequently the precursor polymers assumed expanded coil morphologies. In order for polymers to achieve similar morphologies without solvent, a high temperature ($T = 900K$) was used in the crosslinking simulations. The temperature is located in the coil globule transition region for the atomistic model in vacuum. In reality polystyrene can not survive such a high temperature. But it is doable in the simulation and the temperature can compensate for the absence of a good solvent. In this sense, the temperature can be viewed as an effective temperature which incorporates the effects of both the solvent and the temperature. In an experiment, the morphologies of the precursor polymers can be adjusted by either the temperature or the solvent quality. Therefore, in a temperature-sensitive crosslinking experiment, a desired morphology can be achieved by choosing an appropriate solvent. For example, fig. 3.1 shows that a crosslinking experiment in the coil regime can be done above the reaction temperature threshold T_c by using good solvents.

The original united atom model was slightly modified to adapt to the simulation software LAMMPS[35]. Firstly, harmonic potentials were used to describe bond stretching interaction between united atoms, while in the original model the bond lengths were constrained by the SHAKE algorithm. The strengths of the potentials for bond stretching interaction were taken from experimental data, but they were reduced by a factor of 4 to increase the time step [68]. Secondly, the original model incorporated dihedral potentials between atoms of a phenyl in order to maintain its planar configuration. But in the crosslinking simulations a phenyl was constrained as a rigid body so that its six united atoms moved uniformly as a whole. The total force on a phenyl was calculated as the sum of all external forces on its six united atoms. This treatment of phenyls has two advantages. Not only can it maintain a strict planar configuration for a phenyl, it can also speed up the computer simulation because all the internal forces within a rigid body do not need to be considered. A similar rigid body constraint was also used for benzocyclobutenes in BCB monomers.

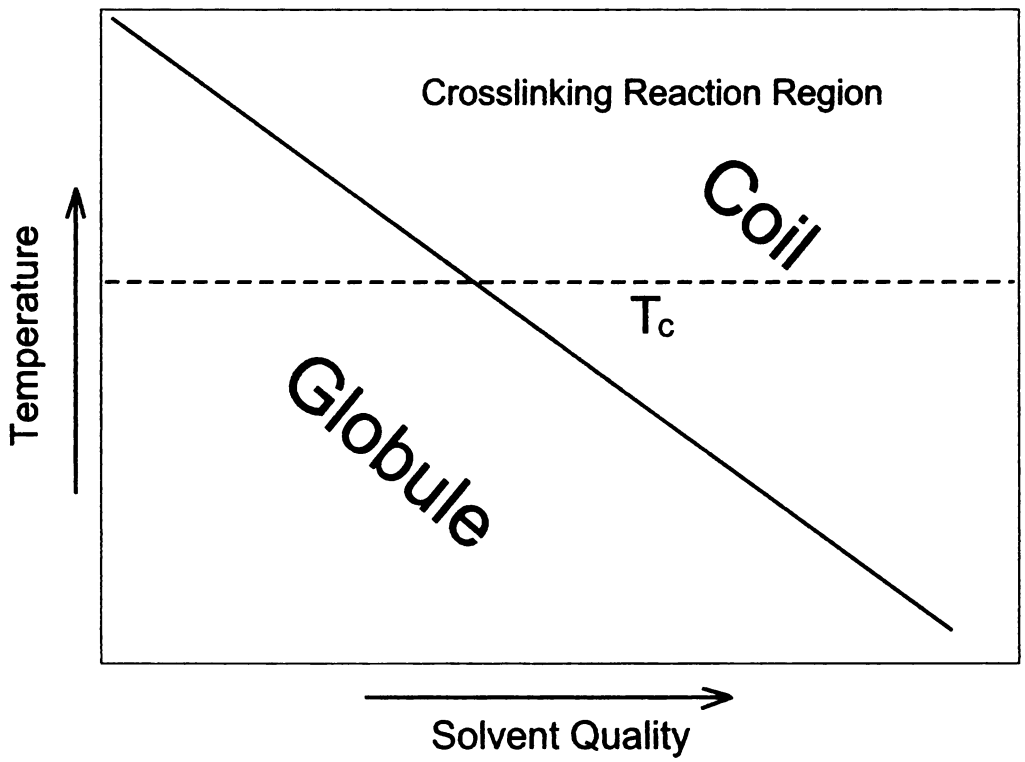

Figure 3.1: Crosslinking experiments in the coil regime can be done above T_c by using good solvents.

Each of them consisted of eight united atoms. Other details of the united atom model in this work were taken from the literature [57].

The force field in the crosslinking simulations took the following forms:

$$E_{LJ} = 4\epsilon \left[\left(\frac{\sigma}{r}\right)^{12} - \left(\frac{\sigma}{r}\right)^{6} \right]$$

$$E_{bond} = K_r(r - r_0)^2 + K(l - l_0)^2$$

$$E_{angle} = K_\theta(\theta - \theta_0)^2 + K_\alpha(\alpha - \alpha_0)^2$$

$$E_{dihedral} = K_\phi(1 + cos(3\phi)) + K_\psi(1 - cos(2\psi))$$

$$E_{improper} = K_\chi(\chi - \chi_0)^2 + K_\omega(\omega - \omega_0)^2$$

The parameters in the above equations are listed in table 3.1. Lennard-Jones interactions between united atoms separated by four or more bonds are considered in the potential energy calculation.

3.4 Simulation

The crosslinking simulations were carried out for BCB/styrene copolymers with 250, 500 and 750 monomers separately. Unlike the experiment where the concentration of BCB monomers was below 30%, the percentage of BCB monomers in the simulations was varied from 5% to 100% to investigate the full range of crosslinker concentrations. Ten samples were studied for each size and each crosslinker concentration and the results were averaged to get better estimates of properties.

The initial configuration for a BCB/styrene copolymer was generated in three steps. First, its backbone was created by a self avoiding walk (SAW) on a diamond lattice. Each site of the walk represented a CH_2 or a CH united atom alternatively. The diamond lattice automatically ensured that two neighboring bonds made an angle of 109.5°. In the second step, the side groups were attached to the CH united atoms.

Table 3.1: The parameters of the force field for the united atom model of a BCB/styrene copolymer. Energy is in kcal/mol, and distance is in Å

Lennard-Jones		
CH_2	$\epsilon = 0.12$	$\sigma = 3.85$
CH	$\epsilon = 0.09$	$\sigma = 3.7$
$C(ar)$, $C(ar)H$	$\epsilon = 0.12$	$\sigma = 3.7$
bond		
$C - C$	$K_r = 80$	$r_0 = 1.54$
$C(ar) - C$	$K_l = 80$	$l_0 = 1.50$
angle		
$C - C(ar) - C(ar)$	$K_\alpha = 70$	$\alpha_0 = 120°$
$C - C - C$	$K_\theta = 60$	$\theta_0 = 109.5°$
dihedral		
backbone	$K_\phi = 1.4$	
phenyl rotation	$K_\psi = 1.0$	
improper		
$C(ar)$	$K_\omega = 80$	$\omega_0 = 0$
C	$K_\chi = 50$	$\chi_0 = 35.26°$

There were two types of side groups with different populations, phenyls and BCBs and they were added in a totally random manner, with concentration x of BCB units. Each side group can be attached to any CH united atom and can be on either side of the backbone, so it essentially generated an atactic random copolymer. However, since it was possible that newly added side groups were too close to other particles of the polymer, a short preliminary NVT simulation was then run for the polymer to resolve any dangerous configurations. In this simulation a soft pair potential was temporarily imposed for all particles to push them apart. The preliminary NVT simulation lasted for only a few picoseconds and led to expanded morphologies for all polymer samples.

Simulation of intramolecular crosslinking of BCB/styrene copolymers began with the initial configurations generated as described above and consisted of three stages, equilibration, crosslinking and re-equilibration. In the equilibration stage, NVT simulations of all samples were run for 3.2 ns at 900K. In the subsequent crosslinking stage, the same NVT simulations were run, however they were paused every 0.8 picoseconds to check if the crosslinking criteria could be met. At each check, the distances between all pairs of BCB monomers were examined. in particular, the distances were measured from C_1/C_2 of one BCB monomer to C_3/C_4 of another BCB monomer, as shown in fig. 3.2. To establish a C_1 bond to C_3 and C_2 to C_4 their distances have to be less than $5\mathring{A}$, or approximately 1.3σ, where σ is the hard core radius of the Lennard-Jones interaction between two CH united atoms. This distance requirement is consistent with previous bulk crosslinking simulations[75]. The relative orientation of two BCB monomers was also checked, so that new chemical bonds were only formed when the four active carbon united atoms C_1, C_2, C_3, C_4 approached each other in a way that their orbital electron clouds overlapped significantly. To impose this condition four angles were examined as listed in table 3.2. All of these angles have equilibrium values of 109.5°, and in the crosslinking simulations their values have to be more than 90°

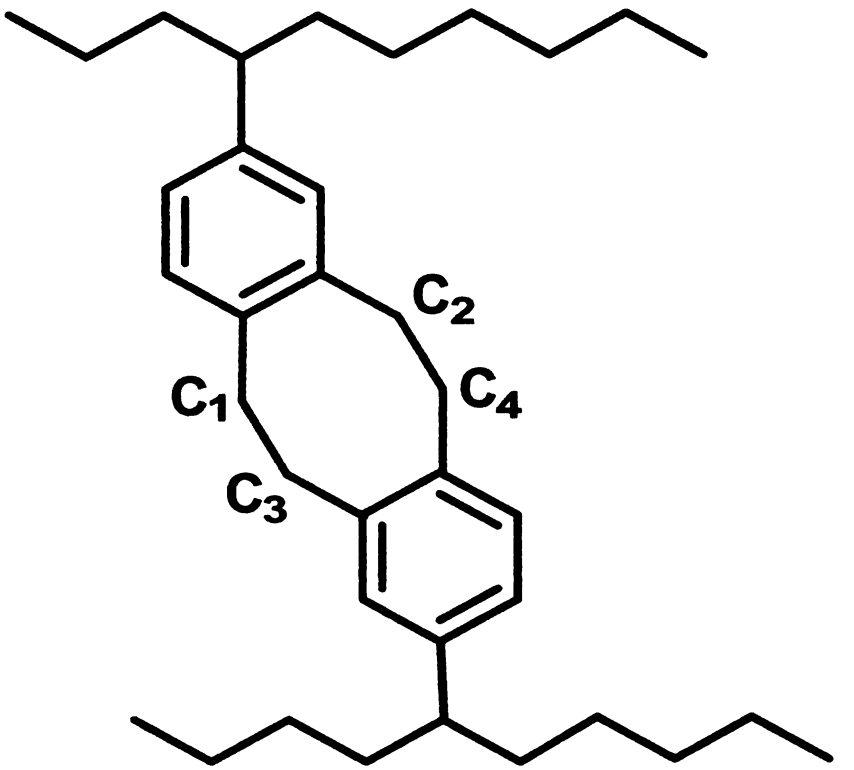

Figure 3.2: The crosslink between two BCB monomers.

Table 3.2: Table of bonded potentials in a crosslink

bond	$C_1 - C_3$	$C_2 - C_4$
angle	$C(ar) - C_1 - C_3$	$C_1 - C_3 - C(ar)$
	$C(ar) - C_2 - C_4$	$C_2 - C_4 - C(ar)$
dihedral	$C(ar) - C_1 - C_3 - C(ar)$	
	$C(ar) - C_2 - C_4 - C(ar)$	

and less than 130° in order for the crosslinking reaction to proceed.

As shown in fig. 3.2, the crosslink between two BCB monomers is a floppy eight-membered ring that introduces a number of extra bonded potentials to the model, which are listed in the table 3.2. In total two bond potentials, four angle potentials and two dihedral potentials are added for each new crosslink and its potential functions and parameters are the same as those of the backbone of a BCB/styrene copolymer.

The check for the reaction criteria was performed every 0.8 picoseconds in the crosslinking simulations. This interval was long enough to allow for the configuration

of a polymer to undergo a nontrivial change, yet it was short enough for the simulated crosslinking to be finished in a reasonable computing time. Once a pair of BCB monomers was found to meet the reaction criteria, the crosslink formed immediately between them. The crosslinking stage lasted until there were less than two BCB monomers left in a polymer or until 17 nanosecond of simulation time had elapsed, whichever occurred first.

Once the crosslinking ceased the last stage consisted of a re-equilibration process for another 3.2 ns. The crosslinked polymers were then analyzed.

3.5 Crosslinking reaction

The simulated reaction rate of the intramolecular crosslinking of a BCB/styrene copolymer is greatly restrained by both orientation and distance requirements for two BCB monomers. For instance, the simulation shows that it takes about 5 checks on average to form a crosslink in a polymer with 750 unlinked BCB monomers, which corresponds to a reaction rate at the picosecond time scale. Moreover, the reaction rate drops quickly as the number of unlinked BCB monomers decreases and is at the nanosecond scale when there are only tens of unlinked crosslinkers left.

Due to its slow kinetics, the simulation of the intramolecular crosslinking of a BCB/styrene polymer can not be completed in a practical computing time. A time limit of 17 nanosecond is thus set on the crosslinking simulations. It is found that a majority of crosslinkers are able to crosslink within this time period though a substantial number of them remain unlinked. In addition, there are no obvious signs that the crosslinking reactions are complete even though the reaction rates finally become extremely slow.

Theoretically it is interesting to know if all crosslinkers can be crosslinked, which also has significance to real applications. For example, unreacted crosslinkers can

function as docking points in drug delivery and they also affect the applicability of the slow addition method to synthesize the polymeric nanoparticles. Note that the number of unlinked crosslinkers was recorded at every check in the crosslinking process (see previous section), i.e. every 0.8 picoseconds. So the theoretical number of final unlinked crosslinkers can be obtained by extrapolation.

The crosslinking of two BCB monomers is an elementary reaction that is approximated by the law of mass reaction, namely the reaction rate is proportional to the product of concentrations of reactants. To leading order, it becomes

$$dx(t)/dt = -kx^2(t) \tag{3.1}$$

where $x(t)$ denotes the number of unreacted crosslinkers in a polymer at time t, and k is a rate constant. Note that in the equation above the number of reactants, *i.e.*, crosslinkers, is used instead of its concentration. As a consequence, the coefficient k should contain an additional factor of $1/V$ with V being the reaction volume. Since the intramolecular crosslinking occurs only in the vicinity of a polymer, the reaction volume is proportional to the size of the polymer. By multiplying by the number of monomers N, a normalized coefficient can be obtained which is $k^* = k \cdot N$. The solution to eq. 3.1 is :

$$x(t) = \frac{x(0)}{1 + At} \tag{3.2}$$

where $A = kx(0)$. This solution predicts that the number of free crosslinkers decays slowly with time and goes to zero at long times. However this simple model omits the influence of steric hindrance on the reaction rate. In particular if crosslinking produces a highly constrained or rigid nanoparticle it may be impossible for some crosslinkers to find a partner. As a result, there can be some free crosslinkers left unreacted even if the crosslinking runs for an infinitely long time.

To approximate the effect of the steric hindrance on crosslinking, eq. 3.1 is

generalized to:

$$x(t) = \frac{x(0)}{B + At} + x_\infty \tag{3.3}$$

where x_∞ is the number of crosslinkers that are left unreacted eventually. The unity in eq. 3.2 is replaced with a parameter B in order to maintain its validity when t goes to zero.

This equation provides an excellent representation of all of the simulation data that have been obtained, except at really low crosslinker concentrations where strong statistical variations render the fitting less reliable. Examples of fits to the data for three different crosslinker concentrations, 80%, 40% and 20% are presented in fig. 3.3. In these graphs all samples have 750 monomers.

From these fits, values for the parameters k^*, B and x_∞ can be found for all crosslinker concentrations but 5%, which has large variations. The normalized coefficient k^* is shown in fig. 3.4, demonstrating that k^* is approximately the same for all concentrations and all sizes. The parameters B and x_∞ are plotted in fig. 3.5 and fig. 3.6 respectively. The parameter B assumes values close to unity, which is reasonable. However the most interesting result is that x_∞ assumes larger values when the concentration of crosslinkers is above 60% and rises roughly linearly with crosslinker concentration beyond this point. In the next section this behavior is found to be related to a rigidity effect.

3.6 Rigidity effect

It is not surprising that higher levels of crosslinking yield more rigid nanoparticles. As noted in the previous section this can lead to some unpartnered BCB crosslinkers even at very long reaction times. The radius of gyration of the crosslinked nanoparticles has been studied and exhibits some rigidity effects in its behavior. Firstly, it is noticed that the radius of gyration of a crosslinked BCB/styrene copoly-

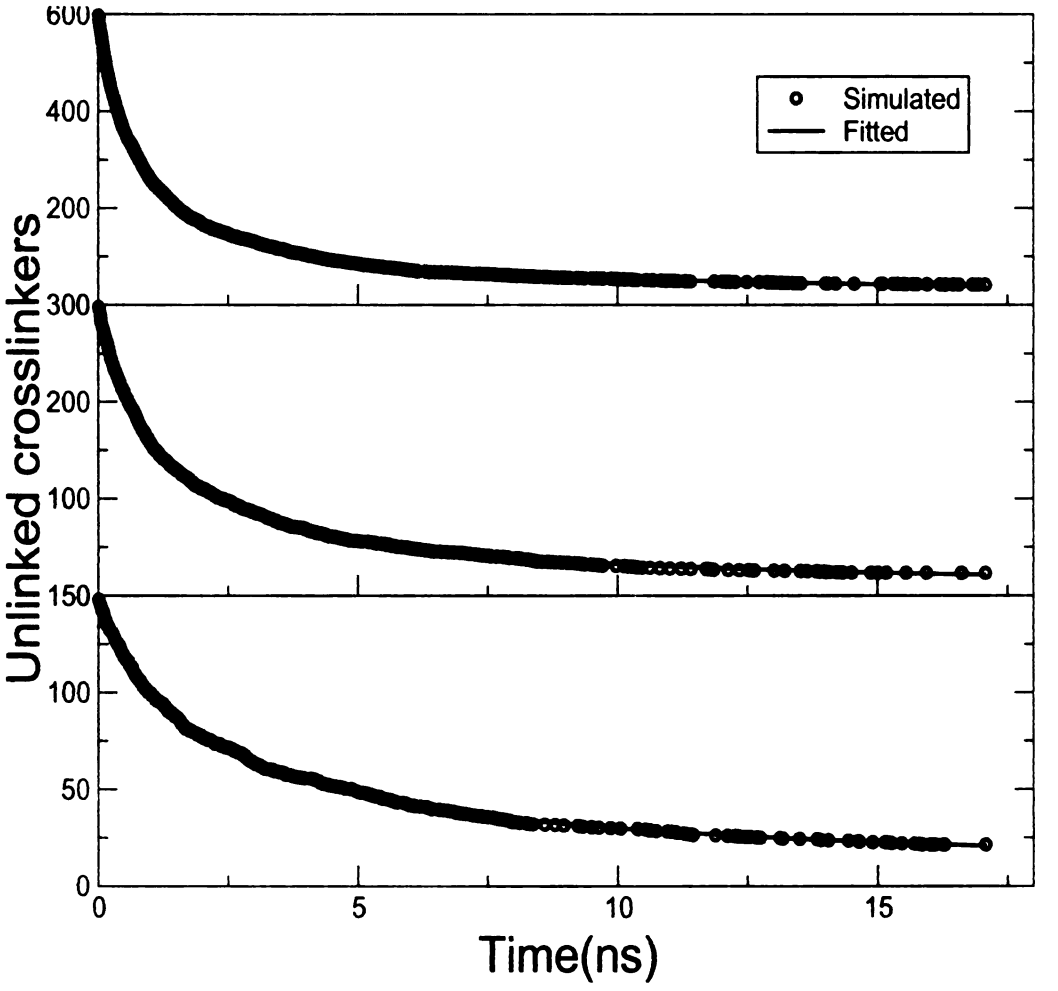

Figure 3.3: The number of unlinked crosslinkers for BCB/styrene copolymers with 750 monomers decreases as the crosslinking simulation proceeds. From the top down, the three panels are for 80%, 40% and 20% BCB monomers respectively.

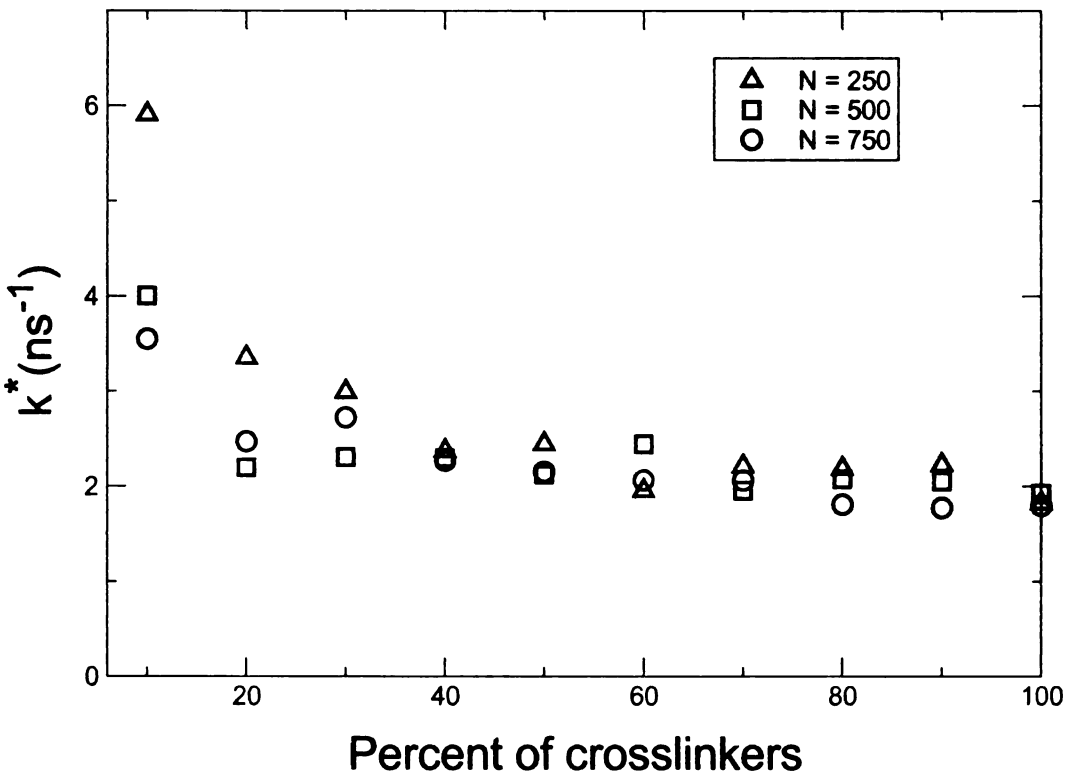

Figure 3.4: The parameter k^* from fitting to eq. 3.3.

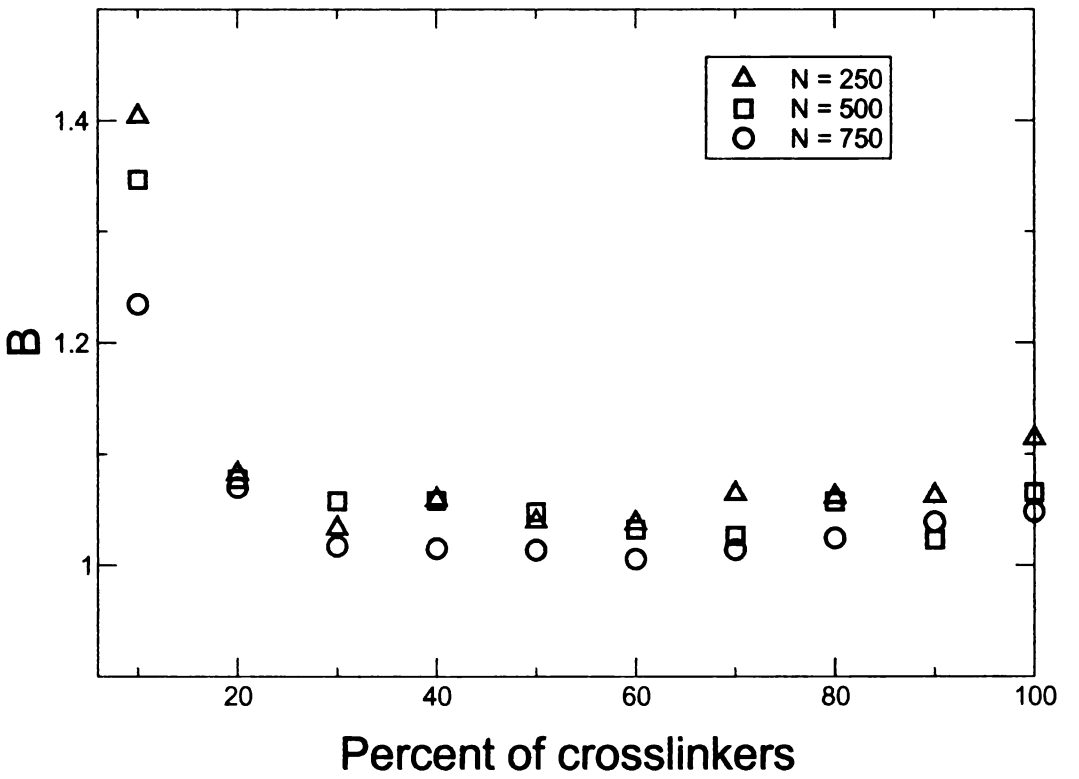

Figure 3.5: The parameter B from fitting to eq. 3.3.

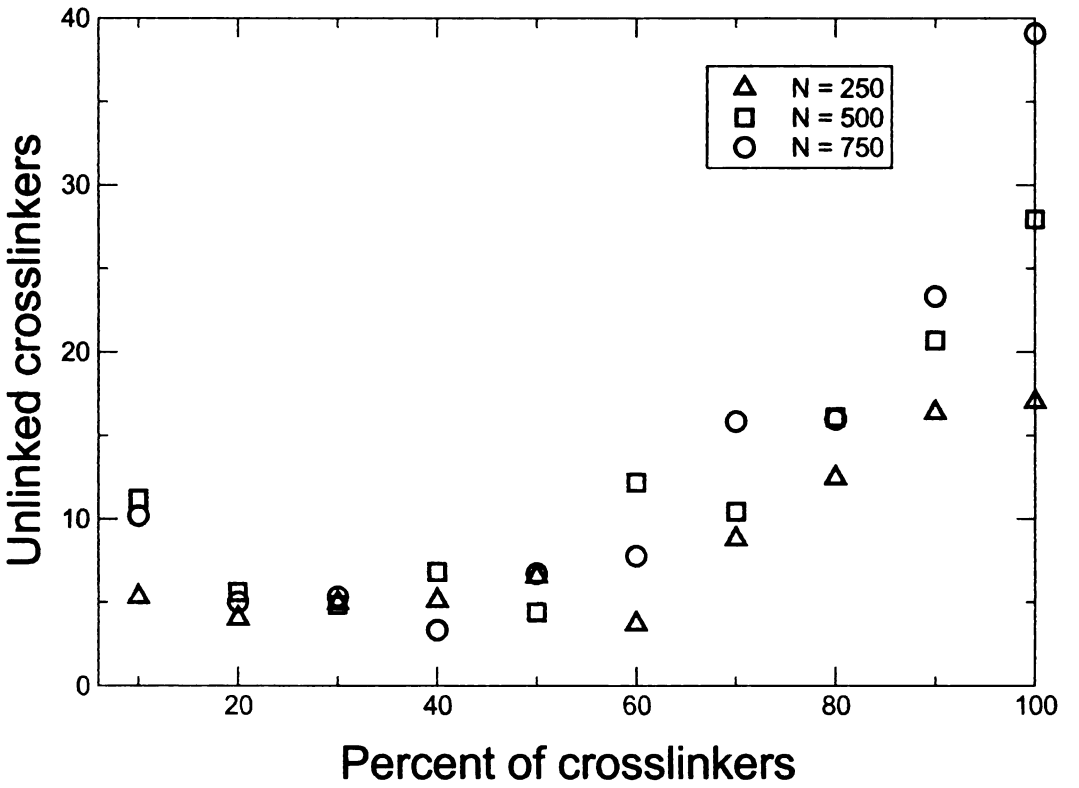

Figure 3.6: The parameter x_∞(unlinked crosslinkers) from fitting to eq. 3.3, showing a rigidity effect at around 60% BCB crosslinkers.

mer in the simulation is comparable to that in the experiment[4]. For instance, in the experiment a precursor polymer with molecular weight 11200 amu and 10% BCB monomers yields a nanoparticle with hydroradius $R_h = 6.2nm$ after crosslinking. This polymer has roughly 100 BCB monomers and 900 styrenes. In the simulations the largest samples have 750 monomers. With 10% BCB monomers, they form nanoparticles with average radius of gyration $R_g = 5.3nm$.

In fig. 3.7, the average radius of gyration found in simulations is plotted for BCB/styrene copolymers with three different sizes. It shows a decreasing trend with the increasing fraction of crosslinkers. However, when the BCB monomer concentration is above 60%, the R_g curves cease to show any decreases. This unusual behavior, as well as large numbers of unlinked crosslinkers observed before suggest that when the crosslinker concentration is above 60%, the nanoparticles are quite rigid.

In a previous work, the rigidity effect on the intramolecular crosslinking of polymers was studied using coarse grained models[76]. It was found that a rigidity transition occurred in some models with increasing crosslinker concentration. For example, the freely rotating chain model (FRC) exhibited a rigidity transition at 40% of crosslinkers. Above the rigidity transition, the R_g of crosslinked polymers showed little change with the crosslinker concentration, and the number of unlinked crosslinkers is higher. The Maxwell counting method[77] was employed to determine the rigidity transition threshold for the coarse grained models and a nice agreement with the simulation result was achieved.

To apply the Maxwell counting technique to BCB/styrene copolymers, both the chain stiffness and the crosslinker concentration need to be incorporated. Stiff polymers can be modeled as freely jointed chains in which each segment represents $m(m > 1)$ monomers. The segment length m is known as *Kuhn length*. Usually in the freely jointed chain (FJC) models, each segment contains only one bead which represents m monomers. But in order to describe the crosslinking, one bead should

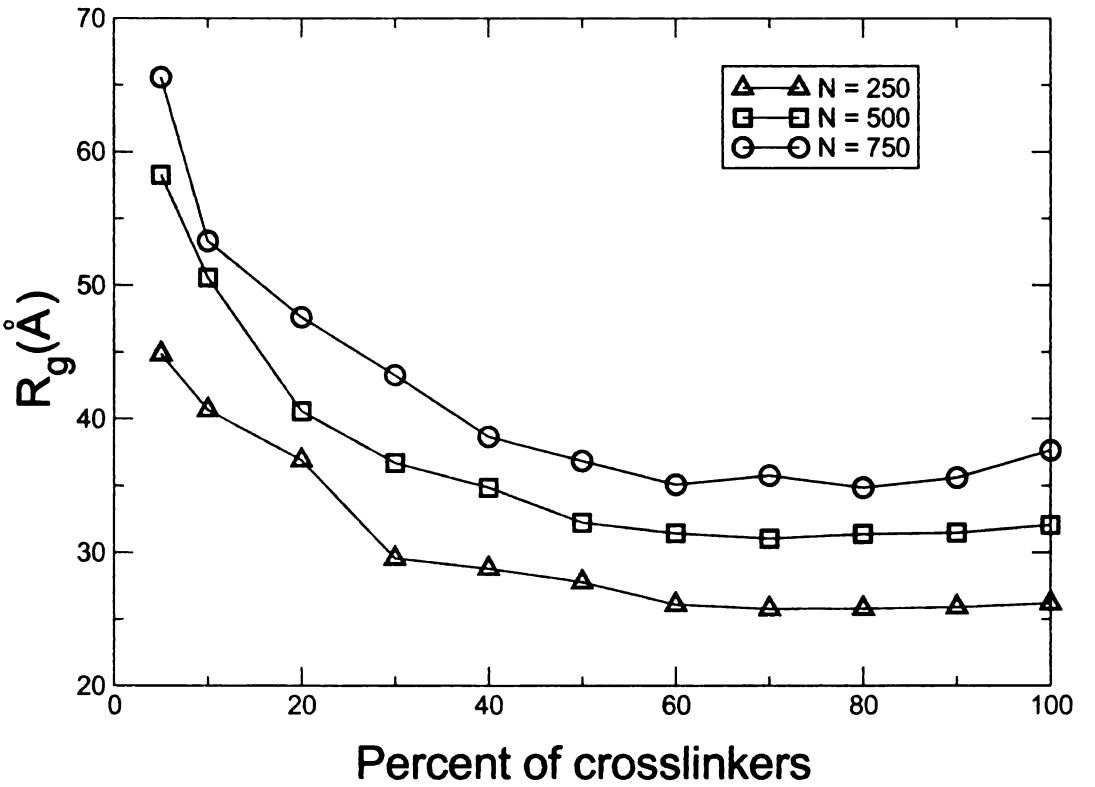

Figure 3.7: The radius of gyration of crosslinked BCB/styrene copolymers, showing a rigidity effect when the crosslinker concentration is above 60%.

represent a single monomer, be it a styrene or a BCB monomer. So one segment contains m beads in the new model for stiff polymers. They are distributed evenly along the whole segment, and are strictly aligned in a straight line all the time.

Before crosslinking, the number of degrees of freedom in the chain is $2N/m$ since the chain is equivalent to a simple FJC with N/m beads with two unconstrained degrees of freedom for each bead. The number of crosslinkers is xN where y is the crosslinker percentage. In the atomistic model, a crosslink brings about 7 additional constraints. However, the only effect of those 7 constraints on two monomers is to limit their distances. Therefore a crosslink adds only one effective constraint in the new coarse grained model. Based on the Maxwell counting, the number of floppy modes F of the model can be written as :

$$F(y) = 2\frac{N}{m} - \frac{xN}{2} \tag{3.4}$$

The rigidity transition should occur when F vanishes, yielding $x_c = 4/m$. Polystyrene has a Kuhn length $m = 7$ [5]. Thus the Maxwell counting estimate of the rigidity threshold gives $x_c = 4/7 \approx 57.14\%$.

On the other hand, based on the simulation data, the rigidity threshold for a crosslinked BCB/styrene copolymer is around $x = 60\%$ (see fig. 3.6 and 3.7), which is in good agreement with the Maxwell counting estimate, indicating that simple constraint counting ideas provide a good starting point for understanding rigidity effects in unimolecular crosslinking. It should be noted that the crosslinks are flexible in the sense that they can rotate somewhat, however they impose limits on the ability of the chain to fluctuate and in particular to extend. In technical terms they are closer to tensegrity constraints rather than pure rigid constraints.

3.7 Summary

A simulation study of intramolecular crosslinking of BCB/styrene copolymers is carried out using an atomistic model. In addition, freely jointed chain models were adopted for a rigidity analysis. Various factors that can affect the crosslinking and the size of the crosslinked end state were considered, including the concentration of crosslinkers, the ambient temperature, and the rigidity effect.

Simulations of the atomistic model of BCB/styrene copolymers show that over a wide regime, the crosslinking rate has a quadratic dependence on the number of free crosslinkers. However, steric hindrance plays an important role in the intramolecular crosslinking where it may prevent a finite fraction of crosslinkers from being crosslinked even at long times. An equation incorporating both the quadratic dependence and the steric hindrance provides a successful description of the crosslinking reaction.

A rigidity transition occurs in the intramolecular crosslinking of BCB/styrene copolymers when the BCB monomer concentration is above 60%. In this region, the number of unsatisfied crosslinkers goes up considerably. Moreover in this regime, R_g of the crosslinked copolymers exhibits little change with increasing number of crosslinks. Maxwell counting was applied to the FJC model of a BCB/styrene copolymer, and found the quantitative dependence of its rigidity threshold on its Kuhn length.

Chapter 4

Temperature series simulation of intramolecular crosslinking

4.1 Introduction

Polymers assume various morphologies under different environmental conditions, which can also play a role in the intramolecular crosslinking process. A single polymer can have two distinct morphologies, *i.e.*, that of a compact globule or of an expanded coil. It can transform from one state to the other on changing either the ambient temperature or the quality of the solvent. Intuitively, when a polymer is in the globule state, the crosslinks are more likely to form between well separated crosslinkers, resulting in a more compact nanoparticle. However, when the polymer is in the coil state the crosslinks tend to occur between neighboring crosslinkers so that a more loosely crosslinked nanoparticle is formed. This fact was briefly acknowledged in previous works[78, 79], however a systematic study of the effect of initial morphologies on intramolecular crosslinking of polymers is not available.

In this chapter, the FJC model is adopted to study the effect of initial morphologies on intramolecular crosslinking, by performing a temperature series of simulations.

The quality of the solvent can also induce a change in the morphology of the precursor polymer, so that the result of the temperature series simulation is also meaningful to the crosslinking experiments in various solvents at least to a first order approximation. The chapter is organized as follows. Firstly, the simulation procedure is described in section 4.2. Then in section 4.3, the contraction ratio of crosslinked polymers are calculated and are compared to a previous work[78]. In section 4.4 a variable *chemical distance density* is introduced to account for the contraction ratio. It is applied to the simulation results of both freely jointed chains and BCB/styrene copolymers. The last section provides a summary of this chapter.

4.2 Simulation

A temperature series of simulations of intramolecular crosslinking were performed on a number of FJC samples using the standard interaction potential,

$$E = \sum_{pairs} 4\epsilon \left[\left(\frac{\sigma}{r}\right)^{12} - \left(\frac{\sigma}{r}\right)^{6} \right] + \sum_{bonds} K(r - r_0)^2 \tag{4.1}$$

where $\epsilon = 1$, $\sigma = 1$, $K = 1000$ and $r_0 = 1$. All of them are in the Lennard-Jones units.

Each FJC sample comprised of 500 beads, of which a fraction, x, were crosslinkers while the remainder were normal beads. Aside from its ability to crosslink, a crosslinker is the same as a normal bead, with both interacting through the force field defined in eq. 4.1. Four different concentrations of crosslinkers were studied, namely 5%, 20%, 50% and 100%.

The temperatures being considered were in the range from $T = 0.5$ to $T = 11$ (also in the Lennard-Jones units), which covered all the temperature points of interest for the FJC model of the simulations. In particular, more points were taken between $T = 3$ and $T = 5$, which lie in the coil globule transition regime and in total 44

temperature points were considered. At each temperature point, 50 FJC samples were studied for each of the four crosslinker concentrations mentioned previously, so the total number of FJC samples was $50 \times 4 \times 44 = 8800$.

The temperature series of simulations started from high temperatures to low temperatures. Firstly, the initial configurations of the FJC samples at the highest temperature $T = 11$ were generated. The chains were constructed by self avoiding walks on a FCC lattice with lattice constant $a = 1$ and the crosslinkers were randomly distributed over the chains. The initial configurations for the samples at lower temperatures were simply copied from the equilibrated samples at the next higher temperature, *e.g.*, the initial configurations of the FJC samples at $T = 10$ were obtained from the FJC samples after equilibration at $T = 11$. Note that in this copy procedure the locations of crosslinkers were rearranged randomly, so that the initial configuration for a sample at lower temperature had a new monomer sequence.

A molecular dynamics simulation of intramolecular crosslinking of the FJC model was similar to that of the atomistic model of BCB/styrene copolymers. It also consisted of equilibration, crosslinking and re-equilibration stages. In the equilibration process, NVT simulations were run for 10000 Lennard-Jones time units. Subsequently, the crosslinking process was carried out, which consisted of 9000 Lennard-Jones time units, with the interval between checks for the crosslinking criteria being 10 Lennard-Jones time units. Unlike the atomistic model, there was no need to check for the orientation between two crosslinkers. The only condition to be met for two crosslinkers to react was that their distance should be less than 1.3σ. The final re-equilibration process consisted of NVT simulations for 10000 Lennard-Jones time units.

4.3 Contraction of polymers

The contraction factor is defined as the ratio of the radius of gyration of a polymer after crosslinking to that of it before crosslinking, denoted as $R_g(x)$ and $R_g(0)$ respectively:

$$\gamma = \frac{R_g(x)}{R_g(0)} \tag{4.2}$$

In fig. 4.1 the contraction factor against temperature is presented and it shows that the largest contraction occurs between $T = 3.5$ and $T = 4$, which is just above the coil globule transition region and close to the Θ temperature of the FJC model.

Intramolecular crosslinking results in a wide structural diversity in the final products because there are numerous ways to crosslink a chain with 500 beads. This is reflected in the wide range of values of R_g especially at higher temperatures, leading to relatively big fluctuations in γ above the Θ temperature. But at lower temperatures, the starting state is already a globule so the effect of intramolecular crosslinking on the size of the polymer decreases and the fluctuation in γ is smaller.

The contraction of an intramolecularly crosslinked polymer is naturally related to its density of crosslinks, and since all crosslinkers can find a partner in the FJC model, which has no rigidity effect, the density of crosslinks in the final state is directly proportional to its crosslinker concentration. As evident in fig. 4.1, larger concentrations of crosslinkers lead to greater contractions in the final states of the FJC samples at all temperatures. This is counter to the effects observed in systems exhibiting a rigidity effect where the contraction of polymers ceases to increase beyond the rigidity threshold.

An early work [78] studied the quantitative relation between R_g and the density of crosslinks, in cases where the precursor polymers were made completely of crosslinkers, i.e. $x = 1$. Using the ideal chain model they argued that for a chain with N monomers and m crosslinks, the ensemble average of its contraction can be

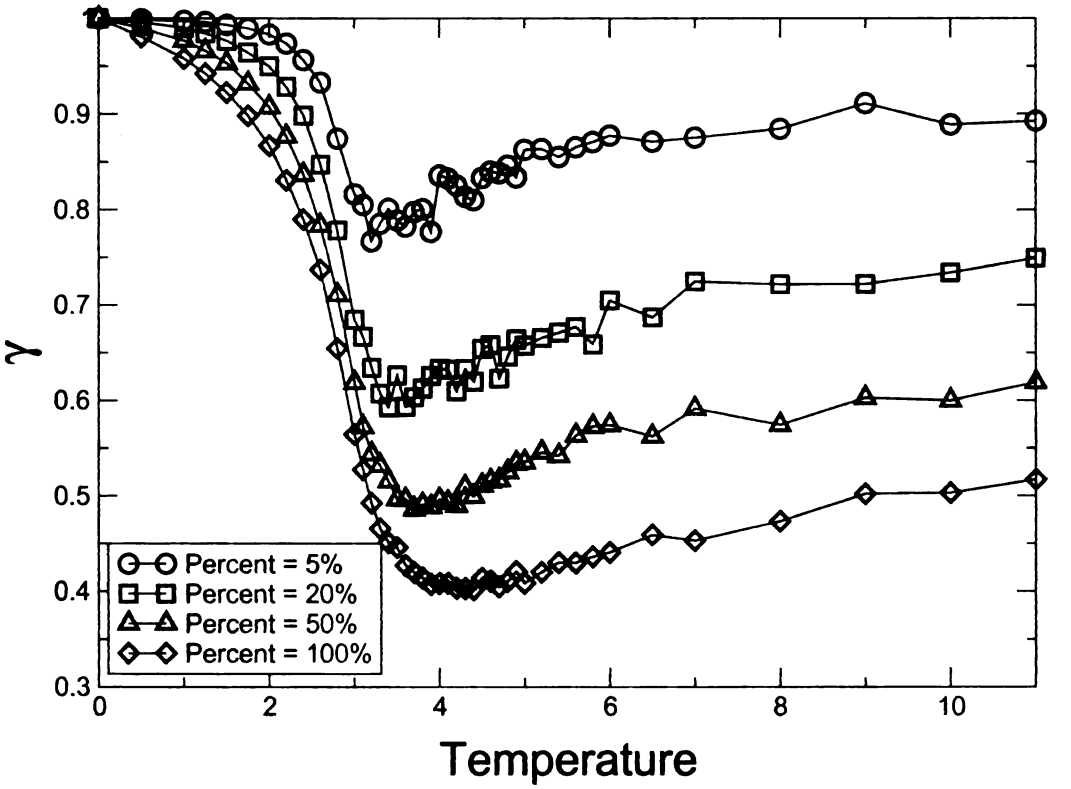

Figure 4.1: The average contraction ratio γ, namely the ratio of the radius of gyration of the polymer after and before crosslinking, as a function of the crosslinking temperature. The four curves correspond to four different concentrations of crosslinkers.

described by

$$\langle g(N,m)\rangle = 1 - \beta\rho^{1/2} \tag{4.3}$$

where $g = R_g^2(x)/R_g^2(0)$, and $\rho = m/N$. This prediction was compared to experiments where the crosslinking reaction could be turned off before it was complete, enabling access to the full range of values of crosslink density. The density of crosslinks ρ can then assume any value from 0 for a chain with no crosslinks to 0.5 for a fully crosslinked chain. The theory agreed well with their experiments. However, the authors pointed out that their theory can not be applied to the intramolecular crosslinking of polymers with only a fraction of randomly distributed crosslinkers. The fundamental reason, they argued, is that the density of crosslinks by itself is insufficient to describe the crosslinks, and instead the distribution of crosslinking rings is the key. The radius of gyration of a crosslinked polymer depends on detailed information about all crosslinking rings, particularly their number and their sizes. The more rings there are or the larger each individual ring is, the greater the contraction of the polymer is. The density of crosslinks, however, only accounts for the number of crosslinking rings but not their sizes. It suffices in the case of crosslinking a fully crosslinkable polymer because the size distribution of its rings can be evaluated[78]. But in the case where the chains are made of randomly distributed crosslinkers, the crosslinking rings with various sizes can arise and are distributed in a totally random way. Therefore, even if two crosslinked polymers have the same crosslinker concentrations, they can have drastically different R_g due to differences in their crosslinking rings.

The FJC samples in this simulation work consisted of randomly distributed crosslinkers. In order to compare the simulation result of the contraction ratio to the theoretical work, the data was fitted to a generalized form of eq. 4.3, namely:

$$\gamma^2 = 1 - \beta\rho^e \tag{4.4}$$

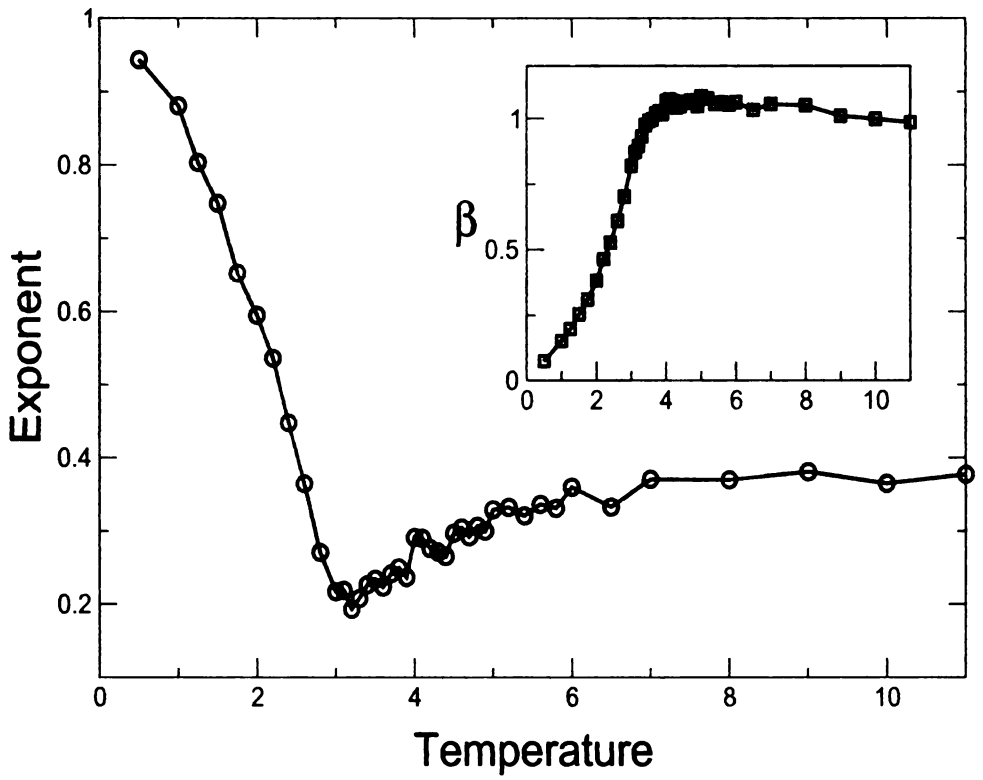

Figure 4.2: The simulation data for the contraction ratio $\gamma = R_g(x)/R_g(0)$ are fitted to the expression $\gamma^2 = 1 - \beta\rho^e$, yielding values for the prefactor β and the exponent e.

The fitting results are presented in fig. 4.2. The theoretical prediction based on the ideal chain model is $\beta = 0.75$, $e = 0.5$ and applies to the theta point that occurs at a temperature of approximately $T = 3.5$ for the FJC model in this chapter. It can be seen that the exponent found by the fitting is considerably smaller than 0.5 though the prefactor is close to that predicted by the theory, implying a stronger contraction effect than predicted by the ideal model. This is most likely due to the fact that the precursor chains are more expanded than ideal chains because of hard core repulsion effects. The non-monotonic behavior in the exponent reflects the non-monotonic temperature dependence of the contraction ratio (see fig. 4.1) and is due to a subtle interplay between the dimension of the precursor chain and the number of large rings that are produced by crosslinking.

4.4 Chemical distance density

To further quantify the effect of the sizes of crosslinking rings on the structure of a crosslinked polymer, the "chemical distance" was introduced as the number of monomers (along the backbone) that separate two crosslinked monomers. And the chemical distance density is defined as:

$$\rho_d = \frac{\sum_{i=1}^{m} d_i}{N} \tag{4.5}$$

where d_i denotes the chemical distance of the ith crosslink and N is the total number of monomers in the polymer. The summation runs over all the crosslinks. Chemical distance density indicates the overall effect of the crosslinking rings, incorporating both their number and their sizes. It can serve as a useful measure of the structure of an intramolecularly crosslinked polymer. The largest value of ρ_d is of the order of the number of monomers N. For example, when every monomer i ($1 \leq i \leq N/2$) is connected to a monomer $N/2 + i$, yielding a chemical distance of $N/2$, the

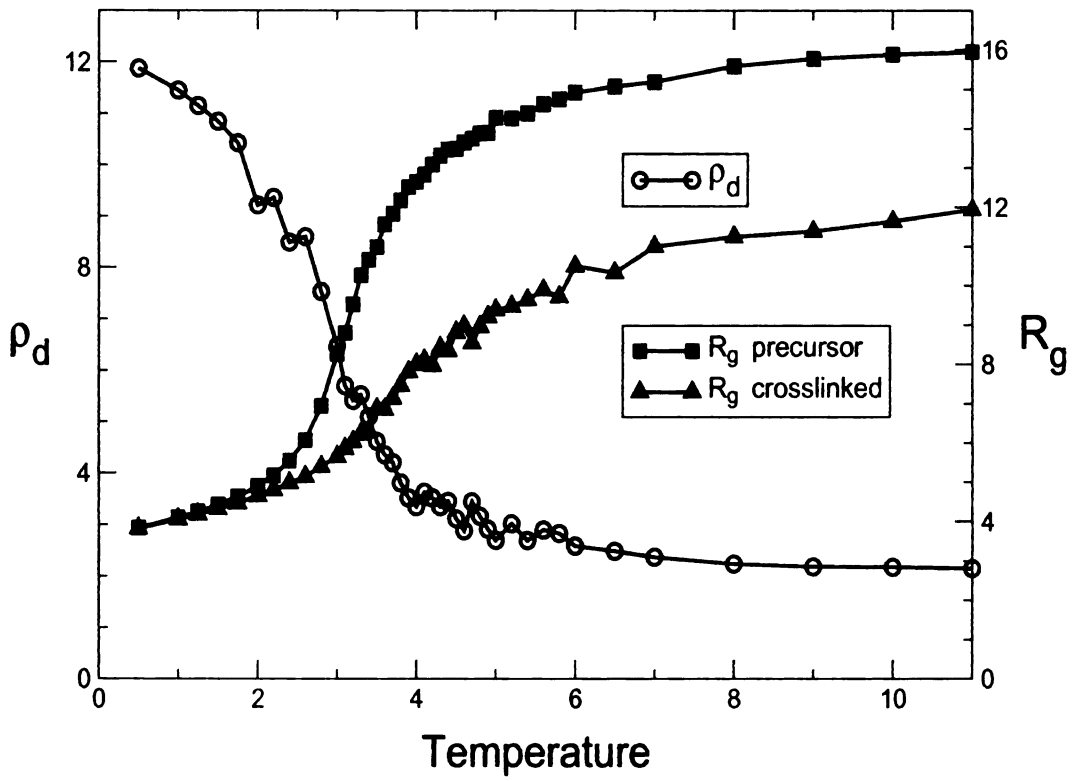

Figure 4.3: The chemical distance density ρ_d and radius of gyration R_g are plotted for different temperatures. This data is for FJC samples with $N = 500$ and $x = 0.2$.

chemical distance density of the crosslinked polymer acquires a value of $N/4$. It is also convenient to extend the definition of the chemical distance to a linear polymer, where each pair of connected monomers contributes a chemical distance of unity, and its chemical distance density is also approximately unity.

The data of fig. 4.3 shows that the chemical distance density has a clear temperature dependence, assuming large values in the globule region and becoming quite small in the coil region. In particular, there is a sharp decline of chemical distance density at the coil globule transition regime.

To find a quantitative relation between the chemical distance density and the radius of gyration, the simulation data at each temperature point are examined separately. By doing so the temperature effect on the radius of gyration can be excluded from the analysis. At each temperature point there are four different crosslinker

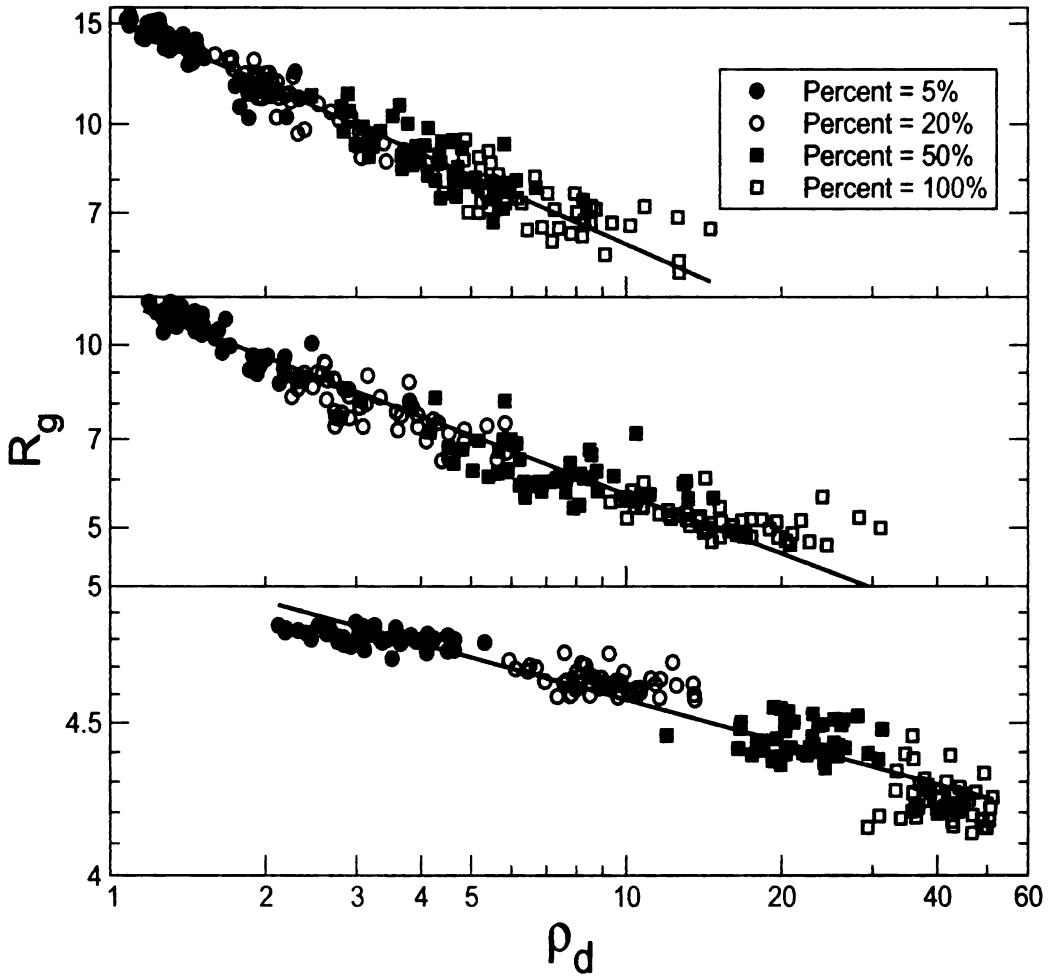

Figure 4.4: Eq. 4.6 is fitted to the simulation data for FJC samples at different temperatures. Starting from the top the data is for crosslinking temperatures $T = 8, 4$ and 2 respectively.

concentrations, and 50 samples for each concentration. This yields 200 data points for R_g and chemical distance density. Based on analysis of this data, a power law dependence is found for R_g on chemical distance density (see fig. 4.4):

$$R_g = R_g(0)(1 + \rho_d)^g \tag{4.6}$$

Unity is added to ρ_d in the equation above to recover the correct limit for precursor chains. The fitting parameters in eq. 4.6 are the exponent g and $R_g(0)$. Note that $R_g(0)$ is the radius of gyration of a polymer before crosslinking. The fitting results

are presented in fig. 4.4, where the fits and the data are compared at T=2.4, and 8, providing an overview of the whole temperature range. Overall eq. 4.6 turns out to be a reasonably good fit to the simulation data, though some deviations can be seen for large chemical distance densities and low temperatures. A large chemical distance density implies that there are complicated interpenetrating ring structures in the intramolecularly crosslinked polymer, while at low temperatures the crosslinking is a less important factor as the precursor polymers take on compact morphologies already.

A series of values for $R_g(0)$ and for g at each temperature are then obtained from the fitting procedure, As shown in fig. 4.5, $R_g(0)$ obtained from the fitting procedure agrees well with that found directly from simulations. The exponent g in eq. 4.6 is plotted in fig. 4.6. It changes smoothly from the lowest temperature (T=0.5) to the highest temperature (T=11), where g is approximately -0.4. Note that though g is temperature dependent, it is not dependent on the crosslinking fraction (see fig. 4.4).

It is also tested whether the power law relation of eq. 4.6 applies to the intramolecularly crosslinked BCB/styrene copolymers using data generated in chapter 3, where the simulations were performed for samples with 250, 500 and 750 monomers. For each size, 11 concentrations from 5% to 100% were studied with 10 samples each, so that in total there were 110 samples for each size. Eq. 4.6 was then used to fit the data as presented in fig. 4.7. It can be seen that the fitting yields good agreements except for a few data points with large chemical distance densities.

To compare the FJC results with those for the BCB/styrene copolymer it is noticed firstly that one FJC bead represents about 7 BCB/styrene monomers[5]. A 500-bead FJC sample in the temperature series of simulations thus approximates a BCB/styrene copolymer with 3500 monomers. Secondly, the crosslinking simulations of the atomistic model were performed at $T = 900K$, which was near the coil globule

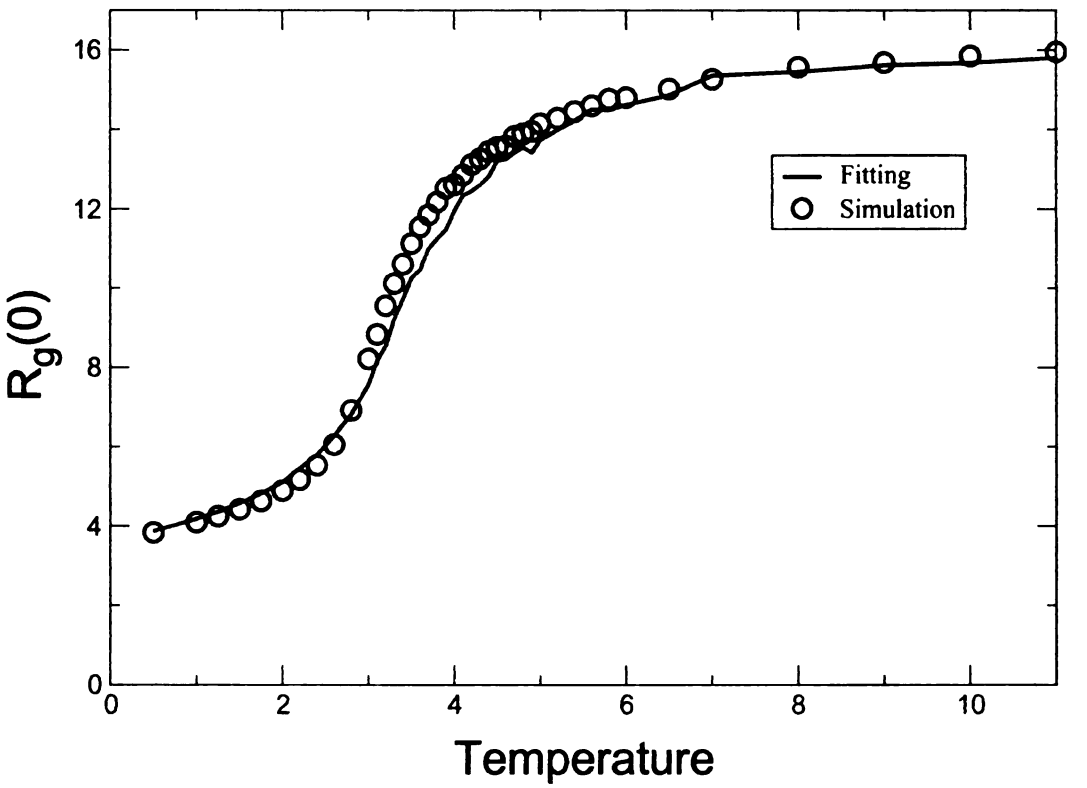

Figure 4.5: The radius of gyration before crosslinking found from fittings of crosslinked FJC samples to eq. 4.6 is compared to the simulation data, showing a good agreement.

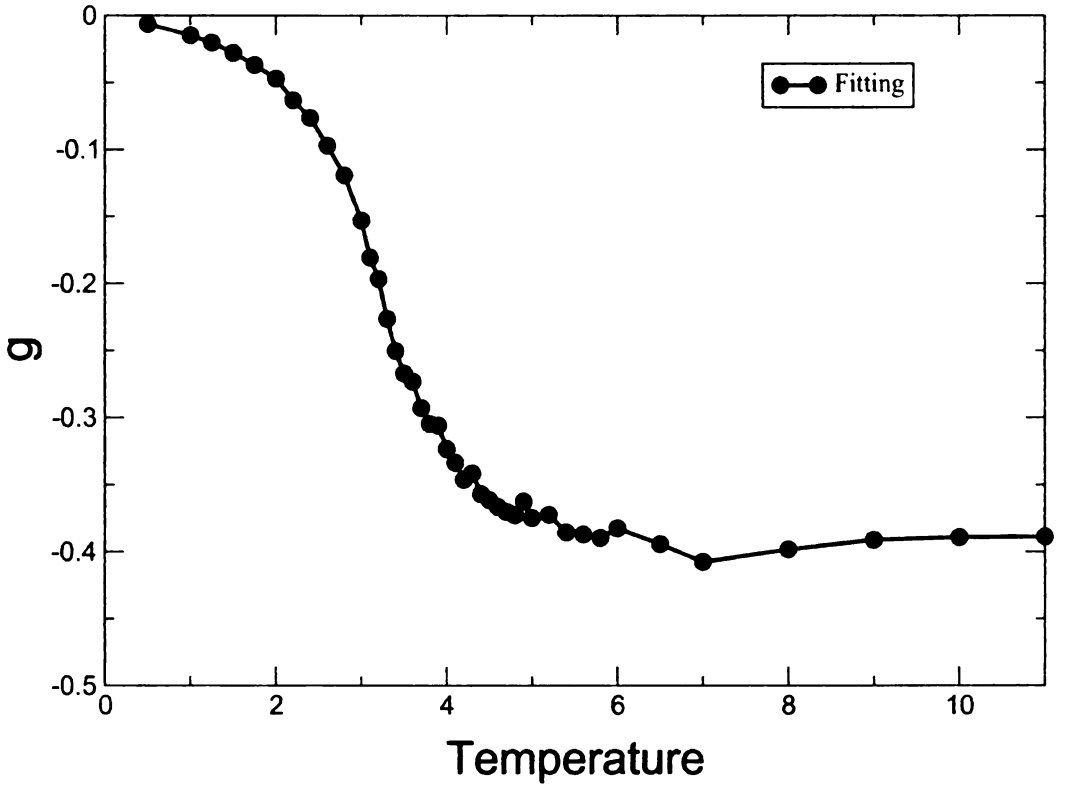

Figure 4.6: The exponent g in eq. 4.6 for the FJC model is obtained from fittings at all temperatures. Note that the exponent is independent of the crosslink density.

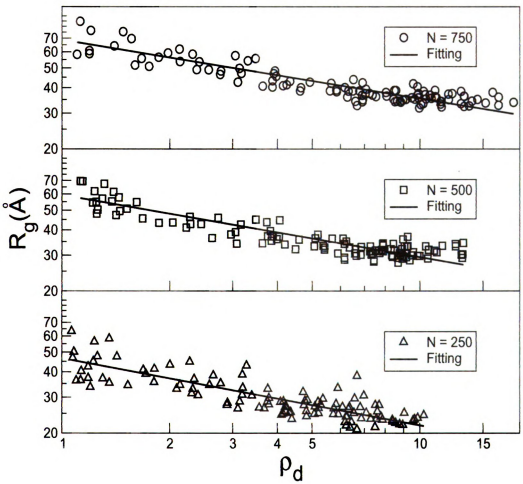

Figure 4.7: The radius of gyration as a function of chemical distance density for intramolecularly crosslinked BCB/styrene copolymers is plotted. From the top down, the three panels are for samples with 750, 500, 250 monomers respectively. In each panel, the data (open symbol) and the fit to eq. 4.6 (solid line) are shown.

transition temperature for the atomistic model in vacuum, and corresponded to a Lennard-Jones temperature between $T = 3$ and $T = 4$ for the FJC model, namely its coil globule transition regime. The exponent g for the FJC model ranges from -0.25 to -0.35 in this regime. Data extracted from simulations of the atomistic BCB/styrene model lead to values of g of -0.33, -0.31, -0.29, for $N = 250, 500, 750$ monomers respectively, which are consistent with each other and also with the results of the FJC model.

4.5 Summary

Freely jointed chain models were adopted for a temperature series of simulations of intramolecular crosslinking. It is showed that the morphologies of the precursor polymers greatly affect intramolecular crosslinking. The change of the morphology of a polymer can be induced by the ambient temperature or by the solvent quality, providing experimental controls of intramolecular crosslinking. The key qualitative effect is that crosslinking of polymers in the globule state yields tightly interconnected particles, while crosslinking of polymers in the coil state leads to relatively loose particles.

The chemical distance density was introduced as a useful measure of the internal structure of a crosslinked polymer. It provides a better account of the contraction of a crosslinked polymer than the density of crosslinks, particularly for a polymer with randomly distributed crosslinkers. A systematic simulation using FJC samples shows that there exists a power law relation between R_g and chemical distance density. The exponent of the power law relation is determined for a series of temperatures by fitting, and approaches -0.4 in the high temperature limit. A power law relation between R_g and chemical distance density is also found for the atomistic model of BCB/styrene copolymers. In the coil globule transition regime of this model and of

the FJC model, the exponent g is found to be approximately -0.3.

Chapter 5

Rigidity effect in the crosslinking of polymers

5.1 Introduction

Polymers are made of a large number of repeating chemical units, namely monomers, connected by covalent bonds. The covalent bonds have fixed bond lengths and bond angles such that the bond stretching and bending motions in polymers are strongly inhibited, however the bond rotations are still allowed. In a long polymer, the bond-rotational degrees of freedom lead to plenty of floppy modes, which makes it highly flexible.

Intramolecular crosslinking connects different monomers of a polymer together by forming extra covalent bonds between them. Due to those extra constraints the floppy modes of the polymer are reduced. As the crosslink density increases, it may happen that at a certain threshold the number of floppy modes in the polymer vanishes, resulting in a rigidity effect. Previously the same rigidity effect as a result of the loss of floppy modes has been studied in other fields, such as network glasses[80, 81] and protein foldings[77, 56]. Network glasses are made of elements with different valence.

When the concentrations of high valence elements in a network glass system increase, more covalent bonds come into being that render it to be rigid. In the folding of a protein, the changes of environmental conditions, such as the temperature or the solvent, induce the formation of non-covalent bonds and consequently the reduction of floppy modes, and result in a rigidity effect. The study of the rigidity effect in the intramolecular crosslinking process is important to the understanding of the rigidity effect in general. Moreover, intramolecular crosslinking has been utilized to manufacture nanoparticles[4], where the rigidity effect has been shown to play an important role [76]. Therefore the study of the rigidity effect in the intramolecular crosslinking process also has practical meanings to the nanoparticle manufacturing.

The methods to intramolecularly crosslink a polymer can vary greatly, as was demonstrated by multiple crosslinking experiments on polystyrenes in the past. In the early 1970's, Allen *et al.* [82] did an experiment to intramolecularly crosslink chloromethylated polystyrene chains with hexamethylene diisocyanate molecules. The crosslink units in this experiment are basically aliphatic chains made of more than ten carbon atoms. Since their conformations can change very easily, the crosslinks are highly floppy. In a recent experiment by Harth *et al.* [4], the precursor polymers are prepared by substituting benzocyclobutene(BCB) for styrene in polystyrenes, and the crosslinking units are eight-membered rings, each connecting two BCB monomers. An eight-membered ring is less floppy than an aliphatic chain. But it is still able to change among multiple conformations and is relatively floppy. Martin *et al.*[78] and Antonietti *et al.*[79] did their crosslinking experiments on polystyrenes using Friedel-Crafts with p-bis(chloromethyl) benzene. The crosslink units are intermediate phenyls which connect phenyls of two styrenes together via two carbon atoms. Because the phenyl rotations in polystyrenes are greatly hindered[83, 84], one can deduce that the rotations of intermediate phenyls are also considerably hindered. Thus its conformational change is the most difficult one among all three types of crosslinks. Those

experiments show that there are a wide variety of crosslinking protocols available, with different levels of rigidities.

Another technical difference among those experiments was discussed in the literature [78], where the authors argued that there were two different types of crosslinking schemes. The first one was adopted in experiments done by Allen *et al.* and Harth *et al.*, where polystyrenes were pretreated so that they contained randomly distributed crosslinkers. Since the locations of crosslinkers on the precursor chains spread apart, this type of crosslinking led to the formations of large rings such that polymers contracted considerably after crosslinking. The second one was employed in the experiments done by Martin *et al.* and Antonietti *et al.*, where crosslinks were made via intermediate chemical units. Therefore all styrenes in the precursor chains were potential crosslinkers. This type of crosslinking favored the formations of small rings and led to a less significant contraction. The authors referred to the crosslinking with preset crosslinkers as "random" crosslinking, and the other as"ring-weighted" crosslinking.

A random network has a continuous rigidity transition, while a protein with its highly ordered structure behaves more like an organized network and consequently exhibits a discontinuous rigidity transition[56]. It is possible that these two types of crosslinks have different rigidity behaviors as well. The random crosslinking of a polymer with preset crosslinkers can be compared to the folding of a protein so that the rigidity effect may emerge in a discontinuous manner, while the ring-weighted crosslinking leads to a rigidity effect which may occur continuously.

5.2 The freely rotating chain model

Freely Rotating Chain (FRC) model is a simple model that incorporates both bond stretching and bond bending constraints. Bonds in this model can rotate about

their connecting bonds in much the same way as in a real polymer. Therefore it is suitable for the simulation study of the rigidity effect in the intramolecular crosslinkings of polymers.

The freely rotating bead-spring chain model adopted in this simulation work has harmonic bond stretching and bond bending potentials. It enforces the Lennard-Jones 12-6 potential between beads that are separated by at least 3 bonds. The force field of this FRC model is:

$$E = K_b(r - r_0)^2 + 4\epsilon\left[\left(\frac{\sigma}{r}\right)^{12} - \left(\frac{\sigma}{r}\right)^{6}\right] + K_\theta(\theta - \theta_0)^2 \tag{5.1}$$

Variables are in the Lennard-Jones units where both σ and ϵ are set to unity. The bond stretching and bond bending potentials are significantly stronger than Lennard-Jones potentials, with $K_b = 1000$, $r_0 = 1.0$ and $K_\theta = 500$, $\theta_0 = 1.91 = 109.47°$.

A FRC sample in the crosslinking simulations contains 1000 beads, where a certain fraction of beads are randomly selected to be crosslinker beads and the rest are normal beads. A crosslinker can form exactly one crosslink with another one of its type, and is identical to a normal bead otherwise. The initial configuration of a FRC sample is generated by a self avoiding walk on a FCC lattice with lattice constant $a = 1$. After a NVT simulation of 2 million time steps (each time step consisting of 0.005 Lennard-Jones time unit) to reach equilibrium, the FRC sample undergoes another NVT simulation to crosslink. This simulation pauses every 500 time steps to check all pairs of unlinked crosslinkers to add new crosslinks. If one pair is within a distance of 1.3σ[75], a crosslink between them will be added immediately. If there are multiple such pairs, the one with the smallest distance should be chosen. So the reaction rate is limited to be no more than one per 500 steps. It ensures the crosslinking occurs in a controlled manner and also prevents the polymer from overheating. The crosslinking process has a maximum of 2 million steps. If less than 2 crosslinkers are left, the

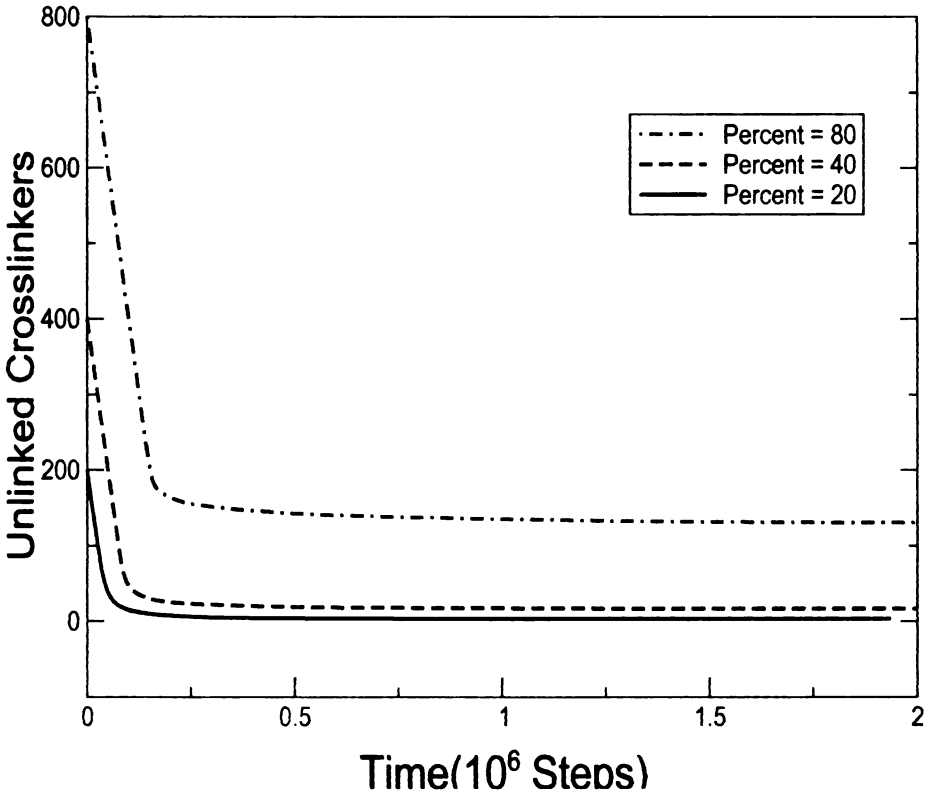

Figure 5.1: The number of unlinked crosslinkers in the FRC model as a function of the simulation time. It shows that the crosslinking reaction goes very fast in the beginning, while it basically stops after about a quarter of a million steps.

crosslinking process is terminated earlier to save the computing time. As an example, fig. 5.1 shows the number of unlinked crosslinkers as a function of the simulation time steps for three concentrations, 20%, 40% and 80%. One can see that the number of unlinked crosslinkers drops quickly in the crosslinking process. After about a quarter of a million steps it becomes almost constant, indicating that the crosslinking process is basically complete. After the crosslinking process, another NVT simulation of 2 million steps is run for the crosslinked polymers to reach equilibrium again.

The simulations on the FRC model were run for the full range of the crosslinker concentrations from 5% to 100%. For each concentration 50 samples were studied. The temperature of the simulation was set to $T = 3.5$, which was right above the coil globule transition of the FRC model. All simulations in this work were carried out

using the LAMMPS software[35].

A crosslink can be associated with various bond stretching and bond bending constraints, as shown by the experiments on the intramolecular crosslinkings of polystyrenes. But for simplicity this simulation work only employed two types of crosslinks, one with angle constraint and the other without. This treatment is similar to that in the rigidity study of protein folding[56]. Protein folding is primarily driven by effective hydrophobic bonds and hydrogen bonds, where an effective hydrophobic bond introduces one distance constraint, while a hydrogen bond produces one distance and four angle constraints. In the crosslinking simulations in this chapter, these two types of crosslinks were applied to the same model under the same conditions. By comparing the polymers crosslinked in these two different ways, the rigidity threshold as well as the rigidity effect can be reliably identified.

In theory, the rigidity threshold in the intramolecular crosslinking process can be determined by the Maxwell constraint counting method, which was proved to be successful by the rigidity study of protein folding[56]. It was also employed before for the intramolecular crosslinking of FRC model with angle constraints and found that the rigidity threshold was about 40%[76]. At this crosslinker concentration, its mean coordination is $2/5 \times 3 + 3/5 \times 2 = 2.4$, which agrees well with the rigidity results of network glasses[77] and protein folding[56]. Certainly the Maxwell constraint counting method can be applied to the FRC model crosslinked without angle constraints as well. In this case a crosslink brings about only one new constraint. A FRC sample with N beads initially has N degrees of freedom. Let x denotes the crosslinker concentration. The equation becomes $N - xN/2 = 0$ for the floppy modes to vanish. It has no solution for $x \leq 1$ which implies that no rigidity effect can exists in this case.

The crosslinking simulations of the FRC model yield nice agreement with the theoretical analysis. Fig. 5.2 shows the linked percent of crosslinkers for these two

types of crosslinks. While the curve for the crosslinking without angle constraints stays high for the full range of crosslinker concentrations, the one with angle constraints exhibits a large decline when the crosslinker concentration goes above 40%, as is predicted by the Maxwell constraint counting method.

R_g is another important measure of crosslinked polymers. It is plotted for both cases in fig. 5.3, showing that two R_g curves split at the crosslinker concentration of 40%. The one crosslinked without angle constraints continues decreasing as the crosslinker concentration grows, while the other one stays flat thereafter due to the rigidity effect. Besides, R_g of the rigid one has a larger variation due to the lack of relaxation in a rigid polymer.

5.3 The stiff chain model

The FRC model allows a bond to rotate freely with respect to one of its neighboring bonds. It does not apply to stiff polymers where the bond rotations are significantly hindered. Thus, a different model is required to study the rigidity effect in the intramolecular crosslinking of stiff polymers.

A stiff polymer can be modeled as a Freely Jointed Chain (FJC)[5]. Normally in the FJC model each segment contains only one bead which represents a number of monomers, known as Kuhn length. However, in order to simulate the crosslinking, every monomer, either a crosslinker or a normal one, has to be explicitly represented in the model. So a stiff chain model based on the FJC model is arrived, where each segment contains more than one bead while each bead represents only one monomer. Beads of a single segment are evenly distributed over it, and angle potentials with equilibrium of 180° are enforced everywhere of the chain except for the joints of its segments. Thus all segments maintain linear configurations and can bend freely with respect to each other. Once again two types of crosslinks were employed for the

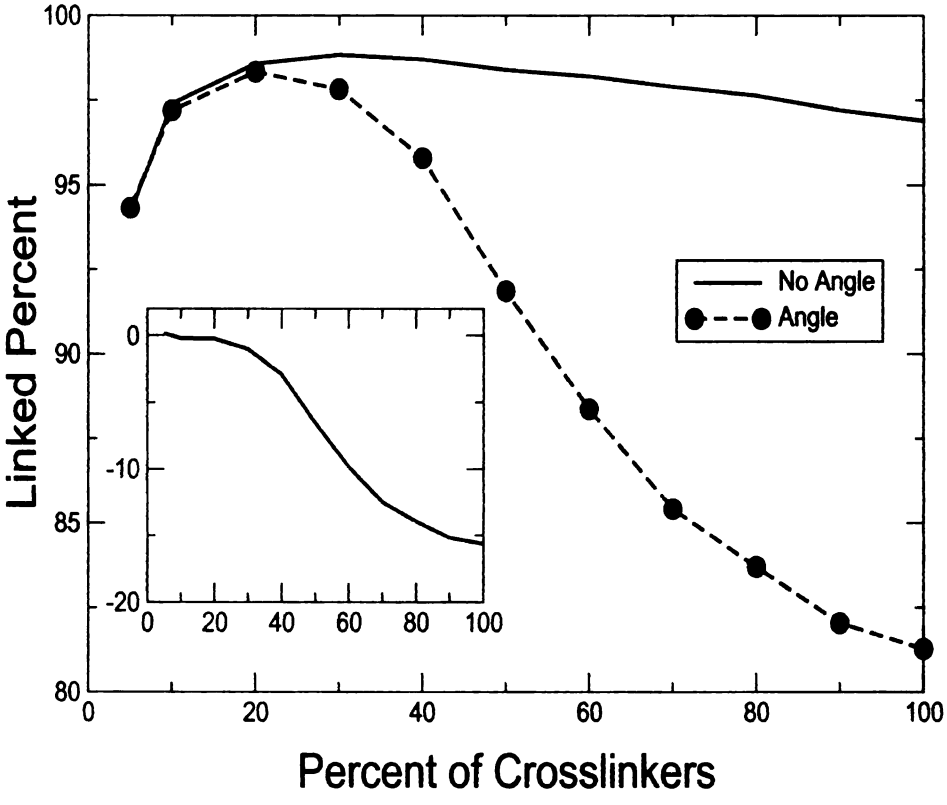

Figure 5.2: The percent of crosslinkers in FJC samples that can find their partners to react. For the crosslinking with angle constraints, a considerable decrease can be observed when the crosslinker concentration is above 40%, which agrees with the estimate of the Maxwell constraint counting that 40% is the rigidity threshold for this model. On the contrary, for the other crosslinking the linked percent changes little when the crosslinker concentration grows, while the Maxwell counting also predicts no rigidity effect for this model. The inset shows the difference between two crosslinking curves.

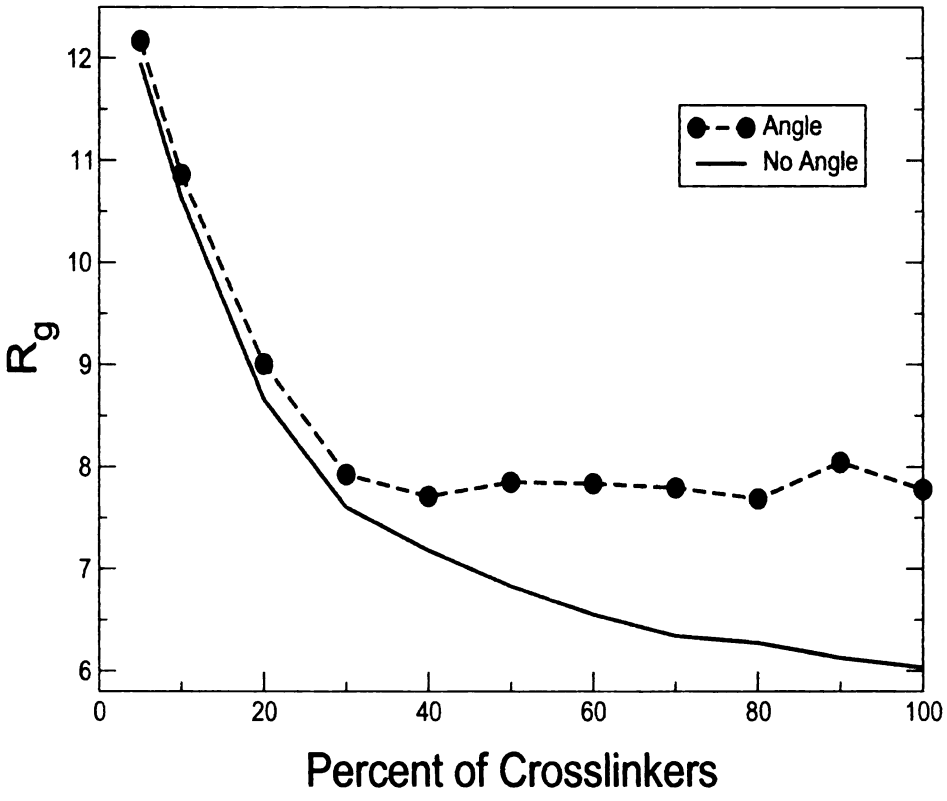

Figure 5.3: R_g of FRC samples crosslinked with angle constraints shows an abrupt change at the crosslinker concentration of 40%. Below this threshold, R_g decreases greatly with the increasing of crosslinks. But above the threshold, it is almost flat. On the contrary, R_g of FRC samples crosslinked without angle constraints lacks a rigidity effect, and decreases over the full range of crosslinker concentrations.

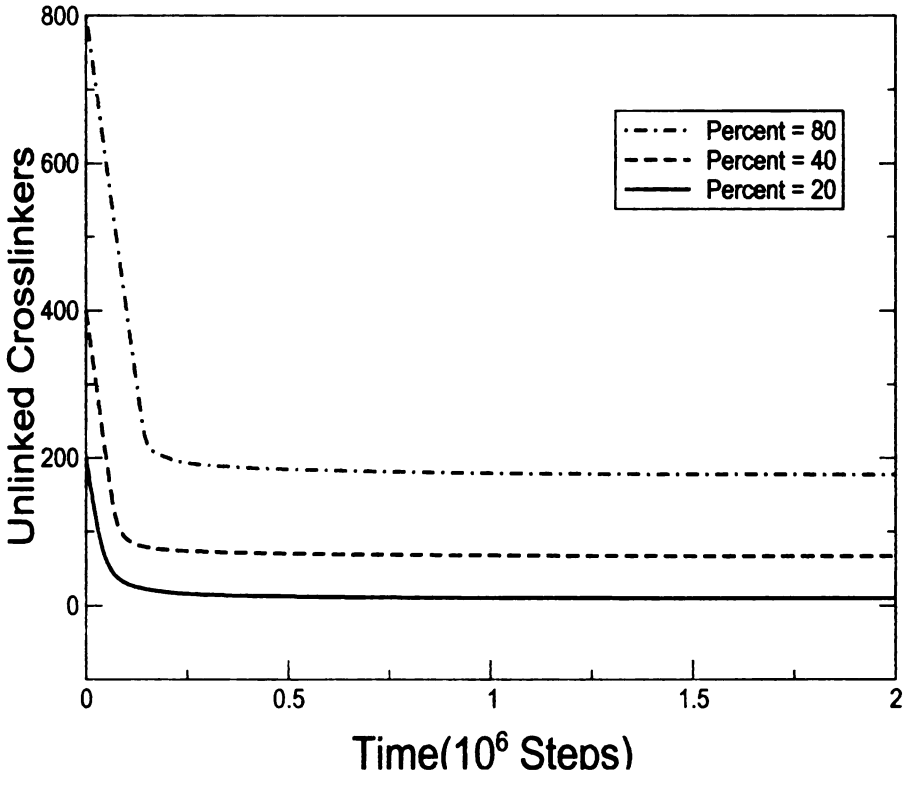

Figure 5.4: The crosslinking reaction rate for a stiff chain with 1000 beads and a segment length $m = 4$ indicates that the reaction saturates after a quarter of a million steps.

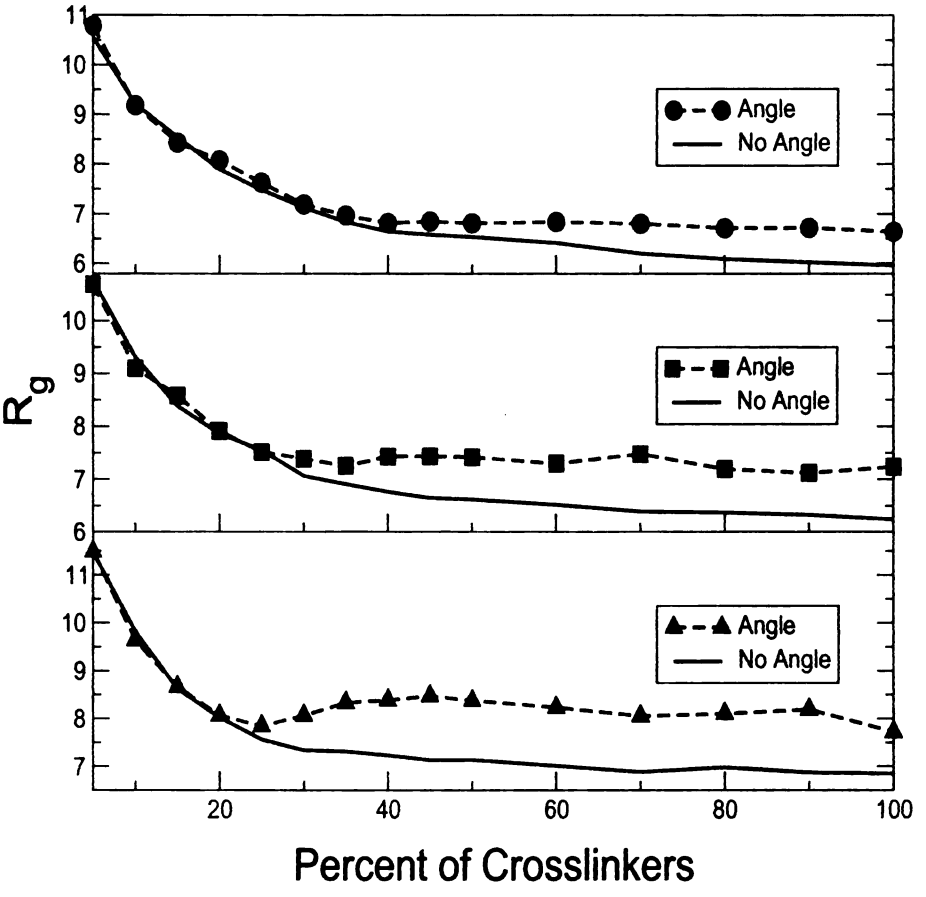

Figure 5.5: R_g of stiff chains with segment length $m = 2, 3, 4$ are plotted in separate panels from top down. By the Maxwell constraint counting method, when they are crosslinked with angle constraints, the rigidity thresholds are 50%, 36.36% and 28.57% respectively, while crosslinking without angle constraints can not cause the rigidity effect in those chains. It can be seen in each panel that two curves corresponding to two types of crosslinks nicely overlap with each other at lower crosslinker concentrations, and split above the rigidity thresholds, showing good agreement with the theoretical estimate.

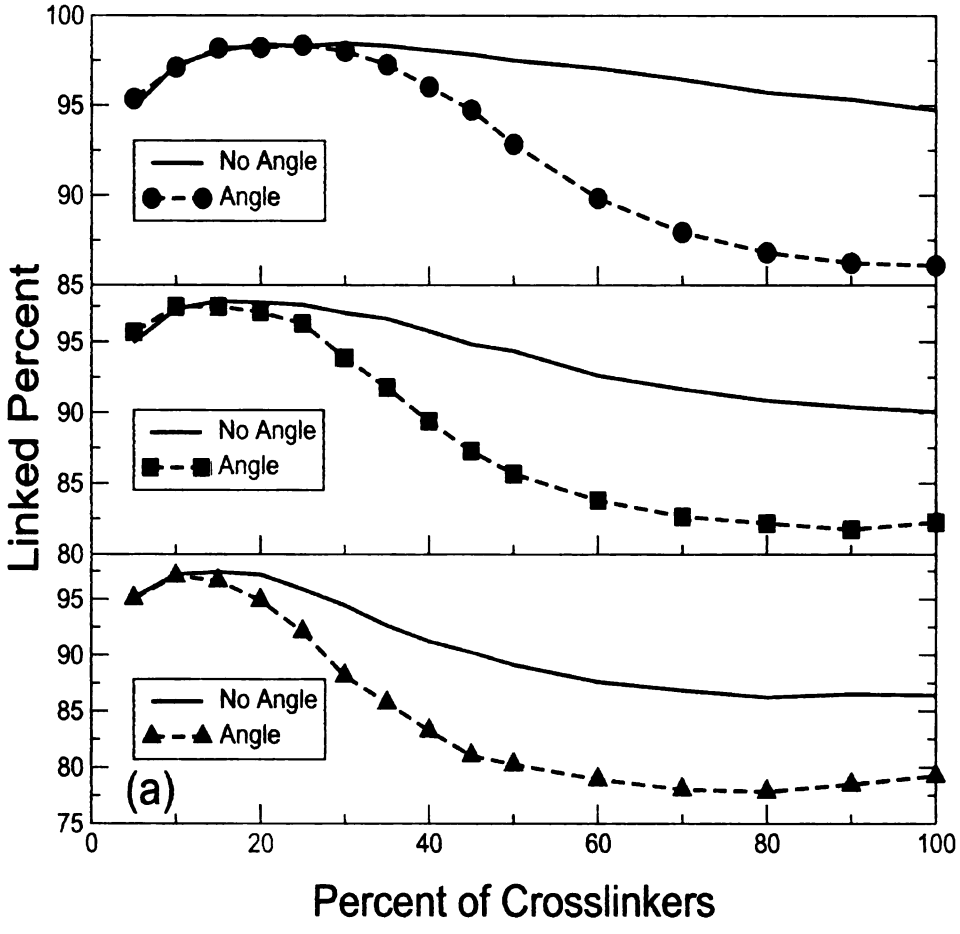

Figure 5.6: The linked percent of crosslinkers in stiff chains with segment length $m = 2, 3, 4$ are plotted in separate panels from top down. In each panel, the results for two types of crosslinks are plotted together for comparison.

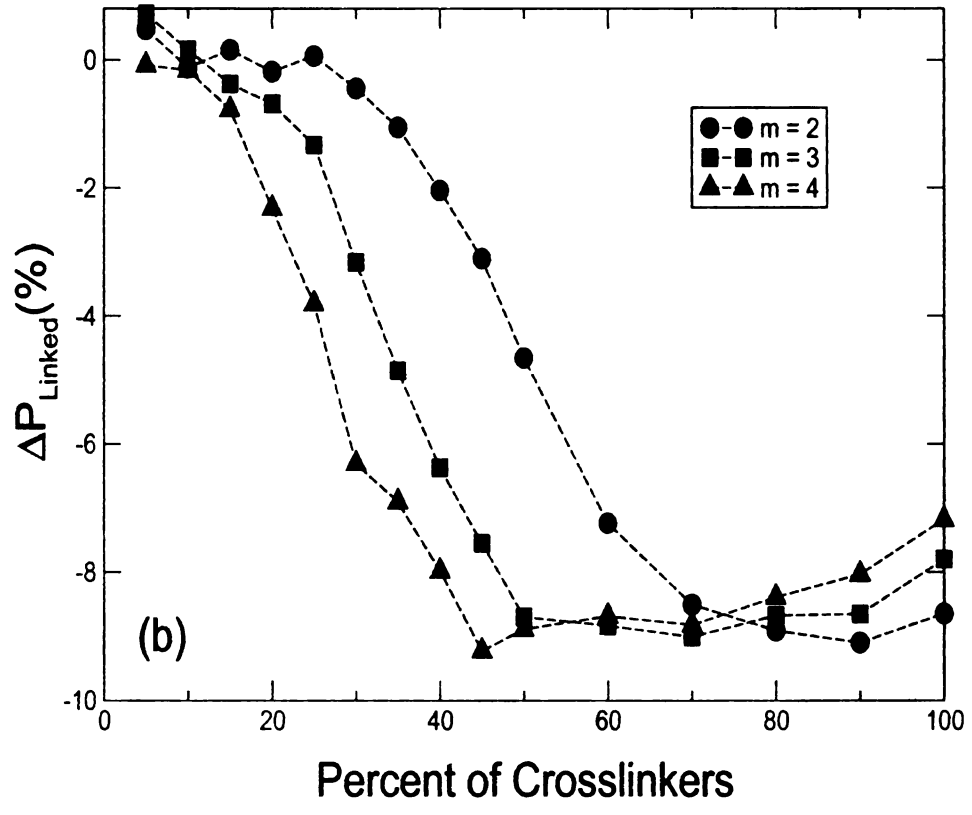

Figure 5.7: The difference between linked percents of two types of crosslinks. They exhibit considerable declines at their respective rigidity thresholds, which are 50%, 36.36% and 28.57% as found by the Maxwell constraint counting method.

comparison purpose, one with and one without angle constraints. The angle potential of a crosslink, if it is applied, has an equilibrium of 90°. Same criteria as in previous chapter are checked for two crosslinkers to react, namely they have to be within the distance of 1.3σ. Besides, because of the chain stiffness, an additional requirement should be enforced that only beads separated by at least two segment lengths can form a crosslink.

In the stiff chain model, only beads at the joints of the segments contribute to the floppy modes. Thus, a N-bead stiff chain model with a segment length m is equivalent to a simple FJC model with N/m beads which has $2N/m$ floppy modes. When the stiff chain model is crosslinked without angle constraints, it can be derived in a way similar to the FRC model that a rigidity effect should emerge when $2N/m - xN/2 = 0$, yielding $x_c = 4/m$. When the angle constraints are enabled for intramolecular crosslinking, one has to distinguish between the beads at the joints and at the middle of the segments, for a crosslink causes two angle constraints for the former but only one for the latter. There are on average N/m beads at the joints of the segments and $N(m-1)/m$ beads that are at the middle of the segments. Thus the rigidity threshold equation becomes:

$$\frac{2N}{m} - \frac{xN}{2} - \frac{1}{m} \cdot 2xN - \frac{m-1}{m} \cdot xN = 0 \tag{5.2}$$

which gives a rigidity threshold at $x_c = 4/(3m+2)$.

The simulations were run on three stiff chain models with segment lengths $m = 2, 3, 4$ respectively. All chains had 1000 beads and their concentrations of crosslinkers varied from 5% to 100%. The crosslinking simulations were run in the same way as for the FRC model, and all of them were run at temperature $T = 3.5$ (in the Lennard-Jones units).

Because the crosslinking without the angle constraints has a rigidity threshold

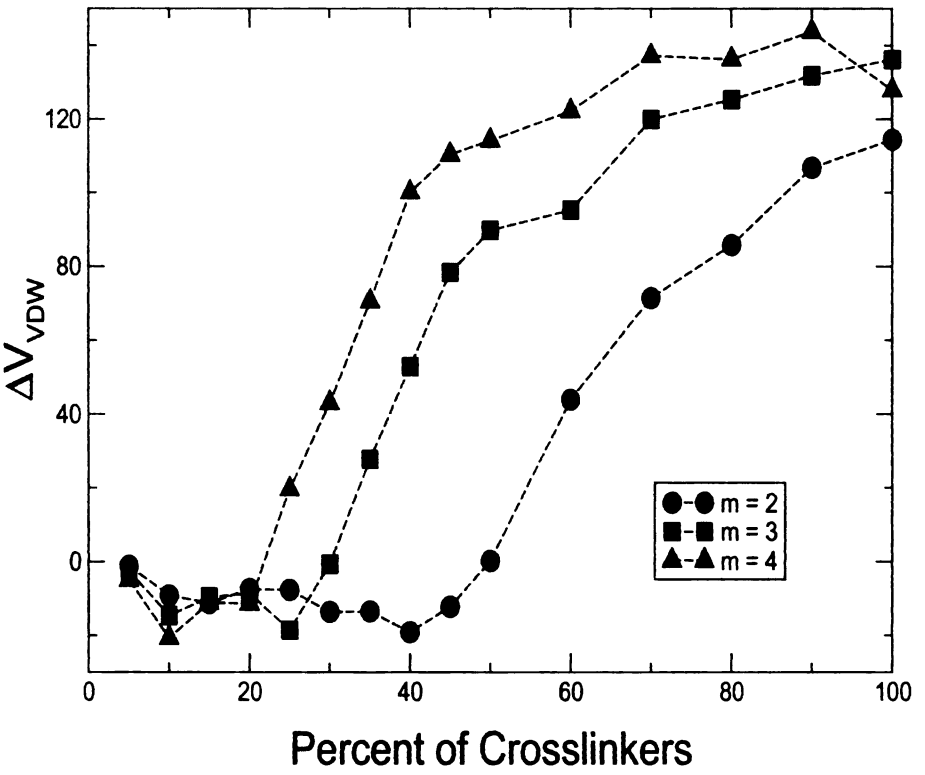

Figure 5.8: The difference between van de Waals volumes of stiff chains crosslinked by two types of crosslinks shows a similar transition for all segment lengths.

$x_c = 4/m$, all three models with $m = 2, 3, 4$ should show no rigidity effect when crosslinking without angle constraints. On the other hand, the crosslinking with angle constraints yields a rigidity threshold at $x_c = 4/(3m + 2)$, which equals to $50\%, 36.36\%$ and 28.57% for three models respectively.

The theoretical estimate of rigidity thresholds is well supported by the simulation results. Fig. 5.5 shows the change of R_g with the crosslinker concentration. For each segment length, two R_g curves for two types of crosslinks overlap with each other nicely at first, and they split when the crosslinker concentration is above the theoretical rigidity thresholds. Moreover, the linked percent of crosslinkers and its difference for two types of crosslinks also exhibit transitions at the theoretical rigidity thresholds, as shown in fig. 5.6 and fig. 5.7 respectively.

Van de Waals volume of a crosslinked polymer turns out to be another indicator

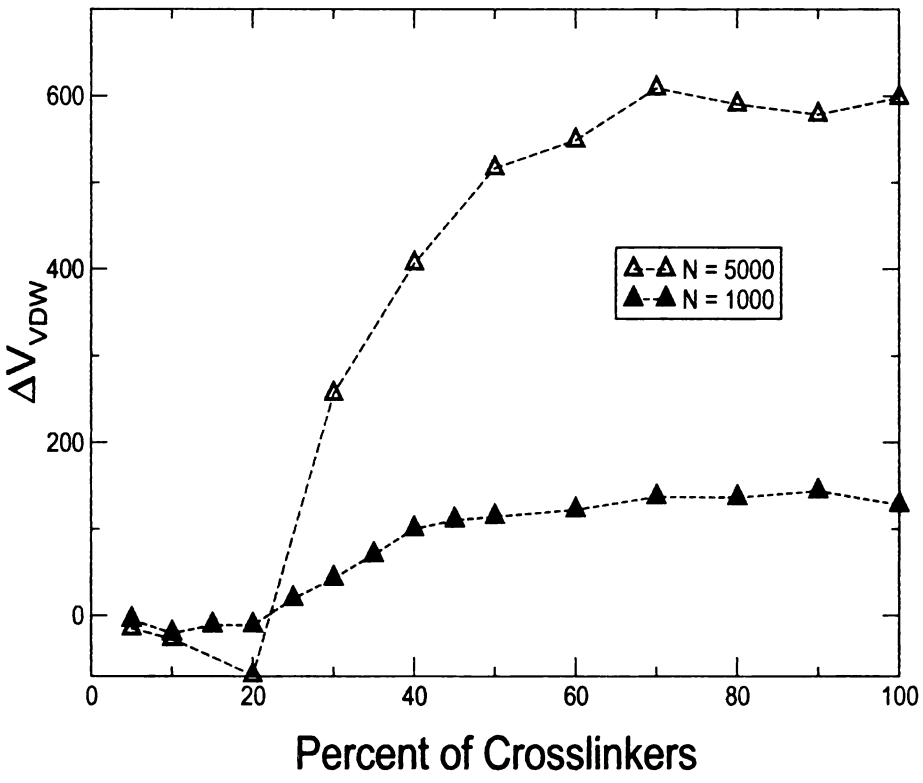

Figure 5.9: ΔV_{vdw} for long chains (5000 beads) and short chains (1000 beads). Both of them have a segment length $m = 4$. The difference in van de Waals volume is approximately proportional to the size of the chain.

of the rigidity effect. In fig. 5.3, the difference between van de Waals volume of stiff chains crosslinked in two ways are plotted, where a sudden change can be observed for all three models with different segment lengths, at their respective theoretical rigidity thresholds, namely 50%, 36.36% and 28.57%.

The rigidity effect was also studied for the intramolecular crosslinking of longer chains with 5000 beads and a segment length $m = 4$. Compared to shorter chains, the changes in their van de Waals volumes are more pronounced as shown in fig. 5.3. The accurate rigidity threshold of intramolecularly crosslinked stiff chains can possibly be determined by a finite size scaling.

5.4 Ring-weighted crosslinking

A ring-weighted crosslinking occurs in a polymer made completely of crosslinkers. It can be simulated in a similar procedure as described in section 5.2. However, their termination criteria are different. A ring-weighted crosslinking simulation should be terminated once the desired crosslinking density is reached, whereas a random crosslinking simulation goes until no more crosslinks can be formed.

The ring-weighted crosslinking simulations were carried out on both FRC and stiff chain models. Their crosslinker concentrations varied from 5% to 100%. 50 FRC and 50 stiff chain samples with 1000 beads each were studied for all concentrations. Without loss of generality, the segment length of all stiff chains was set to be 4. The simulations were performed at $T = 3.5$ using the same force fields as described before.

Similar to the study of random crosslinking, two types of crosslinks were employed for ring-weighted crosslinking on both FRC and stiff chain models, one with angle constraints and the other without. Fig. 5.10 shows R_g for freely rotating chains and stiff chains with these two types of crosslinks. It can be seen that basically all R_g curves are smooth over the full range of crosslinker concentrations without any abrupt changes at their rigidity thresholds. It indicates that the rigidity effect in the ring-weighted crosslinking emerges continuously, similar to that of a random network glass.

5.5 Conclusion

The intramolecular crosslinking of a polymer permanently changes its structure. It reduces the floppy modes of the polymer by forming new covalent bonds. Thus a rigidity effect may emerge in this process.

A molecular dynamics simulation study of the rigidity effect was performed using both freely rotating chain and stiff chain models. And two types of crosslinks were

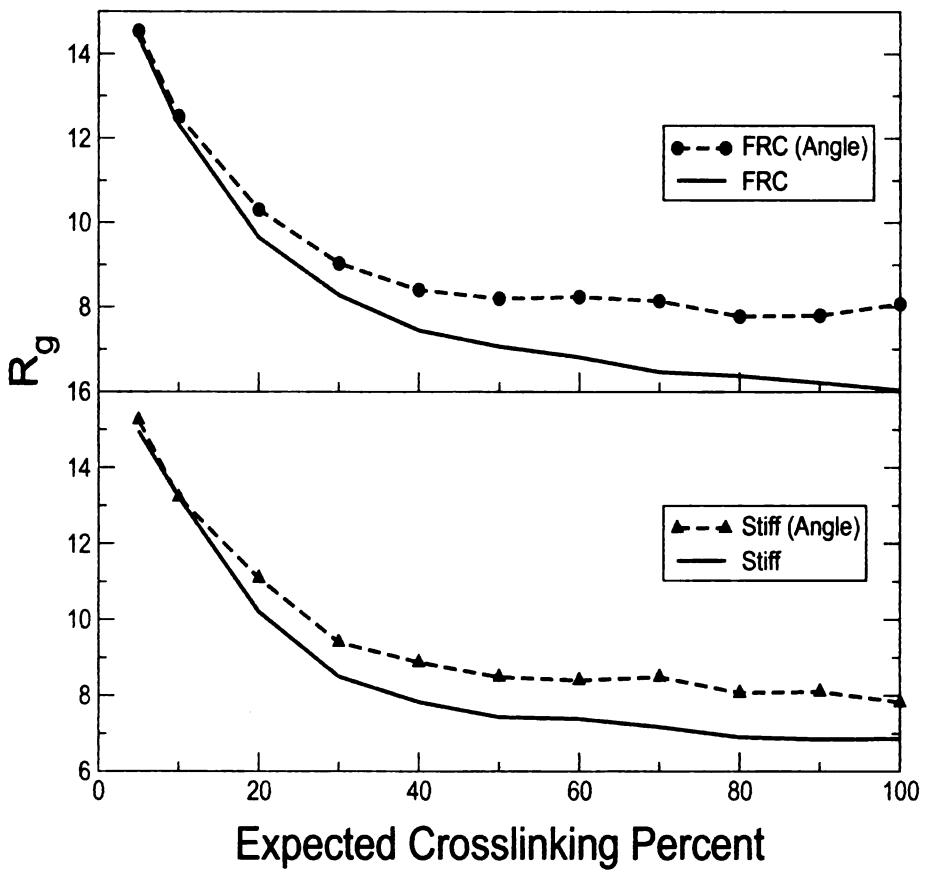

Figure 5.10: R_g for freely rotating chains and stiff chains ($m = 4$) crosslinked by ring-weighed crosslinking. When the angle constraints are employed, crosslinking still leads to a larger R_g for both models. However, in this case all R_g curves are smooth without abrupt changes at theoretical rigidity thresholds.

employed in the crosslinking simulations, one with angle constraints while the other without. Models and parameters in the crosslinking simulations were carefully chosen so that the crosslinking with angle constraints leads to a rigidity effect at certain crosslinker concentration, while the one without angle constraints yields no rigidity effect over the full crosslinker concentration range. Then the rigidity effect can be identified unambiguously by comparing these two cases.

The Maxwell constraint counting method can be employed to calculate the rigidity thresholds. A simple FRC model has a threshold of 40% when being crosslinked with angle constraints, while a stiff chain with Kuhn length m has rigidity thresholds at $4/(3m+2)$ and $4/m$ when being crosslinked with and without angle constraints, respectively.

To detect the rigidity effect, R_g and the percent of linked crosslinkers were evaluated for all models. In models where the rigidity effect is absent, R_g exhibits a continuous decline with increasing of crosslinks. On the contrary, R_g in the rigid regions shows little dependence on the density of crosslinks and is noticeably larger than in the corresponding floppy regions. Moreover, it also exhibits large variations in the rigid regions due to lack of relaxation.

Compared to R_g, the linked percent of crosslinkers of a crosslinked polymer changes more smoothly with the crosslinker concentration, but a considerable decline can still be observed at the rigidity thresholds. By taking the difference between two types of crosslinks, which excludes all other factors but rigidity from the simulation results, nice transition at theoretical rigidity thresholds can be observed.

The van de Waals volume of a crosslinked polymer is closely related to the linked percent and appears to be a good indicator of the rigidity effect, too. Because it is proportional to the size of the polymer, the van de Waals volume of a long chain can be used to determine the rigidity threshold accurately.

In addition, simulations were also run for another crosslinking scheme, the ring-

weighted crosslinking. In this case, the radius of gyration of a crosslinked polymer did not show any abrupt changes at the rigidity thresholds as in the random crosslinking. However, because at higher crosslinker concentrations the ring-weighted crosslinking makes little difference from the random crosslinking, it should also lead to a rigidity effect as the random crosslinking does. The continuous change of R_g simply implies that in the ring-weighted crosslinking the rigidity effect emerges continuously.

Chapter 6

Polystyrene on attractive surfaces

6.1 Introduction

The behavior of a polymer on an attractive surface is dominated by the monomer-monomer and monomer-surface interaction. In addition, if the polymer is immersed in a solvent, interaction between the monomers and the solvent molecules also plays a role. Basically, the interaction between monomers controls the morphology of a polymer, so that it can be either extended or compact; while the interaction between monomers and surfaces affects the adsorption of a polymer, so that it can be either adsorbed or desorbed. Their combination leads to four different states: DE(Desorbed Extended), DC(Desorbed Compact), AE(Adsorbed Extended) and AC(Adsorbed Compact). Moreover, in the intermediate region complex phases arise because of the interplay of these two types of interaction.

In the view of statistical mechanics, polymer adsorption is driven by two factors, the polymer-surface attraction and the entropy of the polymer. It is adsorbed to the surface when the decrease of the polymer-surface attraction energy can compensate for its entropy loss due to adsorption, and is desorbed otherwise.

Polymer adsorption is the key to various fields, such as polymer wetting and

dewetting[85, 86], organic-inorganic interface adhesion[87, 88, 89] and protein ligand binding[90, 91]. It has drawn great interest and been extensively studied in the past few decades[92, 93]. Those researches were fruitful and greatly improved our knowledge of polymer adsorption, but many questions still remain unanswered in areas such as thin films, bio-systems, nano-structured interfaces, even the fundamental adsorption mechanism[94].

In this chapter a molecular dynamics simulation study of polystyrenes on attractive surfaces is presented. It is organized as follows. In section 6.2, the phase diagram of tethered polystyrene chains on attractive surfaces is studied by molecular dynamics simulations. In section 6.3, a simple heating simulation is performed to gain an overview of the dynamic process of the adsorption of a polymer chain. In the last section a summary of this chapter is given.

6.2 Phase diagram

The phase diagram of polymers on attractive surfaces is critical to the understanding of polymer adsorption, which has been studied by various numerical works in the past based on lattice models [95, 96, 97, 98, 99, 100, 101, 102, 103, 104, 105]. Recently an improved simulation study of the phase diagram was carried out[3] which employed the bond fluctuation model[106]. This research presented the phase diagram of tethered polymers on substrates in terms of two field variables. They are $\beta_b = \epsilon_b/kT$ and $\beta_s = \epsilon_s/kT$, where ϵ_b is the Lennard-Jones interaction energy between the monomers and ϵ_s between the monomers and the substrate molecules. The phase diagram is shown in fig. 6.1.

The bond fluctuation model allows the bond length to fluctuate within a range so that the conformations of a polymer can be sampled in more detail. It is basically an intermediate approach between lattice models and off-lattice models. Along this

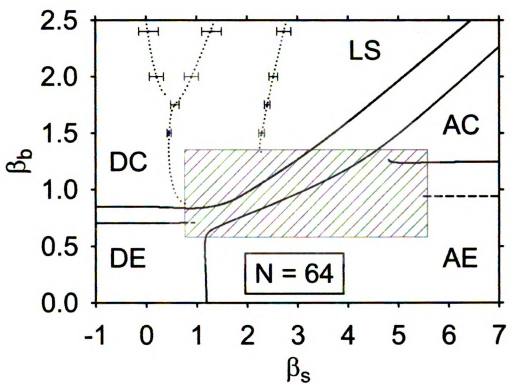

Figure 6.1: The phase diagram of tethered polymers on substrates. It was obtained by a Monte Carlo simulation study using the bond fluctuation model[3].

line the next improvement in the phase diagram study should incorporate true off lattice models. Moreover, many polymers have large side groups which greatly hinder their motion at low temperatures, which cause them to be trapped in glassy states. For example, polystyrene with phenyl groups attached to its backbone assumes a glassy state under 108K. To better describe those polymers atomistic models are often required.

Molecular dynamics simulation has been successfully applied to the study of the dynamics of polymers on surfaces[107, 108] as well as their glassy transitions[109, 110]. A molecular dynamics simulation study is presented below. It investigates the phase diagram of polystyrene chains on surfaces, and compares it to the results of Monte Carlo simulation studies. In particular, by employing the molecular dynamics and an atomistic model of polystyrene, the glassy states can be identified in the phase diagram.

The samples in this molecular dynamics study were 125-monomer atactic polystyrene chains. They were represented by the same atomistic model as is described in section 3.3. Initially, each polystyrene sample was tethered to a substrate by one of its ends. A weak repulsive force was then enforced between the sample and the substrate for a short period of time to ensure that it stayed above the plane $z = 0$ initially.

For simplicity, the simulations were performed in vacuum. Because vacuum is an extremely poor solvent, high temperatures (up to 1600K) have to be used in order to study the coil phase of polystyrenes. The temperature here should be considered as an effective temperature which incorporates the effect of solvent as well.

In the simulation the substrates were not explicitly represented. They were described by the Lennard-Jones 9-3 potential instead:

$$U_{LJ93} = \epsilon_{eff}\left[\frac{2}{15}\left(\frac{\sigma}{z}\right)^9 - \left(\frac{\sigma}{z}\right)^3\right] \tag{6.1}$$

where ϵ_{eff} can be related to the regular Lennard-Jones 12-6 potential well depth ϵ by:

$$\epsilon_{eff} = \frac{2\pi}{3} n\sigma^3 \epsilon \tag{6.2}$$

n is the number density of the substrate molecules. The Lennard-Jones 12-6 potential describes the interaction between monomers and substrate molecules. Based on the equation above, a polystyrene substrate has a ϵ_{eff} of 0.7Kcal/mol (Recall that the density of bulk polystyrene is 1050 kg/m^3). ϵ_{eff} of other substrates can be obtained similarly.

The temperature and surface attraction were varied in a wide range in the simulation to investigate the phase diagram. A total of 30 temperatures from 200K to 1600K, and 28 surface Lennard-Jones potentials with ϵ_{eff} from 0.01 Kcal/mol to 4 Kcal/mol were used. Ten samples were studied for each pair of temperature and surface attraction. Final results were averaged over them. The simulation of each polystyrene sample consisted of a NVT run for 8 nanoseconds to reach equilibrium, and a subsequent NVT run for 2 nanoseconds to take 200 snapshots to calculate its physical properties.

The boundary between AE and DE phases is determined by both the temperature and the surface attraction. Their effects can be combined in the field variable β_s. In fig. 6.2 the z-coordinate of the center of mass for all samples is plotted against β_s, where different curves correspond to different temperatures. Note that there is a special point $\beta_s = 0.25$ where all chains assume approximately equal heights in spite of temperature difference, qualitatively indicating the boundary between AE and DE phases. This height is also approximately the persistence length of polystyrene chains[111].

The extended state and compact state for polymers on attractive substrates are basically the same as the coil state and globule state for free polymers. The transition between them can occur either in 2D space (when the polymer is adsorbed) or 3D

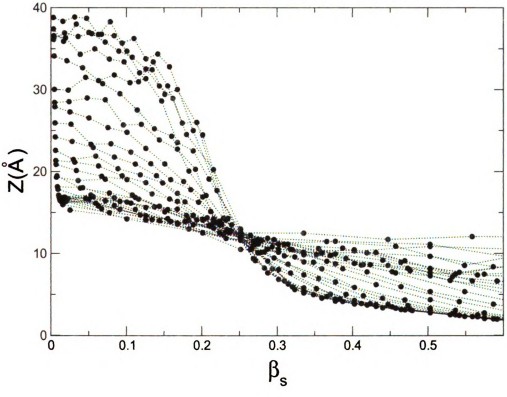

Figure 6.2: The z-coordinate of the center of mass of a polymer is plotted against β_s. Temperature decreases from the top curve to the bottom one. It can be seen that approximately at $\beta_s = 0.25$, the z-coordinate is the same for all temperatures

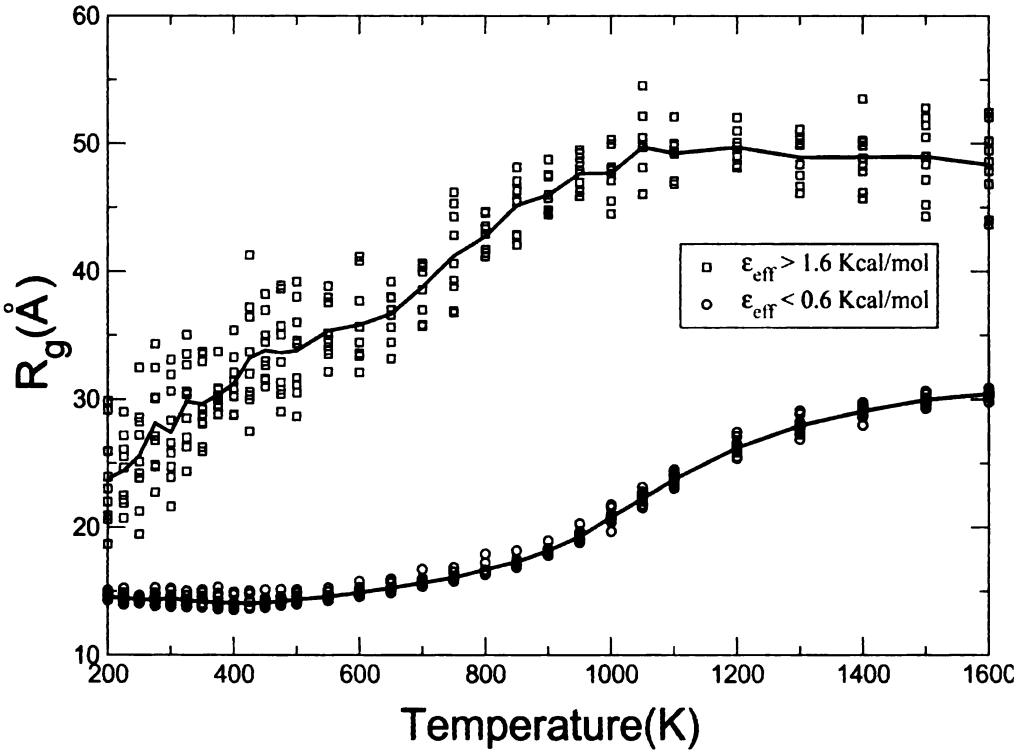

Figure 6.3: R_g of polystyrene chains (with 125 styrenes) on substrates. When ϵ_{eff} is greater than 1.6Kcal/mol, all chains are adsorbed and show a transition from AC to AE; when ϵ_{eff} is less than 0.6Kcal/mol, they are desorbed and the transition is from DC to DE. Two solid lines give average R_g for all desorbed cases and all adsorbed cases respectively. In addition, below 400K the polystyrene chains are frozen in glassy states, so that they keep their initial globule morphologies, even for $\epsilon_{eff} > 1.6 Kcal/mol$, and assume smaller radii of gyration.

space (when the polymer is desorbed). In fig. 6.3, these two transition temperatures can be roughly determined to be the inflection points of R_g curves, namely T=700K for the transition from AC to AE and T=1100K for the transition from DC to DE.

The contour of $R_g = 20\mathring{A}$ can be qualitatively taken as the boundary of DC phase. Polymers in DC phase should have the smallest R_g because they assume globular morphologies. Moreover, the glassy state is marked as the region with larger z-coordinate of the center of mass at low temperatures. Combining all those phase boundaries, a rough phase diagram can be obtained for polystyrene chains on substrates. In fig. 6.4 and 6.5, the contour plot of the z-coordinate of the center of mass

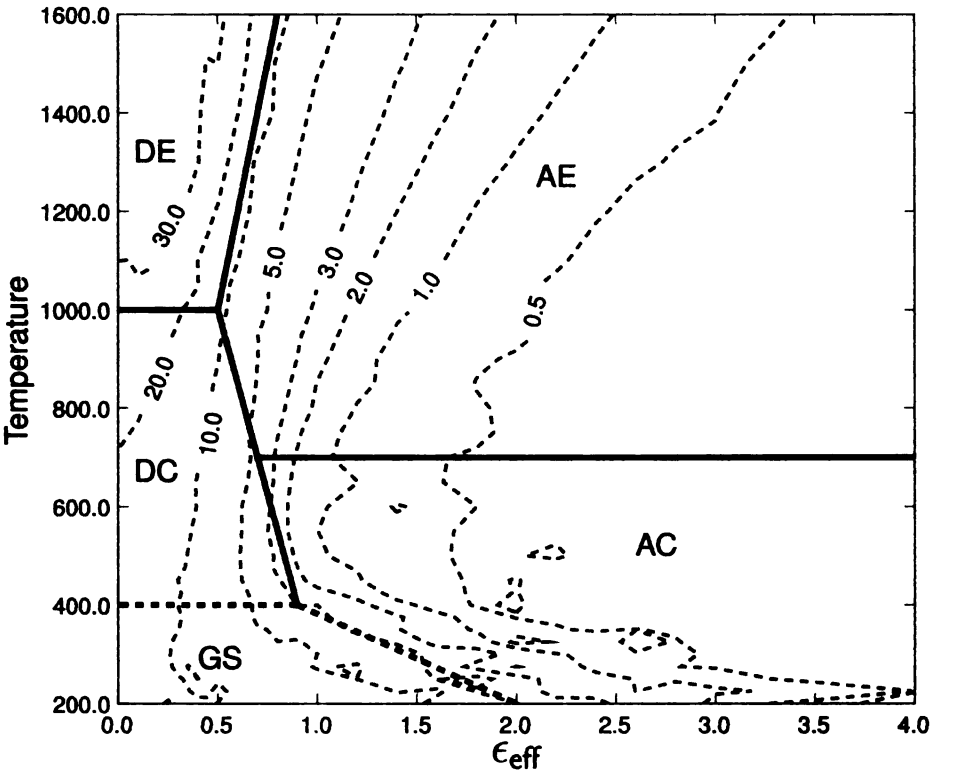

Figure 6.4: The contour plot of the z-coordinate (in $\mathring{A}$) of the center of mass of polystyrene chains with 125 monomers on substrates.

and R_g of polystyrenes are shown, and the phase diagram is overlaid on it.

6.3 The dynamics of polymer adsorption

The dynamics of polymer adsorption firstly depends on the attraction energy between the polymer and the surface. It is also affected by the ambient temperature. An early study on the adsorption of polymer films showed that their adsorptions exhibit an exponential kinetics at high temperatures, and a stretched exponential kinetics at low temperatures[112]. Moreover, the lateral diffusion of a polymer on attractive surfaces also has to do with its adsorption. On the one hand, the diffusion of a polymer on a surface is suppressed by its adsorption to the surface. On the

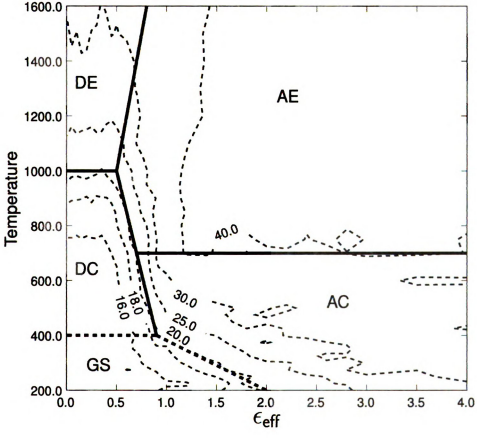

Figure 6.5: The contour plot of R_g (in $\AA$) of polystyrene chains with 125 monomers on substrates.

other hand, it is more difficult for the adsorption to reach equilibrium if its diffusion is restricted by the surface roughness or strong attraction spots on the surface. Such correlation between diffusion and adsorption was observed in an experiment on polymer films[113]. It was also demonstrated by later molecular dynamics simulations on polymer chains[108] and polymer films[114].

In the early years, the research of polymer adsorption focused predominantly on thin film samples. It was since the invention of the technology of direct imaging of single macromolecules, in particular Atomic Force Microscopy (AFM), that single chain samples have been studied more thoroughly. Molecular dynamics simulations of the adsorption of a single polymer have also been performed on both coarse grained[107, 115] and atomistic models [73, 116]. The adsorption of a polymer chain has abundant applications such as single molecule memory device or thermally actuated drug delivery. It is a stepwise process consisting of three stages[107]. In the first stage, a polymer approaches to the vicinity of an attractive surface and deforms into an elongated shape perpendicular to the surface. In the second one, the polymer adsorbs to the surface at an exponential rate. The third one is the relaxation stage where an adsorbed polymer spreads to the surface to reach the final equilibrium state. The relaxation stage takes a significantly longer time to complete compared to previous two stages. In fact, it is often questionable if the true equilibrium is reached.

A rough overview of the dynamics of single chain adsorption was obtained by molecular dynamics simulations of polystyrene chains on attractive substrates. The surface attraction was described by a Lennard-Jones 9-3 potential as before. Its strength ϵ_{eff} varied from 0.5Kcal/mol to 3Kcal/mol. Due to the AC to DC transition, the surface attraction can not be smaller than 0.5 Kcal/mol otherwise the polystyrene chains can not be always adsorbed over the full temperature range of the simulations.

25 samples were studied for each ϵ_{eff}. Their initial configurations were generated in a similar way as in section 6.2, but initially they were simply placed on substrates

instead of being tethered to them. A NVT simulation of 12 nanoseconds at 300K was subsequently performed on each sample to leave it in a compact globule form. Then a heating process started at room temperature (T=300K) and went all the way up to T=600K. It took 20 nanoseconds to finish, corresponding to a heating rate of 15K/ns.

In fig. 6.6, the z-coordinate of the center of mass is plotted for polystyrenes on all substrates. Since the initial temperature is 300K, well below the glassy transition temperature of polystyrenes, all samples were frozen in their initial states, namely compact globules, with relatively large heights. As temperature rose, polystyrene samples became flexible and started to collapse rapidly. Apparently, the temperature thresholds for polystyrenes to collapse are lowered by increasing of surface attraction. Since the glassy transition temperature is positively correlated with the temperature threshold of collapsing, it can be deduced that the glassy transition temperature for single polystyrene chains is lowered as well. In the end of the heating process, the heights of polystyrene samples remain constant on almost all substrates, which implies that they reached a stable adsorbed state. The only exception is the surface with an attraction energy ϵ_{eff}=0.5Kcal/mol, where small oscillations of the height at high temperatures were seen. It can be attributed to the transition from AC to DC, which occurs at around 450K for this surface according to the previous phase diagram study.

6.4 Conclusion

In this chapter, an atomistic model was adopted to study the behavior of polystyrenes on attractive surfaces. The phase diagram was firstly obtained by varying the ambient temperature and the surface attraction. Owing to the adoption of molecular dynamics and an atomistic model, a glassy region can be identified at low temper-

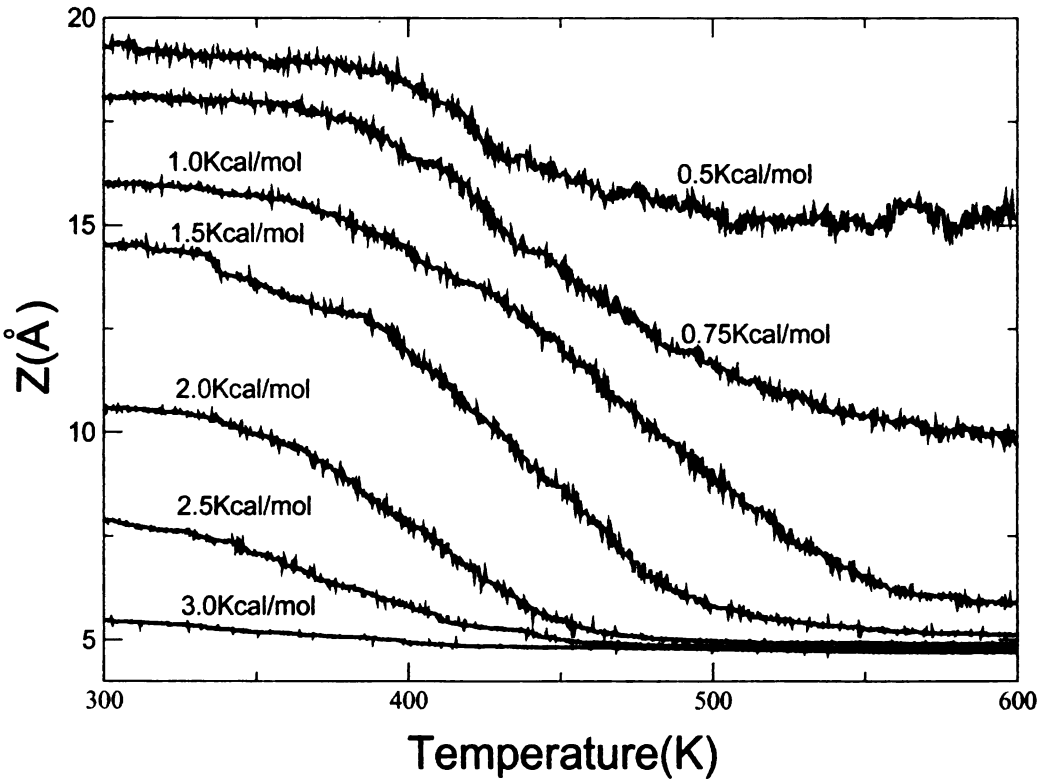

Figure 6.6: The z-coordinate of the center of mass of polystyrene chains on substrates during the heating process.

atures. At high temperatures the result appears to be the same as previous Monte Carlo simulation studies on lattice models or bond fluctuation models.

The heating simulations were performed on polystyrene chains to study their adsorption processes. In the beginning of the heating, the temperature was below the glassy transition temperature for polystyrenes. Consequently all samples were frozen at the compact globule state. As temperature rose, they gained more mobility and started collapsing to take on expanded and adsorbed morphologies eventually. It was found that increasing of the surface attraction can reduce the temperature threshold for polystyrene globules to collapse, indicating the decrease of the glassy temperature of single polystyrene chains. The heating simulation thus provides a good overview of the dynamics of polystyrene chains on attractive substrates.

Chapter 7

Conclusion

Intramolecular crosslinking of polymers is a feasible approach to manufacture polymeric nanoparticles that have found abundant applications in various fields. In this thesis, the intramolecular crosslinking process and its end product, *i.e.*, polymeric nanoparticles, are studied using molecular dynamics simulation. Both atomistic and coarse grained models are employed in the simulations, providing a comprehensive understanding of the intramolecular crosslinking process.

The simulation study discovers a variety of factors that are important to the crosslinking process and, consequently, the properties of final nanoparticles. Those factors can thus be utilized as experimental controls of intramolecular crosslinking. The concentration of crosslinkers in a polymer is a first example. It can be adjusted by polymerization of different numbers of crosslinkable and non-crosslinkable monomers, or by substitution of crosslinkers for a certain number of normal monomers. With more crosslinkers a polymer can usually form more compact nanoparticles, unless a rigidity effect occurs that prevents the complete crosslinking of all crosslinkers.

The morphology of the precursor polymer is another factor in the intramolecular crosslinking process. In the coil phase, the crosslinking of polymers yields loosely connected nanoparticles while in the globule phase it yields tightly connected nanopar-

ticles. The structural difference between these two cases can be described by their chemical distance densities. For precursor chains with the same crosslinker concentration, the crosslinking in the coil phase leads to small chemical distance densities, while large chemical distance densities occur in the globule phase. A power law dependence of the radius of gyration on the chemical distance density is fitted to the simulation data and yields good fitting results.

The rigidity effect plays an important role in the intramolecular crosslinkings of polymers. It is caused by the loss of floppy modes during the crosslinking process. The rigidity effect is dependent on the concentrations of crosslinkers. It only occurs when the crosslinker concentration is above certain threshold. Several other factors also contribute to the rigidity effect, such as the chain stiffness and the crosslinking type. A stiff polymer has less floppy modes initially, such that a rigidity effect can emerge at lower crosslinker concentrations. In principle, the rigidity threshold x_c for a stiff polymer is inversely proportional to its persistence length l, *i.e.*, $x_c \sim 1/l$. Thus a wide range of rigidity thresholds is accessible by using precursor polymers with different stiffness. Different types of crosslinks utilize crosslinking units with different levels of rigidity, so that various rigidity thresholds can also be achieved by adopting different crosslinking protocols.

Furthermore, the analogy between intramolecular crosslinking and protein folding points out another possible control of the crosslinking process that is to use designed sequences of crosslinkers in precursor polymers to direct the manufacturing of nanoparticles with desired shapes and sizes. For example, a recent study[76] shows that Janus particles[117] can be formed by the intramolecular crosslinking of precursor polymers with three different types of crosslinkers using the CLICK chemistry[118].

Future researches in the intramolecular crosslinking may include a more thorough study from theoretical point of view on the reaction rate, the rigidity effect, the structure size relation and so on. Intramolecular crosslinking simulations of other

polymers using atomistic model will also be meaningful. They can provide further realistic crosslinking examples and possibly lead to new discoveries. Moreover, the crosslinked polymers from the simulation can also be taken as the basis for the study of the interaction between polymeric nanoparticles and various other materials, *e.g.*, polymers, solutions and substrates *etc.*

Bibliography

[1] Shao-Tang Sun, Izumi Nishio, Gerald Swislow, and Toyoichi Tanaka. The coil-globule transition: Radius of gyration of polystyrene in cyclohexane. *Journal of Chemical Physics*, 73(12):5971–5975, December 1980.

[2] Leslie Howard Sperling. *Introduction to Physical Polymer Science.* John Wiley & Sons, 2006.

[3] Jutta Luettmer-Strathmann, Federica Rampf, Wolfgang Paul, and Kurt Binder. Transitions of tethered polymer chains: A simulation study with the bond fluctuation lattice model. *Journal of Chemical Physics*, 128:064903, 2008.

[4] Eva Harth, Brooke Van Horn, Victor Y. Lee, David S. Germack, Chad P. Gonzales, Robert D. Miller, and Craig J. Hawker. A facile approach to architecturally defined nanoparticles via intramolecular chain collapse. *Journal of American Chemical Society*, 124(29):8653–8660, June 2002.

[5] Michael Rubinstein and Ralph H. Colby. *Polymer Physics.* Oxford University Press, 2003.

[6] Wayne L. Mattice and Ulrich W. Suter. *Conformational Theory of Large Molecules.* John Wiley & Sons, 1994.

[7] Gert Strobl. *The Physics of Polymers.* Springer, 1997.

[8] Bahattin M. Baysal and Frank E. Karasz. Coil-globule collapse in flexible macromolecules. *Macromolecular Theory and Simulations*, 12:627–646, 2003.

[9] D. A. McQuarrie. *Statistical Mechanics.* New York: Harper & Row, 1976.

[10] F. Sato, S. Hojo, and H. Sun. On the transferability of force field parameterss – with an ab initio force field developed for sulfonamides. *J. Phys. Chem. A*, 107:248–257, 2003.

[11] Kurt Binder, editor. *Monte Carlo and Molecular Dynamics Simulations in Polymer Science.* Oxford University Press, 1995.

[12] Michael Kotelyanskii and Doros N. Theodorou, editors. *Simulation Methods for Polymers.* Marcel Dekker, Inc, 2004.

[13] Loup Verlet. Computer "experiments" on classical fluids. i. thermodynamical properties of lennard-jones particles. *Physical Review*, 159:98–103, 1967.

[14] S. Nose. A molecular dynamics method for simulations in the canonical ensemble. *Molecular Physics*, 52:255–268, 1984.

[15] William G. Hoover. Cannonical dynamics: equilibrium phase-space distribution. *Physical Review A*, 31:1695–1697, 1985.

[16] William G. Hoover. Constant presssure equations of motion. *Physical Review A*, 34:2499–2500, 1986.

[17] *GROMACS User Manual (Version 3.3).*

[18] H. J. C. Berendsen, J. P. M. Postma, W. F. van Gunsteren, A. DiNola, and J. R. Haak. Molecular dynamics with coupling to an external bath. *J. Chem. Phys.*, 81:3684–3690, 1984.

[19] Bernard R. Brooks, Robert E. Bruccoleri, Barry D. Olafson, David J. States, S. Swaminathan, and Martin Karplus. Charmm: A program for macromolecular energy, minimization, and dynamics calculations. *J. Comput. Chem.*, 4:187–217, 1983.

[20] Alexander D. MacKerell, Joanna Wiorkiewicz-Kuczera, and Martin Karplus. An all-atom empirical energy function for the simulation of nucleic acids. *Journal of American Chemical Society*, 117:11946–11975, 1995.

[21] A. D. MacKerell, D. Bashford, M. Bellott, R. L. Dunbrack Jr., J. D. Evanseck, M. J. Field, S. Fischer, J. Gao, H. Guo, S. Ha, D. Joseph-McCarthy, L. Kuchnir, K. Kuczera. F. T. K. Lau, C. Mattos, S. Michnick, T. Ngo, D. T. Nguyen, B. Prodhom, W. E. Reiher III, B. Roux, M. Schlenkrich, J. C. Smith, R. Stote, J. Straub, M. Watanabe, J. Wirkiewicz-Kuczera, D. Yin, and M. Karplus. All-atom empirical potential for molecular modeling and dynamics studies of proteins. *Journal of physical chemistry B*, 102:3586–3616, 1998.

[22] Scott J. Weiner, Peter A. Kollman, David A. Case, U. Chandra Singh, Caterina Ghio, Giuliano Alagona, Salvatore Profeta Jr, and Paul Weinerl. A new force field for molecular mechanical simulation of nucleic acids and proteins. *Journal of American Chemical Society*, 106:765–784, 1984.

[23] Scott J. Weiner, Peter A. Kollman, Dzung T. Nguyen, and David A. Case. An all atom force field for simulations of proteins and nucleic acids. *J. Comput. Chem.*, 7:230–252, 1986.

[24] Wendy D. Cornell, Piotr Cieplak, Christopher I. Bayly, Ian R. Gould, Kenneth M. Merz, David M. Ferguson, David C. Spellmeyer, Thomas Fox, James W. Caldwell, and Peter A. Kollman. A second generation force field for the simulation of proteins, nucleic acids, and organic molecules. *Journal of American Chemical Society*, 117:5179–5197, 1995.

[25] Yong Duan, Chun Wu, Shibasish Chowdhury, Mathew C. Lee, Guoming Xiong, Wei Zhang, Rong Yang, Piotr Cieplak, Ray Luo, Taisung Lee, James Caldwell, Junmei Wang, and Peter Kollman. A point-charge force field for molecular mechanics simulations of proteins based on condensed-phase quantum mechanical calculations. *J. Comput. Chem.*, 24:1999–2012, 2003.

[26] Lijiang Yang, Chun hu Tan, Meng-Juei Hsieh, Junmei Wang, Yong Duan, Piotr Cieplak, James Caldwell, Peter A. Kollman, and Ray Luo. New-generation amber united-atom force field. *J. Phys. Chem. B*, 110:13166–13176, 2006.

[27] Norman L. Allinger, Young H. Yuh, and Jenn Huei Lii. Molecular mechanics. the mm3 force field for hydrocarbons. *J. Am. Chem. Soc.*, 111:8551–8566, 1989.

[28] Jenn-Huei Lii and Norman L. Allinger. The mm3 force field for amides, polypeptides and proteins. *J. Comput. Chem.*, 12:186–199, 1991.

[29] Norman L. Allinger, Kuohsiang Chen, and Jenn-Huei Lii. An improved force field (mm4) for saturated hydrocarbons. *J. Comput. Chem.*, 17:642–668, 1996.

[30] Thomas A. Halgren. Merck molecular force field. *J. Comput. Chem.*, 17:490–519,520–552,553–586,587–615,616–641, 1996.

[31] J. R. Maple, M.-J. Hwang, T. P. Stockfisch, U. Dinur, M. Waldman, C. S. Ewig, and A. T. Hagler. Derivation of class ii force fields. i. methodology and quantum force field for the alkyl functional group and alkane molecules. *J. Comput. Chem.*, 15:162–182, 1994.

[32] A. R. Leach. *Molecular Modeling Principles and Applications.* Prentice Hall Publicatons, 2001.

[33] Jay. W. Ponder and David A. Case. Force fields for protein simulations. *Advances in protein chemistry*, 66:27, 2003.

[34] Alexander D. Mackerell. Empirical force fields for biological macromolecules: Overview and issues. *J. Comput. Chem*, 25:1584–1604, 2004.

[35] S. J. Plimpton. Fast parallel algorithms for short-range molecular dynamics. *J. Comp. Phys.*, 117:1, 1995.

[36] Thomas A. Halgren. Mmff vii. characterization of mmff94, mmff94s, and other widely available force fields for conformational energies and for intermolecular-interaction energies and geometries. *Journal of Computational Chemistry*, 20: 730–748, 1999.

[37] Erik Lindahl, Berk Hess, and David van der Spoel. Gromacs 3.0: a package for molecular simulation and trajectory analysis. *J. Mol. Model*, 7:306–317, 2001.

[38] Berk Hess, Carsten Kutzner, David van der Spoel, and Erik Lindahl. Gromacs 4: Algorithms for highly efficient, load-balanced, and scalable molecular simulation. *J. Chem. Theory Comput.*, 4:435–447, 2008.

[39] H. Sun. Compass: An ab initio force-field optimized for condensed-phase applications-overview with details on alkane and benzene compounds. *Journal of Physical Chemistry B*, 102:7338–7364, 1998.

[40] H. Sun, P. Ren, and J. R. Fried. The compass force field: parameterization and validation for phosphazenes. *Computational and theoretical polymer science*, 8: 229–246, 1998.

[41] Stephen L. Mayo, Barry D. Olafson, and William A. Goddard III. Dreiding: A generic force field for molecular simulations. *J. Phys. Chem.*, 94:8897–8909, 1990.

[42] A. K. Rappé, C. J. Casewit, K. S. Colwell, W. A. Goddard III, and W. M. Skid. Uff, a full periodic table force field for molecular mechanics and molecular dynamics simulations. *J. Am. Chem. Soc.*, 114:10024–10035, 1992.

[43] Thomas A. Halgren. Potential energy functions. *Current opinion in structural biology*, 5:205–210, 1995.

[44] Michael D. Beachy, David Chasman, Robert B. Murphy, Thomas A. Halgren, and Richard A. Friesner. Accurate ab initio quantum chemical determination of the relative energetics of peptide conformations and assessment of empirical force fields. *Journal of American Chemical Society*, 119:5908 - 5920, 1997.

[45] Klaus Gundertofte, Tommy Liljefors, Perola Norrby, and Ingrid Pettersson. A comparison of conformational energies calculated by several molecular mechanics methods. *Journal of Computational Chemistry*, 17:429–449, 1996.

[46] D. Mecerreyes, V. Lee, C. J. Hawker, J. L. Hedrick, A. Wursch, W. Volksen, T. Magbitang, E. Huang, and R. D. Miller. A novel approach to functionalized nanoparticles: Self-crosslinking of macromolecules in ultradilute solution. *Advanced Materials*, 13(3):204–208, February 2001.

[47] J. Jiang and S. Thayumanavan. Synthesis and characterization of amine-functionalized polystyrene nanoparticles. *Macromolecules*, 38(14):5886–5891, July 2005.

[48] H. A. Aliyar, P. D. Hamilton, E. E. Remsen, and N. Ravi. Synthesis of polyacrylamide nanogels by intramolecular disulfide cross-linking. *Journal Of Bioactive And Compatible Polymers*, 20(2):169–181, March 2005.

[49] E. Katz and I. Willner. Integrated nanoparticle-biomolecule hybrid systems: Synthesis, properties, and applications. *Angewandte Chemie-International Edition*, 43(45):6042–6108, 2004.

[50] A. C. Balazs, T. Emrick, and T. P. Russell. Nanoparticle polymer composites: Where two small worlds meet. *Science*, 314(5802):1107–1110, November 2006.

[51] A. Rosler, G. W. M. Vandermeulen, and H. A. Klok. Advanced drug delivery devices via self-assembly of amphiphilic block copolymers. *Advanced Drug Delivery Reviews*, 53(1):95–108, December 2001.

[52] R. S. Krishnan, M. E. Mackay, P. M. Duxbury, A. Pastor, C. J. Hawker, B. Van Horn, S. Asokan, and M. S. Wong. Self-assembled multilayers of nanocomponents. *Nano Letters*, 7(2):484–489, February 2007.

[53] M. E. Mackay, A. Tuteja, P. M. Duxbury, C. J. Hawker, B. Van Horn, Z. B. Guan, G. H. Chen, and R. S. Krishnan. General strategies for nanoparticle dispersion. *Science*, 311(5768):1740–1743, March 2006.

[54] M. E. Mackay, T. T. Dao, A. Tuteja, D. L. Ho, B. Van Horn, H. C. Kim, and C. J. Hawker. Nanoscale effects leading to non-einstein-like decrease in viscosity. *Nature Materials*, 2(11):762–766, November 2003.

[55] A. Tuteja, P. M. Duxbury, and M. E. Mackay. Multifunctional nanocomposites with reduced viscosity. *Macromolecules*, 40(26):9427–9434, December 2007.

[56] A. J. Rader, Brandon M. Hespenheide, Leslie A. Kuhn, and M. F. Thorpe. Protein unfolding: Rigidity lost. *PNAS*, 99:3540, 2002.

[57] M. Mondello, Hyung-Jin Yang, Hidemine Furuya, and Ryong-Joon Roe. Molecular dynamics simulation of atactic polystyrene. 1. comparison with x-ray scattering data. *Macromolecules*, 27:3566–3574, 1994.

[58] Hidemine Furuya, M. Mondello, Hyung-Jin Yang, Ryong-Joon Roe, R. W. Erwin, C. C. Han, and S. D. Smith. Molecular dynamics simulation of atactic polystyrene. 2. comparison with neutron scattering data. *Macromolecules*, 27: 5674–5680, 1994.

[59] Ryong-Joon Roe, M. Mondello, Hidemine Furuya, and Hyung-Jin Yan. Molecular dynamics simulation of atactic polystyrene. 3. short range order. *Macromolecules*, 28:2807–2818, 1995.

[60] Alexey V. Lyulin and M. A. J. Michels. Molecular dynamics simulation of bulk atactic polystyrene in the vicinity of tg. *Macromolecules*, 35(4):1463–1472, 2002.

[61] A. V. Lyulin, B. Vorselaars, M. A. Mazo, N. K. Balabaev, and M. A. J. Michels. Strain softening and hardening of amorphous polymers: Atomistic simulation of bulk mechanics and local dynamics. *Europhysics Letter*, 71:618–624, 2005.

[62] Bart Vorselaars, Alexey V. Lyulin, and M. A. J. Michels. Development of heterogeneity near the glass transition:phenyl-ring-flip motions in polystyrene. *Macromolecules*, 40:6001–6011, 2007.

[63] Alexey V. Lyulin and M. A. J. Michels. Time scales and mechanisms of relaxation in the energy landscape of polymer glass under deformation: Direct atomistic modeling. *Physical Review Letters*, 99:085504, 2007.

[64] Collin D. Wick, Marcus G. Martin, and J. Ilja Siepmann. Transferable potentials for phase equilibria. 4. united-atom description of linear and branched alkenes and alkylbenzenes. *Journal of Physical Chemistry B*, 104:8008–8016, 2000.

[65] V. A. Harmandaris, N. P. Adhikari, N. F. A. van der Vegt, and K. Kremer. Hierarchical modeling of polystyrene: From atomistic to coarse-grained simulations. *Macromolecues*, 39:6708–6719, 2006.

[66] P. V. Krishna Pant, Jie Han, Grant D. Smith, and Richard H. Boyd. A molecular dynamics simulation of polyethylene. *J. Chem. Phys.*, 99(1):597–604, July 1993.

[67] Jie Han and Richard H. Boyd. Small-molecule penetrant diffusion in hydrocarbon polymers as studied by molecular dynamics simulation. *Macromolecues*, 27:5365–5370, 1994.

[68] Jie Han and Richard H. Boyd. Molecular packing and small-penetrant diffusion in polystyrene: a molecular dynamics simulation study. *Polymer*, 37(10):1797–1804, 1996.

[69] William L. Jorgensen and Daniel L. Severance. Aromatic-aromatic interactions: free energy profiles for the benzene dimer in water, chloroform, and liquid benzene. *Journal of American Chemical Society*, 112:4768–4774, 1990.

[70] Florian Müller-Plathe. Local structure and dynamics in solvent-swollen polymers. *Macromolecues*, 29:4782–4791, 1996.

[71] Qi Sun and Roland Faller. Molecular dynamics of a polymer in mixed solvent: Atactic polystyrene in a mixture of cyclohexane and n,n-dimethylformamide. *Journal of Physical Chemistry B*, 109:15714–15723, 2005.

[72] Hua Yang, Li Ze-Sheng, Hu jun Qian, Yong biao Yang, Xiu bin Zhang, and Chia chung Sun. Molecular dynamics simulation studies of binary blend miscibility of poly(3-hydroxybutyrate) and poly(ethylene oxide). *Polymer*, 45:453–457, 2004.

[73] Qi Liao, Jie Fu, and Xigao Jin. Single-chain polystyrene particles adsorbed on the silicon surface: A molecular dynamics simulation. *Langmuir*, 15:7795–7801, 1999.

[74] Theodora Spyriouni, Christos Tzoumanekas, Doros Theodorou, Florian Müller-Plathe, and Giuseppe Milano. Coarse-grained and reverse-mapped united-atom simulations of long-chain atactic polystyrene melts: Structure, thermodynamic properties, chain conformation, and entanglements. *Macromolecues*, 40:3876-3885, 2007.

[75] Dana R. Rottach, John G. Curro, Gary S. Grest, and Aidan P. Thompson. Effect of strain history on stress and permanent set in cross-linking networks: A molecular dynamics study. *Macromolecules*, 37:5468–5473, 2004.

[76] J. W. Liu, M. E. Mackay, and P. M. Duxbury. Nanoparticle formation by crosslinking a macromolecule. *Epl*, 84(4):46001, November 2008.

[77] D. J. Jacobs, A. J. Rader, L. A. Kuhn, and M. F. Thorpe. Protein flexibility predictions using graph theory. *Proteins-Structure Function And Genetics*, 44 (2):150–165, August 2001.

[78] James E. Martin and B. E. Eichinger. Dimensions of intramolecularly crosslinked polymers. *Macromolecules*, 16:1345,1350, 1983.

[79] Markus Antonietti, Hans Sillescu, Manfred Schmidt, and Horst Schuch. Solution properties and dynamic bulk behavior of intramolecular cross-linked polystyrene. *Macromolecules*, 21:736, 1988.

[80] M. F. Thorpe. Continuous deformations in random networks. *Journal Of Non-Crystalline Solids*, 57(3):355–370, 1983.

[81] M. F. Thorpe, D. J. Jacobs, M. V. Chubynsky, and J. C. Phillips. Self-organization in network glasses. *Journal of Non-Crystalline Solids*, 266-269: 859 - 866, 2000. ISSN 0022-3093.

[82] G. Allen, J. Burgess, S. F. Edwards, and D. J. Walsh. On the dimensions of intramolecularly crosslinked polymer molecules. *Proc. R. Soc. Lond. A.*, 334: 453,465,477, 1973.

[83] Alan E. Tonelli. Phenyl group rotation in polystyrene. *Macromolecues*, 6:682–683, 1973.

[84] D. Y. Yoon, P. R. Sundararajan, and P. J. Flory. Conformational characteristics of polystyrene. *Macromolecues*, 8:776–783, 1975.

[85] G. Reiter. Dewetting of highly elastic thin polymer films. *Physical Review Letters*, 8718(18):186101, October 2001.

[86] J. Forsman and C. E. Woodward. Prewetting and layering in athermal polymer solutions. *Physical Review Letters*, 94(11):118301, March 2005.

[87] S. R. Whaley, D. S. English, E. L. Hu, P. F. Barbara, and A. M. Belcher. Selection of peptides with semiconductor binding specificity for directed nanocrystal assembly. *Nature*, 405(6787):665–668, June 2000.

[88] K. Goede, P. Busch, and M. Grundmann. Binding specificity of a peptide on semiconductor surfaces. *Nano Letters*, 4(11):2115–2120, November 2004.

[89] R. L. Willett, K. W. Baldwin, K. W. West, and L. N. Pfeiffer. Differential adhesion of amino acids to inorganic surfaces. *Proceedings Of The National Academy Of Sciences Of The United States Of America*, 102(22):7817–7822, May 2005.

[90] E. Balog, T. Becker, M. Oettl, R. Lechner, R. Daniel, J. Finney, and J. C. Smith. Direct determination of vibrational density of states change on ligand binding to a protein. *Physical Review Letters*, 93(2):028103, July 2004.

[91] M. Ikeguchi, J. Ueno, M. Sato, and A. Kidera. Protein structural change upon ligand binding: Linear response theory. *Physical Review Letters*, 94(7):078102, February 2005.

[92] E. Eisenriegler. *Polymers Near Surfaces: Conformation Properties and Relation to Critical Phenomena.* World Scientific, Singapore, 1993.

[93] G. J. Fleer, M. A. Cohen Stuart, J. M. H. M. Scheutjens, T. Cosgrove, and B. Vincent. *Polymer at Interfaces.* Chapman & Hall, London, 1993.

[94] S. Granick, S. K. Kumar, E. J. Amis, M. Antonietti, A. C. Balazs, A. K. Chakraborty, G. S. Grest, C. Hawker, P. Janmey, E. J. Kramer, R. Nuzzo, T. P. Russell, and C. R. Safinya. Macromolecules at surfaces: Research challenges and opportunities from tribology to biology. *Journal Of Polymer Science Part B-Polymer Physics*, 41(22):2755–2793, November 2003.

[95] T. Vrbova and S. G. Whittington. Adsorption and collapse of self-avoiding walks and polygons in three dimensions. *Journal Of Physics A-Mathematical And General*, 29(19):6253–6264, October 1996.

[96] T. Vrbova and S. G. Whittington. Adsorption and collapse of self-avoiding walks at a defect plane. *Journal Of Physics A-Mathematical And General*, 31 (34):7031–7041, August 1998.

[97] T. Vrbova and S. G. Whittington. Adsorption and collapse of self-avoiding walks in three dimensions: A monte carlo study. *Journal Of Physics A-Mathematical And General*, 31(17):3989–3998, May 1998.

[98] M. S. Moghaddam, T. Vrbova, and S. G. Whittington. Adsorption of periodic copolymers at a planar interface. *Journal Of Physics A-Mathematical And General*, 33(25):4573–4584, June 2000.

[99] R. Rajesh, D. Dhar, D. Giri, S. Kumar, and Y. Singh. Adsorption and collapse transitions in a linear polymer chain near an attractive wall. *Physical Review E*, 65(5):056124, May 2002.

[100] Y. Singh, D. Giri, and S. Kumar. Crossover of a polymer chain from bulk to surface states. *Journal Of Physics A-Mathematical And General*, 34(8):L67–L74, March 2001.

[101] Y. Singh, S. Kumar, and D. Giri. Surface adsorption and collapse transition of a linear polymer chain in three dimensions. *Journal Of Physics A-Mathematical And General*, 32(36):L407–L411, September 1999.

[102] J. Krawczyk, A. L. Owczarek, T. Prellberg, and A. Rechnitzer. Layering transitions for adsorbing polymers in poor solvents. *Europhysics Letters*, 70(6): 726–732, June 2005.

[103] A. L. Owczarek, A. Rechnitzer, J. Krawczyk, and T. Prellberg. On the location of the surface-attached globule phase in collapsing polymers. *Journal Of Physics A-Mathematical And Theoretical*, 40(44):13257–13267, November 2007.

[104] Michael Bachmann and Wolfhard Janke. Conformational transitions of nongrafted polymers near an absorbing substrate. *Physical Review Letters*, 95: 058102, July 2005.

[105] Michael Bachmann and Wolfhard Janke. Substrate adhesion of a nongrafted flexible polymer in a cavity. *Physical Review E*, 73:041802, 2006.

[106] I. Carmesin and K. Kremer. The bond fluctuation method - a new effective algorithm for the dynamics of polymers in all spatial dimensions. *Macromolecules*, 21(9):2819–2823, September 1988.

[107] Niklas Källrot and Per Linse. Dynamic study of single-chain adsorption and desorption. *Macromolecues*, 40:4669–4679, 2007.

[108] T. G. Desai, P. Keblinski, S. K. Kumar, and S. Granick. Modeling diffusion of adsorbed polymer with explicit solvent. *Physical Review Letters*, 98(21):218301, May 2007.

[109] J. Baschnagel and F. Varnik. Computer simulations of supercooled polymer melts in the bulk and in-confined geometry. *Journal Of Physics-Condensed Matter*, 17(32):R851–R953, August 2005.

[110] F. Varnik, J. Baschnagel, and K. Binder. Reduction of the glass transition temperature in polymer films: A molecular-dynamics study. *Physical Review E*, 65(2):021507, February 2002.

[111] G. D. Wignall, J. Schelten, and D. G. H. Ballard. Measurements of radius of gyration and persistence length in bulk atactic polystyrene by low-angle neutron-scattering. *Journal Of Applied Crystallography*, 7(APR1):190, 1974.

[112] J. F. Douglas, H. E. Johnson, and S. Granick. A simple kinetic-model of polymer adsorption and desorption. *Science*, 262(5142):2010–2012, December 1993.

[113] H. E. Johnson and S. Granick. New mechanism of nonequilibrium polymer adsorption. *Science*, 255(5047):966–968, February 1992.

[114] D. Mukherji and M. H. Muser. Glassy dynamics, aging in mobility, and structural relaxation of strongly adsorbed polymer films: Corrugation or confinement? *Macromolecules*, 40(5):1754–1762, March 2007.

[115] S. Jeon, S. C. Bae, and S. Granick. Local chain dynamics of adsorbed polystyrene studied by time-resolved fluorescence anisotropy. *Macromolecules*, 34(24):8401–8404, November 2001.

[116] T. K. Xia, O. Y. Jian, M. W. Ribarsky, and U. Landman. Interfacial alkane films. *Physical Review Letters*, 69(13):1967–1970, September 1992.

[117] A. Perro, S. Reculusa, S. Ravaine, E. B. Bourgeat-Lami, and E. Duguet. Design and synthesis of janus micro- and nanoparticles. *Journal Of Materials Chemistry*, 15(35-36):3745–3760, 2005.

[118] H. C. Kolb, M. G. Finn, and K. B. Sharpless. Click chemistry: Diverse chemical function from a few good reactions. *Angewandte Chemie-International Edition*, 40(11):2004, 2001.